UNIVERSITÀ DELLA CALABRIA

UNIVERSITA' DELLA CALABRIA

Dipartimento di CHIMICA

Scuola di Dottorato

Scienza e Tecnica "B. Telesio"

Indirizzo

Scienze E Tecnologie Delle Mesofasi E Materiali Molecolari

CICLO XXVI

AGGREGATE STRUCTURES ANALYSIS OF BITUMEN FOR THE PRODUCTION OF MODIFIED BINDERS IN ASPHALT INDUSTRY.

Settore Scientifico Disciplinare Chim/02

Direttore: Ch.mo Prof. Roberto Bartolino

Supervisore: Dr. Cesare Oliviero Rossi

Dottorando: Dott. Luigi Filippelli

Contents.

Abstract

Since antiquity bitumen had been used as a construction material. Nowadays, most of the huge global production of bitumen each year, are functional to the roads paving industry where they are employed as binders for mineral aggregates to produce asphalt mixes. In the paving industry, a suitable bitumen should be fluid enough at to be pumpable and workable for a uniform covering of the mineral aggregates upon amalgamation. Furthermore, once the asphalt has been laid to build the roads, bitumen has to become sufficiently rigid at the highest pavement temperature to oppose rutting, depending on local climate conditions. Conversely, it must stay flexible enough at the lowest pavement temperature to resist cracking. For these purposes, additives such as polymers, acids, etc., are used to calibrate the operative range of bitumen. In addition asphalt industry is interested to reduce the costs of production, the environmental impact of the production and the safety condition for the paving workers. Bitumen is currently modeled as a dispersion of colloidal particles of asphaltenes, surrounded by a layer of stabilizing polar resins in a continuous oil phase (maltene). Although one can write a very simple definition of bitumen, its chemical composition is very complex and still not completely known. However the characterization of the bituminous materials for its convenient application, is still made by empirical standardized tests. This research project aimed to the deeper understanding of the behavior of bituminous systems, in order to correlate the macroscopic properties to the microstructure of the aggregates that constitute the bitumen colloidal network. We explored the possibility of taking advantage from chemical-physics techniques such as NMR, Rheology and AFM. In particular we have investigated the effect and overall the mechanism through which some chemical additives, already in use by paving companies, explicate their action to modulate the bitumen performances. Several samples different in nature and differently modified were analyzed. The rheological analysis, performed by the measurements under kinematic and dynamic control, helped to determine the material properties related to the structure of the system. The parameters thus obtained, being independent of the measurement conditions may be correlated with the microstructure of the sample investigated by the other techniques we used. As for NMR we exploited the spin-spin relaxation time measurement firstly to find the soften point of bituminous materials whether modified or not. As a novel approach to the understanding of the colloidal nature of the bitumen, the Inverse Laplace Transform (ILT) of the NMR spin-echo decay (T2) was applied. The *ILT was used to draw the map of the macro-aggregates inside bitumen at different temperatures providing indication on the nature of the interaction between additives and the colloidal network. The efficiency of the ILT method was proved by atomic force microscopy images. As matter of fact collecting the AFM analysis, the ILT and the rheological results, we were able to describe the correlation between the aggregates at supra-molecular level inside fresh and doped bitumen. This research constituted a new inside bitumen chemistry overcoming the limits of the empirical tests to verify the efficiency of the bitumen modifiers.*

INTRODUCTION

In the last years, hundreds of new roads were built over the world in order to satisfy the growing traffic load. However many of the existing roads are in use since more than 20 years and the volume of vehicles has noticeably increased. For these two main reasons an increase in roads maintenance is required. In this particular historical moment with one of the worst financial crisis after the second world war, it is not easy to rise adequate funds for roads maintenance leading to a quick deteriorated asphalt pavement. Hence it is essential to innovate and find alternative processes to build up asphalt roads. Recycling aged road pavements is one of this methods. The main points for recycling asphalts are: Reduction of the raw materials; reduction of wasting areas; reduction of pollution; energy saving; economical convenience. Bitumen is the crucial component used for the road constructions in the world, as it is the typical binder adopted for road asphalt conglomerate and, being the only deformable component, it is the main responsible for pavement performance. It is a dark brown to black, cement-like semisolid or solid or viscous liquid produced by the non-destructive distillation of crude oil during petroleum refining. It can also be found in nature as “natural asphalt”. The chemical composition and mechanical properties of bitumen strongly depend on the origin of the crude oil . Indeed bitumen is a complex chemical mixture of molecules that are predominantly hydrocarbons of different molecular sizes with a small amount of structurally analogous heterocyclic species (heteroatoms) and functional groups containing sulphur, nitrogen and hydrogen atoms . Metals like nickel, iron and vanadium are also present. However the elemental analysis is very similar for all the bitumen with a prevalence of hydrocarbons that have a number of carbon atoms higher than 25. Due to this complex chemical composition, bitumen is currently classified for the convenient use by means of empirical standardized tests that were defined since the early 1970s under the USA project SHRP (strategic highway research project). However a more analytical approach is needed to obtain a real improvement of the recycling process and bitumen performance. Hence a better depiction of the molecular and supra-molecular structure of bitumen is essential to understand the action of some additives already in use and to design new ones. Bitumen is currently modeled as a colloidal

dispersion of asphaltene particles, coated with layers of stabilizing polar resins, in a continuous oil phase. Basically it can be viewed as a two phase material with no distinct boundaries between the two fractions. For this reason the mechanical properties of bitumen are the result of the chemical composition and phases arrangement of the molecular structures. This thesis deals with the chemical-physics modification of bitumen binders that produce changes in the supra-molecular arrangement. These changes in turn are reflected on the mechanical properties. In this view we investigated the action of the polyphosphoric acid (PPA) as modifier, that is employed to obtain stiffer binders. However we focused our efforts on the recycling process of bitumen that loses elasticity with aging. This is mainly due to the oxidation of aromatic compounds and resins. Some of the additives already employed by manufacturers to rejuvenate aged bitumen were investigated and their action revealed. To reach this goal we exploited rheology, atomic force microscopy, nuclear magnetic resonance with inverse Laplace transform.

1. Bitumen Production, Structure and Composition.

1.1 Production.

In the early 20th century, bitumen was only taken from natural sources [1]. Nowadays, it is basically obtained by the distillation of crude oil [2,3]. Only one tenth of the available crude oil is suitable to yields adequate amounts of bitumen. More or less, the heavier the petroleum, the higher its bitumen amount [2,3]. Native bitumen is poorly used in the paving industry, normally as an additive for other derivated bitumen [4].The distillation (Figure 1.1) is made by separating the light components from the crude oil by atmospheric distillation at about 350 °C. In a successive step, the residue is further refined at a slightly higher temperature (350–425 °C) under vacuum with [5]. The resulting material properties, depend on the crude origin and real operating conditions. Usually, refiners manufacture only a soft and a hard bitumen, and the intermediate are obtained by blending them [2]. When new vacuum distillation columns came with structured packing internals, harder grades can now be obtained by distillation [4].

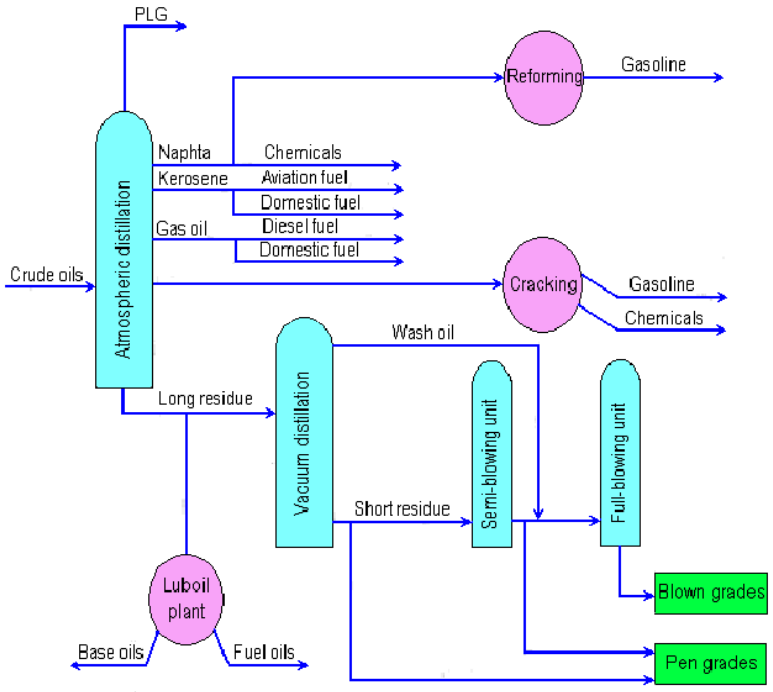

Figure 1.1. Scheme of crude oil refinery plant.

Furthermore another multigrade bitumen, can have a wider operating temperature range than normal bitumen and can be also obtained through acid modification. Other techniques still exist to obtain bitumen from petroleum. Air-blowing was the first process that allowed the manufacture of bitumen from a very fluid crude oil [5,6]. the oil (or soft bitumen) is air-oxidized at 200–275 °C, sometimes in the presence of a catalyst [2]. The properties of the oxidized material, depend on the crude oil origin (or the soft bitumen) and the operating conditions, temperature and time. It still is the best process to make very hard bitumens, especially for waterproofing. However they are not in use for paving applications, because they were too vulnerable to cracking [4]. When a soft bitumen is gently blown to pass paving specifications, the corresponding bitumen is sometimes called semi-blown bitumen.

Another process of minor commercial meaning is the so-called solvent deasphalting, [2]. The heavy fraction of a crude oil (or soft bitumen) is added with 3–10 times its volume of liquid propane and then left to settle [10]. Characteristic conditions are a temperature in the 25–70 °C range and a pressure of 12 bars to maintain propane in the liquid state. The precipitate is bitumen. It still is a good way for recovering lubricants, and the bitumen is a by-product [5,6].

1.2 Physical and chemical properties of Bitumen.

A natural source of heavy crude oil is called bitumen when its density go over 1 g/cm3 at 15.6 °C. However density of bitumen at room temperature is between 1.01 and 1.04 g/cm3, depending on the oil source and paving grade [3]. Normally, the harder it is, the denser the bitumen. Bitumen has a glass transition around −20 °C, although it varies in a range from +5 °C down to −40 °C again depending on the crude origin and somewhat on the process [7,8]. Hence from a thermodynamical point of view, bitumen is a very viscous liquid at room temperature. The complexity of bitumen chemistry lies in the fact that many different chemicals are present. In general the chemical nature of the crude oil is described as paraffinic, naphthenic or aromatic if a majority of saturate, cyclic or aromatic structures, respectively, are present [5]. This classification of the petroleum is sometimes applied to the corresponding bitumen. For example, Venezuelan bitumens are generally known as naphthenic bitumens. The elemental composition of a bitumen depends primarily on its crude source and it is difficult to give geographical generalization [3,9]. For instance materials from the USA or Canada can have quite different compositions. Indeed the first systematic classification of bitumen came with the extraordinary work on bitumen chemistry, structure and properties realized in the USA as part of the Strategic Highway Research Program (SHRP) in the late 1980s [10]. From this data bitumen mainly consists in carbon (typically 80–88 wt.%) and hydrogen atoms (8–12 wt.%). This gives a hydrocarbon

content generally superior to 90wt.% with an hydrogen-to-carbon molar ratio H/C around 1.5. This H/C ratio is therefore intermediate between that of aromatic structures (benzene has H/C=1) and that of saturate alkanes (H/C =2) [3,11] . In addition, heteroatoms such as sulphur (0–9 wt.%), nitrogen (0– 2 wt.%) and oxygen (0–2 wt.%) are generally present. Traces of metals are also found, the most numerous being typically vanadium, and nickel (up to 200 ppm) [3,5,8,11]). Sulfur is generally the most present polar atom. It appears in the form of sulfides, thiols and, to a lesser extent, sulfoxides (Figure 1.2). Oxygen is typically present in the form of ketones, phenols and, to a lesser extent, carboxylic acids (Fig. 2). Nitrogen exists typically in pyrrolic and pyridinic structures and also forms amphoteric species such as 2-quinolones [3,5] (Figure 1.2). Most of the metals form complexes such as metalloporphyrins [5].

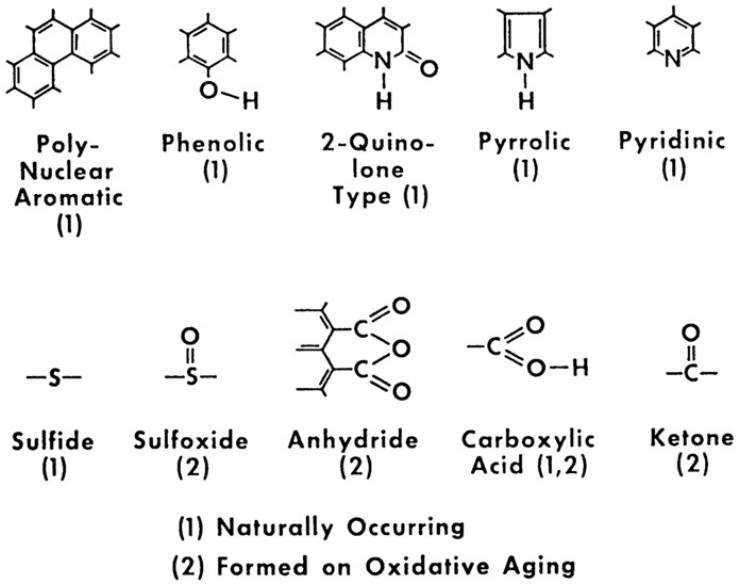

Figure 1.2. Classes of chemicals species present in bitumen binder.

Given the concentration of polar atoms, functional groups generally do not amount for more than a few 0.1 mol/l for straight run bitumens [11]. The number-average molecular weight of bitumen falls typically in the range 600–1500 g/mol [11]. Average molecular structures for bitumen have been proposed (Figure 1.3)[12]. Note that bitumen molecules are therefore not macromolecules in the polymeric sense. Hence it is not easy trying to compare the properties of polymers to that of bitumen, particularly when modeling the viscoelastic properties based on a

molecular approach. Given these molecular weights and the proportion of polar

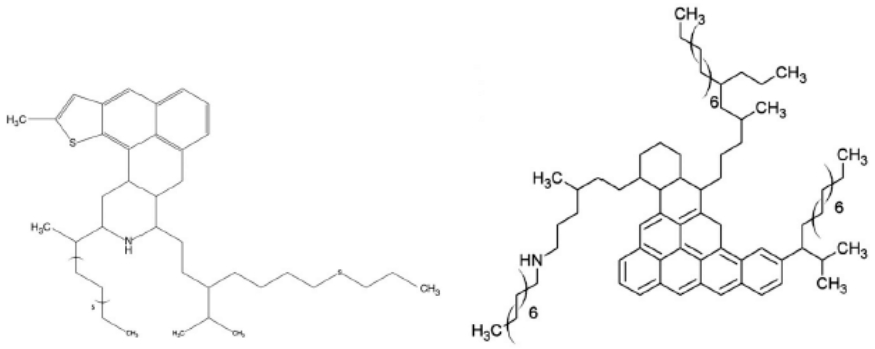

Figure 1.3 Average molecular structures for bitumen as taken from ref. [12].

atoms, only 1–3 polar atoms are present on average in each bitumen molecule. In addition, approaching bitumen chemistry on a global basis is not sufficient when one tries to understand the properties of bitumen. Thus, the molecules are generally separated into different chemical species, depending on their size and solubility in polar, aromatic or non-polar solvents.

1.3 SARA fractions.

As early as 1836, Boussingault separated by distillation two components of a native bitumen : he called petrolene a distillable fraction of about 85 wt.% and the remaining 15 wt.% of a solid fraction, that he called asphaltene [13,14]. Petrolene appeared a yellow liquid of density 0.891 at 21 °C, consisting of a pure hydrocarbon with H/C=1.56. Asphaltene was found to be a solid with H/C=1.58 and contained 14.8 wt.% of oxygen. Asphaltene was a compound very similar in composition and properties to natural asphalt. For their similar H/C ratio, Boussingault suggested that asphaltene originated from the oxidation of petrolene [13]. The soluble part was called the malthenes, because of their resemblance to maltha, a soft kind of native bitumen [15]. The most common spelling is now maltenes. In this view, petrolene would be limited to the distillable fraction of bitumen whereas maltenes would be the bitumen fraction soluble in n-heptane taken as the oily constituent of bitumen as opposed to the asphaltenes. Asphaltenes and maltenes are complex blends of hydrocarbons . Since maltenes are the most numerous components, separating bitumen into only two

fractions is not satisfying. Hoiberg and co-workers in 1939 separated the n-hexane maltenes into resins and oils, defining the resins as the pentane precipitate and the oils as the soluble part [16]. The separation of the maltenes into more fractions really improved with the advent of modern chromatographic methods [16]. The reference method is now elution-adsorption liquid chromatography on active alumina with solvents of increasing polarity and aromaticity as proposed by Corbett [17]. His set-up is now the reference method for the separation of the maltenes into saturates, aromatics and resins, according to their elution by, respectively, n-heptane, benzene and a final two-steps elution by first a 50/50 blend of benzene and methanol followed by trichloroethylene. This method allows to give the composition of bitumen in terms of the relative quantity of its so-called SARA fractions for Saturates, Aromatics, Resins and Asphaltenes (Figure 1.4).

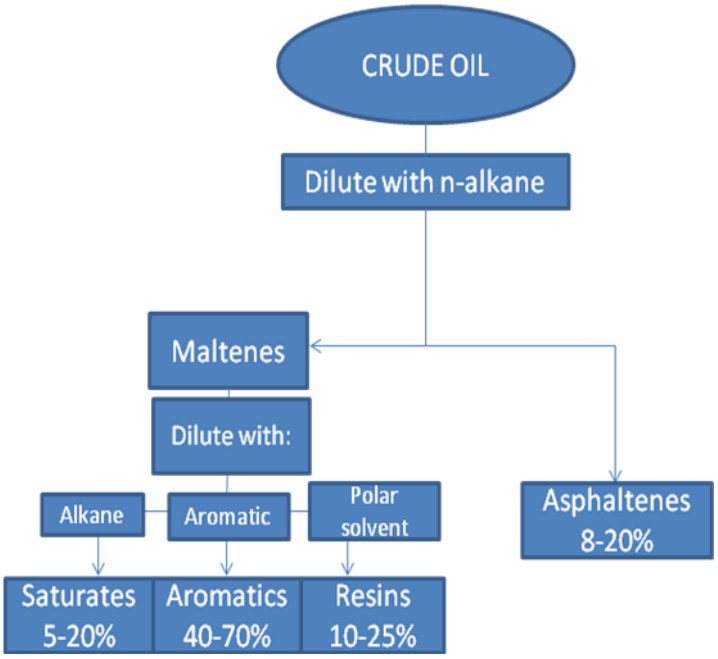

Figure 1.4. Scheme for the separation of SARA fractions.

Nowadays, other solvents if not experimental set-ups are preferred for safety reasons and convenience [5]. The reference method is the ASTM D-4124 [18], also in use for crude oil [5]. The first step consists in separating the asphaltenes by n-heptane precipitation. This is done by blending typically 12 g of bitumen in 1.2 L of n-heptane and recovering the insoluble part after stirring 1 h near the boiling point of n-heptane

(98 °C). The deasphaltened bitumen is called maltenes as it is the more generally accepted name. In a second step, the maltenes in solution at typically 10 g in 50 ml of n-heptane, are passed through a chromatographic column containing CG-20 chromatographic grade alumina. Saturates are first separated using n-heptane as an eluant. Then, pure toluene followed by a blend 50/50 with methanol, are used to separate the aromatics. In the end, trichloroethylene is used to separate the resins.

1.3.1 Saturates

The 5–15 wt.% of a paving grade bitumen is the Saturates component [17]. They present as a colourless or lightly coloured liquid at room temperature [17] due to a very low glass transition temperature around −70 °C, that is typically 40 °C below the glass transition of their source bitumen. Their H/C ratio is close to 2, with only traces of hetero atoms. They contain a few crystalline linear n-alkanes, typically in amounts of 0– 15 wt.% of the overall fraction [19]. Saturates in bitumen are mainly aliphatic, very few polar atoms or aromatic rings are present [20].

1.3.2 Aromatics

Aromatics, are the most abundant constituents of a bitumen together with the resins, since they amount for 30–45 wt.% of the total bitumen [17]. They present as a yellow to red liquid at room temperature [17]. They are somewhat more viscous than the saturates at the same temperature, because of a higher glass transition temperature around −20 °C, which is similar to that of the parent bitumen [19]. Their carbon skeleton is slightly aliphatic with lightly condensed aromatic rings [20].

1.3.3 Resins.

Resins, or polar aromatics, can be abundant (30–45 wt.%) [17]. Resins form a black solid at room temperature [17] and it is not clear whether they exhibit a glass transition [19]. Koots and Speight showed that their composition is close

to that of asphaltenes except for their lower molar mass, of circa 1100 g/mol, a somewhat higher H/C ratio between 1.38 and 1.69 and most of all a less complex aromatic structure [21]. Piéri showed that they can sometimes be more polar than asphaltenes, but again with less condensed aromatic rings [20]. They typically contain fused aromatic rings, with a most probable structure corresponding to 2–4 fused rings . They are believed to play a crucial role in the stability of bitumen, since they act as a stabilizer for the asphaltenes as will be detailed later.

1.3.4 Asphaltenes

Asphaltenes are normally between 5 and 20 wt.% of a paving grade bitumen [17,22] and are the most studied bitumen fraction due to their viscosity building role [11]. They are also of great interest to petroleum chemists for their importance in the processing of crude oil [23]. Asphaltenes are defined as the insoluble part of a bitumen (or a crude oil) in n-heptane (ASTM D3279) but soluble in toluene. In this contest solubility must be viewed as “not generating a precipitate" and not as molecular solubility, since asphaltenes are known to form micelles in toluene. When dealing with high wax content materials, the procedure might generate a co-precipitation of poly-crystalline waxy materials as observed with crude oils [24]. Asphaltenes form a black powder at room temperature [17] and are largely responsible for the black colour of the bitumen. They do not display any thermal transition in the normally investigated temperature range (up to 200 °C [20]). Their number-average molecular weight is estimated to be 800– 3500 g/mol by Vapor Pressure Osmometry ,one of the very few techniques allowing dissociating the micelles [5,22]. Their elemental analysis is stable from one asphalt to the other with a H/C ratio between 0.98 and 1.56 [21]. Ultra-Violet fluorescence [20], FTIR [20,25], X-Ray Raman spectroscopy [56] and Nuclear Magnetic Resonance [25,26] show that they contain fused aromatic rings, with a most probable structure corresponding to 4–10 fused rings. In comparison to other bitumen

molecules, asphaltenes contain more condensed aromatic rings and more polar groups [27] but the presence of fused aromatic structures seems to be the fundamental feature differentiating the asphaltenes from the rest of the bitumen molecules. Due to the many condensed aromatic rings, asphaltenes form almost planar molecules that can associate through π–π bonding to form graphite-like stacks [23,25]. Note that multimer formation may be enhanced by the presence of polar interactions between oxygen functional groups as observed on model pyrene compounds [28]. Because of this association behaviour, X-Ray diffraction spectra of solid asphaltenes show an average of 5 unit sheets [29]. Using other experimental techniques, it was deduced that aggregates with more than 8 sheets are improbable [30]. When put in a solvent, the asphaltenes still associate and the aggregation process leads to what is generally called “micelles” [5,31,32]. The aggregation process persists inside the bitumen and it is the basis of the colloidal structure of bitumen.

1.4 Sol and Gel bitumens and bitumen modeling.

The first description of the colloidal structure of bitumen is generally accredited to Nellensteyn in 1923 [33,34], even if Rosinger suggested a colloidal structure for bitumen in 1914 [35]. Nellensteyn supposed that asphaltenes are very similar to free carbon and form a colloidal suspension within the maltene phase. This was supported by the Tyndall effect of asphaltenes solutions, ultramicroscopic observation of the Brownian motion of asphaltenes in such solutions and the absence of diffusion through membranes [34]. Pfeiffer and coworkers successively developed the colloidal model to explain the difference in rheological properties between what they called sol and gel bitumens [36,37]. Sol bitumens exhibited Newtonian behaviour, whereas gel bitumens (generally blown ones) were highly non-Newtonian. Between these two extremes, a majority of bitumens was found to have an intermediate behaviour due to a mixed “sol–gel” structure. In modern terms, the non-Newtonian behaviour would be described as delayed elasticity together with some

nonlinearity in the viscoelastic properties [38]. In structural terms, the sol type was thought to occur when the asphaltenes micelles were fully dispersed and non-interacting (Figure 1.5 A). The non-Newtonian behaviour was thought to originate from a gel structure due to fully interconnecting asphaltenes micelles (Figure 1.5 B). The sol–gel structure consists in the coexistence of sol-type micelles and a gel structure.

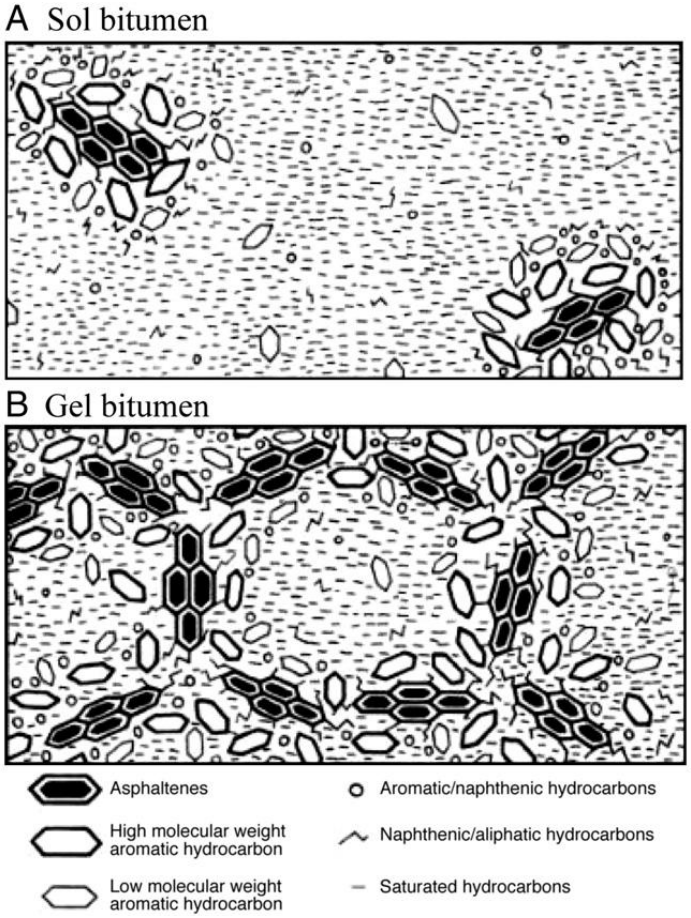

Figure 1.5. (A) scheme of Sol type bitumen. (B) scheme of Gel type bitumen.

this interpretation was in line with the well-known result that a soft grade differs from a harder grade from the same crude oil by higher asphaltenes content and lower aromatics content with almost unchanged resin and saturate contents [3].

1.4.1 The homogeneous model.

Some researchers, concluded that asphalt is a simple homogeneous fluid and Some of them called this model the Dispersed Polar Fluid (DPF) [39,40]. They discarded the colloidal hypothesis based on a series of arguments, such as the inexistence of a elastic plateau for gel bitumens, the monotonic time dependence and the unimodal relaxation spectrum found for bitumen viscoelasticity, that was believed to be a key argument in favour of an homogeneous model. These arguments discarding the colloidal structure of bitumen can not withstand a critical scientific analysis and the arguments based on the rheological properties of bitumen simply ignores that some heterogeneous materials can still display a monotonic time-dependence, a unimodal relaxation spectrum and thermo-rheological simplicity [41]. Moreover, the proponents of the homogeneous model of bitumen can not explain why direct investigation of bitumen structure using X-ray or neutron scattering, confirm its heterogeneous nature [42-44]. Also, and as many experimental results can not be interpreted without introducing the colloidal hypothesis. For all these reasons, the colloidal model is the only one at the moment that can reasonably explain the peculiar features of bitumen properties.

1.4.2 The colloidal model

Small Angle X-Ray Scattering (SAXS) and Small Angles Neutrons Scattering (SANS) confirm that asphaltenes form micelles in organic solvents [45,46], in crude oil [45, 47] and in bitumen [42,48]. It was also shown that the diffusion pattern observed in SAXS or SANS experiments, disappeared once the asphaltenes were removed from the bitumen [42] or the crude oil [49]. The colloidal model is also consistent with results obtained by thermal analysis. As previously described, bitumen undergoes a glass transition at a temperature very close to that of its aromatics. This strongly suggests that the asphaltenes exist as dispersed solid particles and do not directly participate to the glass

transition. All these evidences make it difficult to deny the colloidal nature of bitumen. The most convincing evidence is the one coming for diffusion experiments. In all diffusion studies, the scattering techniques highlighted an elementary structure consisting in diffusive particles of radius 2−8 nm. Such a particle size is reminiscent of the crystal size of asphaltenes [29,48]. Various geometrical shapes were proposed for the asphaltenes micelles: some authors suggested they were spherical [43,44], whereas others proposed they formed flat sheets [46] and others believed they made cylinders [50]. Therefore, it must be kept in mind that the spherical description remains an approximation. The role of the resins in asphaltenes micelles stabilization remains to be fully understood. However many papers showed that asphaltenes precipitate when mixed with only the oily components of their parent bitumen, [51] and that the resins could help disperse asphaltenes in benzene, highlighting their key role in asphaltenes stabilization inside bitumen [51]. More recently, Lian et al. showed that the resins could better stabilize asphaltenes in toluene than a non-ionic surfactant such as ethoxylated nonylphenol [52]. Some other authors quantified that at least 75% of the original resin content were necessary in order to prevent asphaltenes precipitation [21]. Interestingly, they also observed that the resins from one crude oil could not stabilize the asphaltenes from another crude oil. There is therefore some molecular recognition effect that permits the resin to enter the asphaltenes micelles. This helps smother the differences in polarity between the asphaltenes and the maltenes, and therefore creating this surfactant-like behaviour. Asphaltenes micelles and their organization at a higher scale remains quite supposed due to experimental difficulties [53]. A more precise picture of asphaltenes micelles aggregation arises from SAXS or SANS experiments [54]. These results suggest that the aggregation state of

asphaltenes in solvents like toluene [31] and in bitumen is consistent with that a

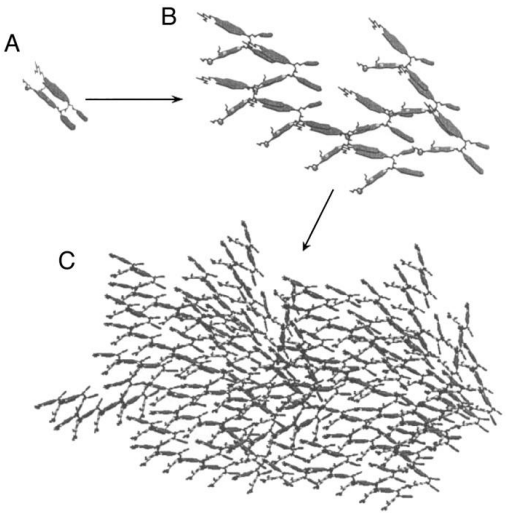

Figure 1.6. Possible molecular arrangement of asphaltene particles.

of fractal aggregates of fractal dimension 2. A possible schematic description of such an asphaltenes aggregate is given in Figure 1.6 C. In parallel, observations of bitumen with Atomic Force Microscopy (AFM), Scanning Electron Microscopy (SEM) have been published. The AFM shows a peculiar “bee” structure that was initially only found for a “gel” bitumen (Figure 1.7 - [55]).

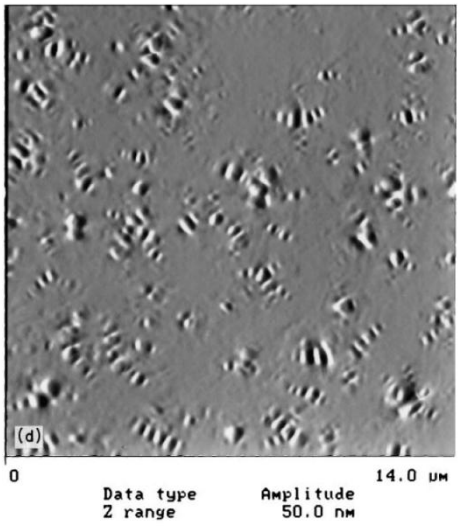

Figure 1.7. AFM of a bitumen sample as taken from ref. [55]

Apart from the bee structure, some bitumens displayed a rather flat structure and some others displayed “flake”-like domains [56]. The additional use of AFM in the Phase Detection Microscopy mode (PDM) suggests that at least three phases are present and temperature-dependent . A full interpretation of these features remains to be given. The SEM observation of the same “gel” bitumen that gave “bee” structure in AFM ,showed connecting aggregates of what was believed to be asphaltene particles of diameter around 100 nm (Fig. 1.8 - [55]). Here, it is not clear how the preparation procedure affects the observed morphology and whether it is representative of the structure inside the bitumen.

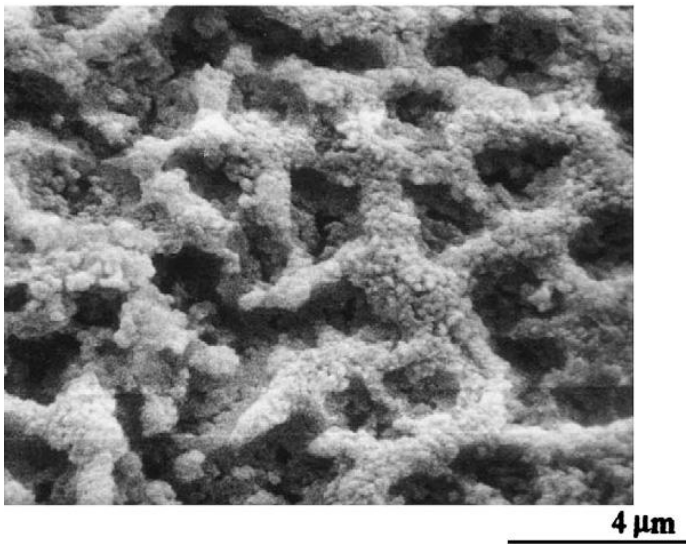

Figure 1.8. SEM image of a Gel-like bitumen as taken from ref. [55].

As previously cited, resins act as somewhat like a surfactant, creating a so-called solvation layer, and help maintain them in suspension. However, it must be remembered that the asphaltenes themselves also act as their own surfactant. In all cases, it is believed that the extent of the solvation layer is temperature dependent and therefore, modeling bitumen as a colloid necessitates considering that the amount of total solid phase in a bitumen (asphaltenes and adsorbed resins) is temperature dependent. Considered that the amount of resins can be around 50% and that at least the 75% of which is required to stabilize the asphaltenes the amount of solid phase (that is

asphaltenes+stabilizing resins) within a given bitumen must be significantly higher than its asphaltene content. In this context, the modern colloidal picture essentially differs from the earlier one in the sense than all bitumens are thought to have the same structure and that the only difference between former sol and gel bitumens would be the amount of solvated asphaltenes, i.e. the volume fraction of dispersed solid phase.

1.5 Bitumen ageing.

From the above picture, bitumen structure is quite complex with slow temperature-dependent evolutions arising from molecular organization processes that are far from being fully understood. In addition to that, the molecules may irreversibly evolve through chemical ageing which is generally thought to be a sum of oxidation reactions and polymerization, and to a lesser extent, lighter components evaporation [3,57]. As a result, chemical ageing leads to a global hardening of the material, which in turns increases the cracking probability. Apart from the manufacturing process, two ageing conditions are generally separated for bitumen. First, there is a rapid chemical ageing upon mixing the hot bitumen in thin film with the hot aggregate. Second, there occurs an in-situ ageing during the service life of the pavement. The first one, sometimes called short-term ageing, occurs for a short time at a high temperature of typically 160 °C and is well simulated by the Rolling Thin Film Oven Test (RTFOT - ASTM D2872 -EN 12607) which “cooks” the bitumen in 1.25-mm thick moving films at 163 °C for 75 min. In the mean time, the asphaltenes content typically increases by 1–4 wt.%. The second one, sometimes called long-term ageing, occurs for a much longer period of time since service life of the pavement can extend to several decades. It depends of course on the position of the bitumen inside the pavement, the top layers being more exposed than the base course. Mix formulation also comes into play, the bitumen thickness and the mix porosity being important parameters. It finally depends on the local climate and all these involved parameters make

it quite complicated to accurately describe in-situ ageing. In chemical terms, ageing leads first to a decrease in aromatic content and subsequent increase in resin content, together with a higher asphaltene content. Therefore, it is generally accepted that the aromatics generate resins which in turn generate asphaltenes [3,58]. The saturates remain essentially unchanged, as
could be assessed from their low chemical reactivity. All these changes result in a slightly higher but almost unchanged glass transition temperature. The rate of asphaltenes production was found to be essentially linear with time in RTFOT laboratory experiments at 163 °C with 6–7 wt.% asphaltenes produced in 340 min [165]. This linear increase was also observed for in-situ aging of bitumen recovered from real pavement sites, with increases between 2 and 10 wt.% in a 90 months period under French southern climate (near Marseilles) [59]. More precisely, ageing was seen to result in the formation of first sulfoxides, and, although at a somewhat slower rate, ketones that finally yields anhydrids and carboxylic acids . Based on oxygen up-take, the ageing kinetics is initially linear and tends to slow down as the reaction proceeds. Bitumen oxidation is generally said to proceed in an auto-catalytic way. Typical antioxidants for lubricating oil or rubber, such as alkylphenylenediamine or phenothiazene at 0.5 wt.%, were observed to be essentially useless to prevent bitumen hardening . Free radical inhibitors such as phenols were also observed to be essentially useless as bitumen antioxidant [11]. In fact, the naturally present phenols seem to regulate bitumen oxidation. Among the few chemicals having a demonstrated antioxidant effect, lime, phenothiazine , amines and phosphate such as zinc dialkyldithiophosphate are generally mentioned. In addition, ultra-violet light is known to increase the oxidation process by activating photo-oxidation reactions [57]. Photo oxidation is believed to generate polymerisation reactions, not only for the asphaltenes, but also for the lower fractions down to the saturates .

1.5.1 Effects of bitumen ageing on its mechanical properties.

Ageing is highly studied because of its impact on the mechanical properties of the binder (hardening). Therefore, all rheological indicators are used to quantify its importance. In general, viscosity is mostly used as an indicator for ageing, an ageing index being usually defined either directly as the viscosity ratio or as the relative increase in viscosity versus time [57]. Room temperature viscosity was observed to increase linearly versus aging time up to 15 h in thin film (3.2 mm) at 163 °. The viscosity increase rate was observed to be higher for the more structured bitumens ("gel type"). More recently, it was observed that some asphaltenic bitumens displayed a different kinetics at high and low temperature whereas "normal" bitumens only showed a single kinetics and the proposed explanation was that the asphaltenes were believed to strongly aggregate at low temperature (60 °C), thus preventing oxygen to diffuse inside the aggregates which in turn lowered the oxidation rate. At high temperature however (130 °C), the dispersion was better therefore allowing for a better oxygen diffusion and higher oxidation rate. A full characterization of the bitumen structure and rheology at the ageing temperature is still to come.

REFERENCES.

[1] Lay MG. Ways of the World. New Brunswick: Rutgers Univ. Press; 1992.

[2] Corbett LW. Manufacture of petroleum asphalt. In: Hoiberg AJ, editor. Bituminous Materials: Asphalts, Tars and Pitches. New York: Interscience Publishers; 1965. p. 81–22. Vol. 2, Part 1.

[3] Read J, Whiteoak D. The Shell Bitumen Handbook. 5th Ed. London: Thomas Telford Publishing; 2003.

[4] PIARC (World Road Association), Use of Modified Bituminous Binders, Special Bitumens and Bitumens with Additives in Road Pavements, Routes/Roads 303 also available from LCPC Eds, Paris (France), 1999.

[5] Speight JG. The Chemistry and Technology of Petroleum. 3rd. Ed. New-York: Marcel Dekker; 1999.

[6] Krchma LC, Gagle DW. A U.S.A. history of asphalt refined from crude oil and its distribution. Proc Assoc Asphalt Paving Techn 1974;43A:25–88.

[7] Schmidt RJ, Santucci LE. A practical method for determining the glass transition temperature of asphalts and calculation of their low temperature viscosities. Proc Assoc Asphalt Paving Techn 1966;35:61–85.

[8] Jiménez-Mateos JM, Quintero LC, Rial C. Characterization of petroleum bitumens and their fractions by thermogravimetric analysis and differential scanning calorimetry. Fuel 1996;75:1691–700.

[9] Mortazavi M, Moulthrop JS. SHRP Materials Reference Library, SHRP report A-646. Washington D. C.: National Research Council; 1993.

[10] Committee for a study for a future strategic highway research program, stategic highway research. Transportation Research Board Special Report 260. Washington D. C.: National Research Council; 2001.

[11] Branthaver JF, Petersen JC, Robertson RE, Duvall JJ, Kim SS, Harnsberger PM, et al. Binder Characterization and Evaluation – vol. 2 Chemistry, SHRP Report A-368. Washington D. C.: National Research Council; 1994.

[12] Jennings PW, Desando MA, Raub MF, Moats R, Mendez TM, Stewart FF, et al. NMR spectroscopy in the characterization of eight selected asphalts. Fuel Sci Techn Int 1992;10:887–907.

[13] Boussingault JB. Extrait d'un mémoire sur la composition des bitumes. C R Acad Sci 1836;3:375–8.

[14] Boussingault JB. Mémoire sur la composition des bitumes. Ann Chim Phys 1837;64:141–51.

[15] Richardson C. The Modern Asphalt Pavement. 2nd Ed. New York: Wiley; 1910.

[16] Rostler FS. Fractional composition: Analytical and functional significance. In: Hoiberg AJ, editor. Bituminous Materials: Asphalts, Tars and Pitches. New York: Interscience Publishers; 1965. p. 151–222. Vol. 2, Part 1.

[17] Corbett LW. Composition of asphalt based on generic fractionation, using solvent deasphaltening, elution-adsorption chromatography and densimetric characterization. Anal Chem 1969;41:576–9.
[18] American Society for Testing and Materials. ASTM D-4124: Test Methods for Separation of Asphalt Into Four Fractions. Philadelphia: ASTM; 2001.
[19] Claudy P, Létoffé JM, King GN, Planche JP. Caractérisation des bitumes routiers par analyse calorimétrique différentielle (ACD). Analyse thermo-optique (ATO). Corrélation entre propriétés physiques et résultats ACD. Bull Liaison Lab Ponts Chaussées 1992;177:45–51.
[20] Piéri, N., Etude du Vieillissement Simulé et In-Situ des Bitumes Routiers par IRTF et Fluorescence UV en Excitation-Emission Synchrones, Ph. D. Thesis: Univ. Aix-Marseille St-Joseph (France), 1995.
[21] Koots JA, Speight JG.Relation of petroleumresins to asphaltenes. Fuel 1975;54:179–84.
[22] Speight JG. Petroleum asphaltenes. Part 1. Asphaltenes, resins and the structure of petroleum. Oil Gas Sci Technol 2004;59:467–77.
[23] Becker JR. Crude Oil –Waxes, Emulsiones and Asphaltenes. Tulsa: PennWell; 1997.
[24] Thanh NX, Hsieh M, Philp RP.Waxes and asphaltenes in crude oils. Org Geochem1999;30:119–32
[25] Scotti R, Montanari L. Molecular structure and intermolecular interaction of asphaltenes by FT-IR, NMR, EPR. In: Mullins O, Sheu EY, editors. Structures and Dynamics of Asphaltenes. New-York: Plenum Press; 1998. p. 79–113.
[26] Michon L, Martin D, Planche JP, Hanqueta B. Estimation of average structural parameters of bitumens by 13C nuclear magnetic resonance spectroscopy. Fuel 1997;76:9–15.
[27] Zhao S, Kotlyar LS, Sparks BD, Woods JR, Gao J, Chung KH. Solids contents, properties and molecular structures for various asphaltenes from different oilsands. Fuel 2001;80:1907–14.
[28] Akbarzadeh K, Bressler DC, Wang J, Gawrys KL, Gray MR, Kilpatrick PK, et al. Association behavior of pyrene compounds as models for asphaltenes. Energy Fuels 2005;19:1268–71
[29] Yen TF, Erdman JG, Pollack SS. Investigation of the structure of petroleum asphaltenes by X-ray diffraction. Anal Chem 1961;33:1587–94.
[30] Di Primio R, Horsfield B, Guzman-Vega MA. Determining the temperature of petroleum formation from the kinetic properties of petroleum asphaltenes. Nature 2000;406:173–6.
[31] Roux JN, Broseta D, Demésans B. Study of asphaltene aggregation: concentration and solvent quality effects. Langmuir 2001;17:5085–92.

[32] Priyanto S, Mansoori GA, Suwono A. Measurement of property relationships of nano-structure micelles and coacervates of asphaltene in a pure solvent. Chem Eng Sci 2001;56:6933–9.
[33] Nellensteyn, F.J., Bereiding en Constitutie van Asphalt, Ph. D. Thesis: Delft University (Netherland), 1923.
[34] Nellensteyn FJ. The constitution of asphalt. J Inst Pet Technol 1924;10:311–25.
[35] Rosinger A. Beiträge zur Kolloidchemie des Asphalts. Kolloid-Z 1914;15:177–9.
[36] Pfeiffer JP, Saal RNJ. Asphaltic bitumen as colloid systems. J Phys Chem1940;44:139–49.
[37] Saal II RNJ. Physical properties of asphaltic bitumen. 1. Rheological properties. In: Pfeiffer JP, editor. The Properties of Asphaltic Bitumen. Amsterdam: Elsevier; 1950. p. 50–76.
[38] Saal RNJ, Labout JWA. Rheological properties of asphaltic bitumens. J Phys Chem1940;44:149–65.
[39] Petersen JC, Robertson RE, Branthaver JF, Harnsberger PM, Duvall JJ, Kim SS, et al. Binder Characterization and Evaluation Volume 1, SHRP report A-367. Washington D. C. : National Research Council; 1994.
[40] Christensen DW, Anderson DA. Rheological evidence concerning the molecular architecture of asphalt cements. Proc.Chemistry of Bitumen 2, Rome; 1991. p. 568–95.
[41] Lesueur D, Gérard JF, Claudy P, Létoffé JM, Planche JP, Martin D. A structure related model to describe asphalt linear viscoelasticity. J Rheol 1996;40:813–36.
[42] Bodan AN. Polyquasispherical structure of petroleum asphalts. Chem Technol Fuels Oils 1982;18:614–8.
[43] Storm DA, Sheu EY, De Tar MM. Macrostructure of asphaltenes in vaccuum residue by small-angle X-Ray scattering. Fuel 1993;72:977–81.
[44] Storm DA, Barresi RJ, Sheu EY. Rheological study of Ratawi vacuum residue in the 298–673 K temperature range. Energy Fuels 1995;9:168–76.
[45] Dwiggins Jr CW. A small angle X-Ray scattering study of the colloidal nature of petroleum. J Phys Chem 1965;69:3500–6.
[46] Ravey JC, Ducouret G, Espinat D. Asphaltene macrostructure by small angle neutron scattering. Fuel 1988;67:1560–7.
[47] Mason TG, Lin MY. Asphaltene nanoparticle aggregation in mixtures of incompatible crude oils. Phys Rev E 2003;67:1–4 050401.
[48] Yen TF. The colloidal aspect of a macrostructure of petroleum asphalt. Fuel Sci Technol Int 1992;10:723–33.
[49] Hénaut I, Barré L, Argillier JF, Brucy F, Bouchard R. Rheological and structural properties of heavy crude oils in relation with their asphaltene content. Proc. Soc. Petrol. Eng. Int. Symposium on Oilfield Chem., Houston; Feb. 2001. Paper SPE 65020

[50] Ravey JC, Ducouret G, Espinat D. Asphaltene macrostructure by small angle neutron scattering. Fuel 1988;67:1560–7.
[51] Swanson JM. A contribution to the physical chemistry of the asphalts. J Phys Chem 1942;46:141–50.
[52] Lian H, Lin JR, Yen TF. Peptization studies of asphaltene and solubility parameter spectra. Fuel 1994;73:423–8.
[53] Gawrys KL, Kilpatrick PK. Asphaltene aggregation: techniques for analysis. J Instr Sci Techn 2004;32:247–53.
[54] Sirota E. Physical structure of asphaltenes. Energy Fuels 2005;19:1290–6.
[55] Loeber L, Sutton O, Morel J, Valleton JM, Muller G. New direct observations of asphalts and asphalt binders by scanning electron microscopy and atomic force microscopy. J Microsc 1996;182:32–9.
[56] Jäger A, Lackner R, Eisenmenger-Sittner C, Blab R. Identification of microstructural components of bitumen by means of atomic force microscopy (AFM). Proc Appl Math Mech 2004;4:400–1.
[57] Bell C. Summary Report on Aging of Asphalt-Aggregate Systems, SHRP Report A-305. Washington D. C.: National Research Council; 1989.
[58] Isaccson, Zeng H. Cracking of asphalt at low temperature as related to bitumen rheology. J Mater Sci 2003;33:2165–70.
[59] Groupe National Bitume, Susceptibilité au vieillissement des bitumes – Expérimentation A08, LCPC Research report CR19, Paris (France): LCPC Ed., 1997.
[60] Wurstner RG, HigginsWA, CraigWG. Laboratory evaluation of factors influencing the performance of paving asphalts — the effect of antioxidants, polymers and methods of processing. Proc Assoc Asphalt Paving Techn 1960;29:253–69.

2. Rheology, Nuclear Magnetic Resonance and Atomic Force Microscopy.

2.1 Fundamentals Rheology of Viscoelastic Matter.

Fluids deform irreversibly under shear; in other words, they flow. In contrast, solids deform elastically when subjected to a small shearing force and recover their original shape when the force is removed. The behavior of what is termed soft matter is somewhere in between. Soft matter systems are typically viscoelastic, that is they display a combination of viscous (fluid-like) and elastic (solid-like)behavior. Measuring the flow behavior and the mechanical response to deformation of viscoelastic materials provides us with information that can be interpreted in terms of their small-scale structure and dynamics. The mechanical properties of soft materials depend on the length scale probed by the measurements due to the fact that the materials are structured on length scales intermediate between the atomic and bulk scales [1]. For example, a colloidal suspension has structure on the scale of the spacing between the colloidal particles; a concentrated polymer system, on the scale of the entanglements between large molecules. As a result, their bulk properties can be quite different from properties on length scales smaller than or comparable to the structural scale. Making measurements on both macroscopic and microscopic length scales can help us to develop a better understanding of the relationship between microstructure and bulk properties in soft materials.

Following a brief introduction to viscoelasticity, this chapter will focus on two methods of measuring the viscoelastic properties of soft matter. On the macroscopic scale, rotational shear rheometry provides a well-established set of techniques for determining the mechanical properties of complex fluids. We will summarize the principles of rheology and describe the types of measurements one can perform [2–4]. Typically shear rheometry will be performed using a commercial rheometer, and we will discuss the types of instrument commonly available. We will not discuss extensional rheology or other rheometrical methods; the interested reader is referred to a number of excellent textbooks [2–4]. Techniques for making rheological measurements on the microscopic scale have been developed more recently, and the

field of microrheology is still evolving. Several reviews of the field have been published recently [5–9]. We will summarize the theoretical background and describe a frequently used experimental method based on tracking the motion of micron-sized tracer particles as they diffuse through the material of interest [6, 7, 10, 11]. Such experiments are typically home-built, and we will describe one implementation. In both cases, we will provide examples that illustrate how rheological measurements can provide information about the structure and dynamics of soft materials.

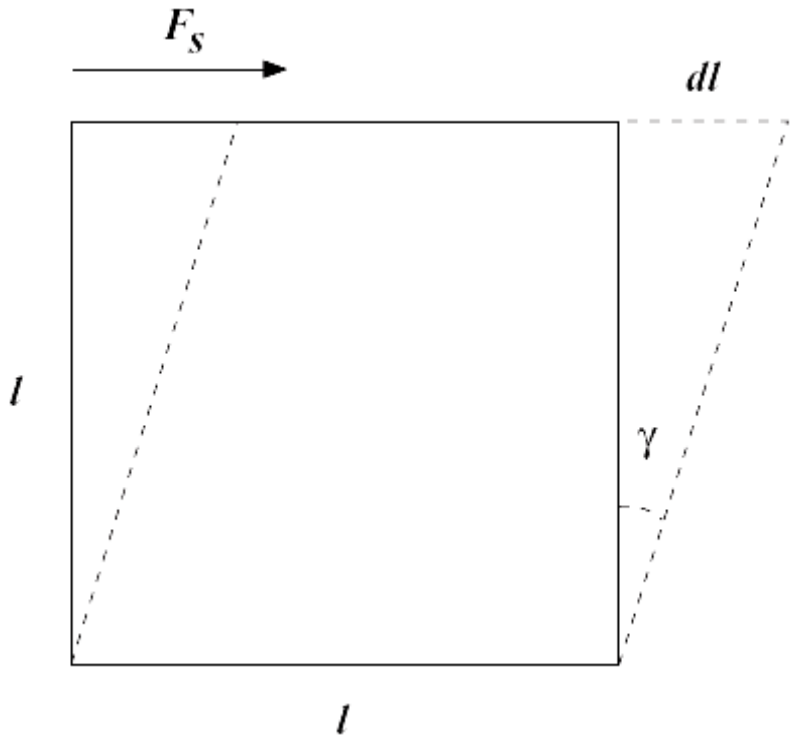

Figure 2.1 A small element of material subject to a shear force Fs . The bottom edge of the material is held fixed. The material experiences a shear strain γ = dl/l.

Consider a small solid cube having sides of length l and area $A = l^2$, as shown in Figure 2.1. Suppose that the bottom surface is held in place, and that we apply a shear force Fs parallel to plane of the top surface. The shear stress σ is the shear force divided by the surface area:

$$\sigma = F_s/A \qquad 2.1$$

In response to the applied shear force, the solid will deform by an amount dl. The shear strain γ is the relative deformation, given by:

$$\gamma = dl/l \qquad 2.2$$

For small strains, this is the same as the angle γ shown in Figure 2.1. For a perfectly

elastic solid, Hooke's Law tells us that stress and strain are linearly proportional, that is:

$$\sigma = G'\gamma \qquad 2.3$$

where the elastic modulus G' is a measure of the elastic energy stored in the material when it is deformed. Hooke's Law implies reversibility – the deformation immediately returns to zero when the shear stress is removed. Now imagine applying the same shear stress to a cubic element of a Newtonian fluid. In this case, the material flows continuously – the strain continues to increase for as long as the stress is applied. If the stress is increased, the fluid flows faster. Newton's law of viscosity states that:

$$\sigma = \eta\dot{\gamma} \qquad 2.4$$

where $\dot{\gamma} = d\gamma/dt$ is the strain rate. Here the strain rate, not the strain, is proportional to the stress. Equation (2.4) can be considered to define the viscosity η, which is related to the dissipation of energy in the flow. η can be thought of as the tendency of a material to resist flow. The discussion above (and throughout this chapter) is very much simplified by our neglect of the fact that stress, strain, and strain rate are all, in general, tensor quantities. For example, the shear stress σ referred to in the above equations is really just one component of a symmetric second-rank stress tensor. Since the focus of this book is on experimental techniques, we will ignore this rather important detail and use a simple scalar description. This implies a neglect of any material anisotropy and, more seriously, of several interesting and important physical phenomena, some of which will be mentioned very briefly below. More mathematically rigorous discussions can be found in textbooks such as references [2, 3, 12]. In general, the response of soft matter systems or complex fluids to an applied deformation or stress is time-dependent, they typically behave as solids on short time scales or at high frequencies and as viscous liquids over long times or at low frequencies. For example, when a viscoelastic material is subjected to a step increase in strain by an amount γ_0, the stress σ in the material undergoes a step change followed by, in the simplest case, an exponential relaxation. For small strains, one can define a relaxation modulus $G(t) = \sigma(t)/\gamma_0$, which is independent of γ_0, so

$$d\sigma = G(t)d\gamma \qquad 2.5$$

Analogously, in a creep experiment, the stress is suddenly increased from zero to some value σ_0. In this case, the strain will initially change rapidly in response, then continue to evolve more slowly as a function of time. The creep compliance J (t) is defined as.

$$J(t) = \gamma(t)/\sigma_0 \qquad 2.6$$

and is conceptually equivalent to the reciprocal of the relaxation modulus G(t).

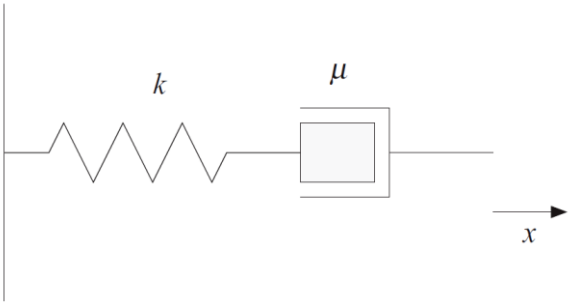

Figure 2.2 The spring-dashpot representation of the Maxwell model for a viscoelastic medium. The viscous and elastic elements are combined in series and stretched by a distance x.

The range of strains in which stress and strain are linearly related is called the linear viscoelastic regime. In this regime, the strain is small enough that it does not seriously disrupt any structure in the material, and one thus probes the response of the material to small perturbations of its equilibrium configuration. At higher strains, the structure is disrupted and the response of the material changes accordingly. In particular, the material properties become functions of strain or strain rate, and often functions of time as well. For example, outside of the linear regime, the viscosity of polymer solutions typically decreases as the strain rate is increased (shear thinning), because the shear stretches out the polymer molecules and allows them to partially disentangle. On the other hand, a concentrated clay suspension, which is a gel at rest, will become liquid when subjected to a large enough strain as the small-scale arrangement of the interacting clay particles is changed. It will then slowly gel again over time [13] as the clay particles rearrange and reorient. The interpretation of rheological measurements in the nonlinear regime is complex, and a subject of substantial current research [14, 15]. The simplest model of a viscoelastic material is originally due to Maxwell [16], and is mechanically equivalent to a spring in series with a viscous damper (a dashpot), as in Figure 2.2. If we stretch this combined system by a displacement x, a force F is developed that obeys the differential equation

$$F + \frac{\mu}{k}\frac{dF}{dt} = \mu\frac{dx}{dt} \qquad 2.7$$

where k is the spring constant and μ the viscosity of the dashpot. In terms of the viscoelastic properties of a complex fluid, the Maxwell model takes the form

$$\sigma + \varphi \frac{d\sigma}{dt} = \eta \frac{d\gamma}{dt} \tag{2.8}$$

where the viscosity η is assumed to be constant and ϕ is a time scale for the relaxation of the material. We can derive the integral form of the Maxwell model by imagining that the stress in a material depends on the strain to which it has been subjected over all time, from the distant past to the present [2]. The stress due to an arbitrary deformation can be calculated by integrating over contributions due to a series of small deformations as long as the relaxation modulus G(t) depends only on time and not on γ . In this case, we can rewrite Equation (2.5) in the form

$$d\sigma = G \frac{d\gamma}{dt} dt = G\dot{\gamma} dt \tag{2.9}$$

Integrating, we have

$$\sigma = \int_{-\infty}^{t} G\left(t - t'\right) \dot{\gamma}\left(t'\right) dt' \tag{2.10}$$

where t' runs from $-\infty$ to the present time t , and in general the strain rate $\dot{\gamma}$ is a function of time. In this context, the relaxation modulus G(t – t') is referred to as a memory function. If G(t) can be represented by an exponential decay with a decay time ϕ, that is, $G(t) = G0e^{-t/\phi}$, then Equation (2.10) becomes

$$\sigma = \int_{-\infty}^{t} G_0 e^{-(t-t')/\varphi} \dot{\gamma}(t') dt' \tag{2.11}$$

which gives the stress as a sum of infinitesimal contributions weighted by the memory function. Differentiating Equation (2.11) with respect to time recovers Equation (2.8), showing that the two formulations are equivalent. At steady state, dσ/dt = 0 and Equation (2.8) becomes Newton's law of viscosity, while for rapid changes, $d\sigma/dt >> \sigma/\phi$ and Hooke's law is recovered.

2.1.2 Shear rheometry.

The principle of shear rheometry is straightforward: the material of interest is subjected to shear in a controlled way, and the mechanical response measured. Typically one either applies a controlled shear strain and measures the resulting shear stress, or applies a known shear stress and measures the strain. Commercial rheometers are available that can do either, and many modern instruments do a good job of both. A schematic representation of a layer of fluid subjected to simple shear is shown in Figure 2.3. The fluid to be studied is sandwiched between two parallel plates separated by a gap d. In a strain-controlled experiment (Figure 2.3(a)), one plate say the upper plate, is moved to the right at a constant speed v_0, while the other plate is fixed. The no-slip boundary condition ensures that the flow velocity is $v = 0$ at the bottom plate, while $v = v_0$ at the top plate. As a result, a uniform shear is set up in the fluid, and the strain rate within the fluid layer is $\dot{\gamma} = \partial v/\partial y = v_0/d$. The horizontal (shear) force required to hold the lower plate fixed in position is measured by a transducer and the corresponding shear stress calculated from the geometry of the experiment. In a stress-controlled measurement, shown in Figure 2.3(b), the lower plate is again fixed. A known force applied to the upper plate causes it to move, and its displacement and velocity are measured.

Most commercial shear rheometers are rotational rheometers, meaning that the rheometer tool has cylindrical symmetry and shear is applied by rotating the tool about its axis. In a strain-controlled shear rheometer, a motor rotates the lower element of the rheometer tool in a precisely controlled manner. Depending on the type of measurements being performed, this can mean rotation at a constant angular velocity, a sinusoidally varying angular velocity, or a rapid jump to a specified angular displacement. The upper element of the tool is connected to a sensitive torque transducer. The rotation of the lower element induces deformation in the fluid, which in turn causes a torque to be exerted on the upper element. This torque is used to calculate the shear stress, as outlined below for three common tool geometries. In the case of a stress-controlled rheometer, the lower element is rigidly fixed. A motor

applies a controlled torque to the upper tool, causing it to rotate, and the resulting angular displacement and angular velocity are measured.

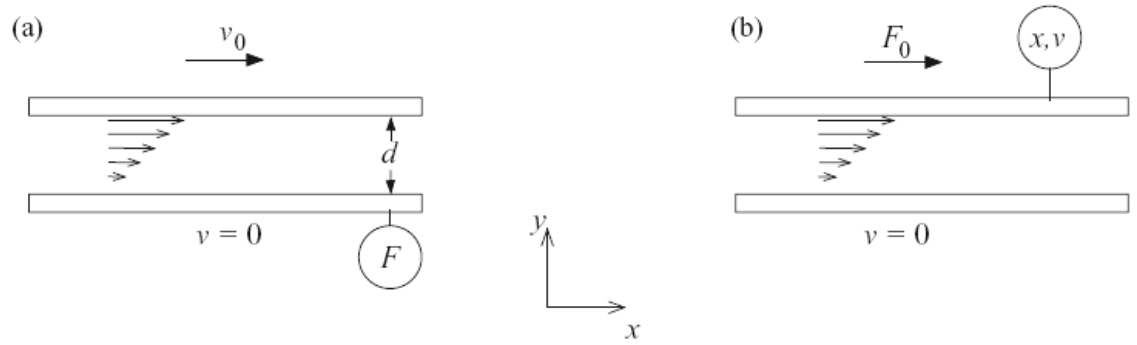

Figure 2.3 The distinction between strain- and stress-controlled deformation. (a) In a strain-controlled measurement, a fluid sample sandwiched between two plates is deformed by moving the upper plate at a controlled velocity v0, while the bottom plate is kept stationary. The force required to hold the lower plate fixed is measured by a transducer, indicated by the circle. (b) In a stress-controlled measurement, a controlled shear force is applied to the top plate, and the resulting velocity is measured.

Many rheometers can also measure the normal (upward or downward) force produced in response to the shear. Normal forces are a tensor phenomenon and will not be discussed in detail here, but they are significant in many complex fluids. The normal force or, more correctly, the normal stress difference, is the cause of the well-known rod-climbing (or Weissenberg) effect seen when a rotating rod is immersed in an elastic polymer solution [17]. The difference between stress and strain-controlled measurements is analogous to the difference between voltage and current-controlled measurements in electronics. In many cases, the same information can be obtained with either technique, a resistor has the same resistance no matter whether one measures it using a voltage supply or a current supply. On the other hand, the mode of measurement can make a difference for complex systems. The current–voltage curve for a tunnel diode, which has a negative differential resistance over a range of bias voltages, would look quite different in the two cases. It is thus important to be aware of the mode of operation and limitations of any instrument being used. There is really no “better” or “worse” mode, but some things are more easily measured in one mode than the other. For example, stress relaxation by definition involves measuring a time-dependent stress. This is most straightforwardly measured with a strain-controlled instrument, by applying and maintaining a known strain and measuring the stress. Creep measurements involve applying a fixed stress and measuring the time-

dependent strain, and consequently are most easily performed using a stress-controlled rheometer. Extending the analogy with the tunnel diode, stress and strain-controlled measurements will give very different results on materials for which the stress is a decreasing function of strain rate, such as clay suspensions under certain conditions [18, 19]; the negative slope of the stress–strain-rate curve signals the presence of a flow instability, which leads to shear localization. This said, however, many currently available rheometers can effectively perform both stress- and strain-controlled measurements by making use of fast computer control. For example, an instrument might actually function by applying a known torque to the tool, but its control system can continuously adjust the torque so that the net result is a constant strain rate. Given this, the distinction is perhaps not so much whether the instrument is stress- or strain-controlled, but whether the measurement transducer is on the part of the tool that is moved by the motor, or that which is fixed.

There are several high-quality rotational rheometers available commercially. Published specifications for high-end instruments quote minimum torques of a few times 10^{-9} Nm with a resolution of 10^{-11} Nm, minimum angular velocities on the order of 10^{-9} rad/s, and 10^{-8} rad resolution in angular position. As with any instrument, there is a trade-off between cost and performance, and less expensive instruments will have less impressive specifications. For the most accurate torque measurements, the body or frame of the rheometer should be very stiff, so that the torques applied to or generated by the sample act only on the rheometer tool and do not twist the instrument itself. High sensitivity and low frictional losses are extremely important for accurate measurements, particularly at low stresses or strain rates. Typically an air bearing or, in some commercial instruments, a magnetic thrust bearing, is used to reduce friction and inertial effects to a very low level. Other important features include the available range of applied shear rates or torques, the range of tool geometries, temperature control capabilities, and ease of use. Some rheometers have the capability for in-situ optical visualization of the sample while it is under shear, or even for small angle light scattering, which is useful for studies of structure under shear. All commercial instruments come with control software, which allows for several standard

preprogrammed measurement sequences and has some data analysis capability; rheological software packages that perform more detailed data analysis can also be purchased.

Measurements.

There are three primary types of measurements that one can perform with a rotational rheometer oscillatory shear, steady shear, and transient measurements. These are directly analogous to ac, dc, and transient electronic measurements. Small-amplitude oscillatory shear measurements are used primarily to determine the linear viscous and elastic moduli. When a material is subjected to a small sinusoidal strain – small enough that the material remains in the linear viscoelastic regime – the resulting stress oscillates sinusoidally at the same frequency, but in general with a phase shift ϕ with respect to the strain. Thus, if γ is given by

$$\gamma = \gamma_0 \sin \omega t \tag{2.12}$$

the resulting stress is

$$\sigma = \sigma_0 \sin (\omega t + \phi) \tag{2.13}$$

The stress in Equation (2.13) can be decomposed into a component in phase with the strain and another 90◦ out of phase:

$$\sigma = \sigma' + \sigma'' = \sigma'_0 \sin \omega t + \sigma_0'' \cos \omega t \tag{2.14}$$

The in-phase component is the elastic part of the response, with the elastic modulus defined as

$$G' = \frac{\sigma'_0}{\gamma_0} \tag{2.15}$$

while the out-of-phase component is the viscous part, with the viscous modulus given by

$$G'' = \frac{\sigma''_0}{\gamma_0} \tag{2.16}$$

Note that the viscous response is out of phase with the strain, but in phase with the strain rate $\dot{\gamma}$. It is common to define a complex modulus G^* as

$$G^* = G' + iG'' \tag{2.17}$$

G’ is a measure of the elastic energy stored per unit volume per cycle, while G’’ is a measure of the energy dissipated per unit volume per cycle [2]. Note that G’(ω) and G’’(ω) are not independent quantities, but satisfy the Kramers–Kronig relations [20].

For a Maxwell model with a single relaxation time ϕ, it is straightforward to show that G’ and G’’ depend on the frequency of oscillation as

$$G'(\omega) = G_0 \frac{\omega^2\varphi^2}{1+\omega^2\varphi^2} \qquad 2.18$$

and

$$G''(\omega) = G_0 \frac{\omega\varphi}{1+\omega^2\varphi^2} \qquad 2.19$$

Thus at low frequencies, G’ ∝ ω^2 and G’’ ∝ ω. This is in agreement with observations for linear polymer melts and micelle solutions [2]. More generally, the frequency dependence of the elastic and viscous moduli reflects the time dependence of the small-scale dynamics within the material. In steady shear experiments, shear is applied at a series of constant strain rates and, once the system has reached a steady state, the stress is measured at each rate. Such experiments are inherently nonlinear, since the strain increases steadily with time for the duration of the experiment. The material typically exhibits a transient stress response as its microscopic structure is driven from its equilibrium state, then settles to a constant stress once the microstructure has reorganized into a new non equilibrium configuration, which depends on the strain rate. The result of such a measurement is a plot of stress versus strain rate, commonly called a flow curve. Since the viscosity η = σ/$\dot{\gamma}$, η($\dot{\gamma}$) is also determined from steady shear experiments. Several different geometries can be used for the rheometer tool, which contains and deforms the sample being studied. Three commonly used tool geometries are illustrated in Figure 2.4. Figure 2.4(a) shows a cone-and-plate tool. One part of the tool, here the lower part, is a horizontal plane, while the other part is a truncated cone. The gap between the cone and plate is set such that the extrapolated tip of the cone would just touch the surface of the plate. The angle between the surface of the cone and the plate is small, typically a few degrees (that is, so that the small-angle approximation is valid). The sample fills the gap between the two parts of the tool, remaining confined by surface tension. A parallel-plate tool is shown in Figure 2.4(b). As the name implies, both parts of the tool are planar, and the sample again fills the gap between them. In this case, the separation between the two parts of the tool can be varied. The Couette geometry, shown in Figure 2.4(c), consists of an outer cup of radius R_o and a coaxial inner cylinder of radius R_i and length L. The sample fluid fills the annular gap between the two cylinders, as well as the volume below the end of the inner cylinder. The shape and depth of this lower volume should be designed to minimize its effects on the measurements.

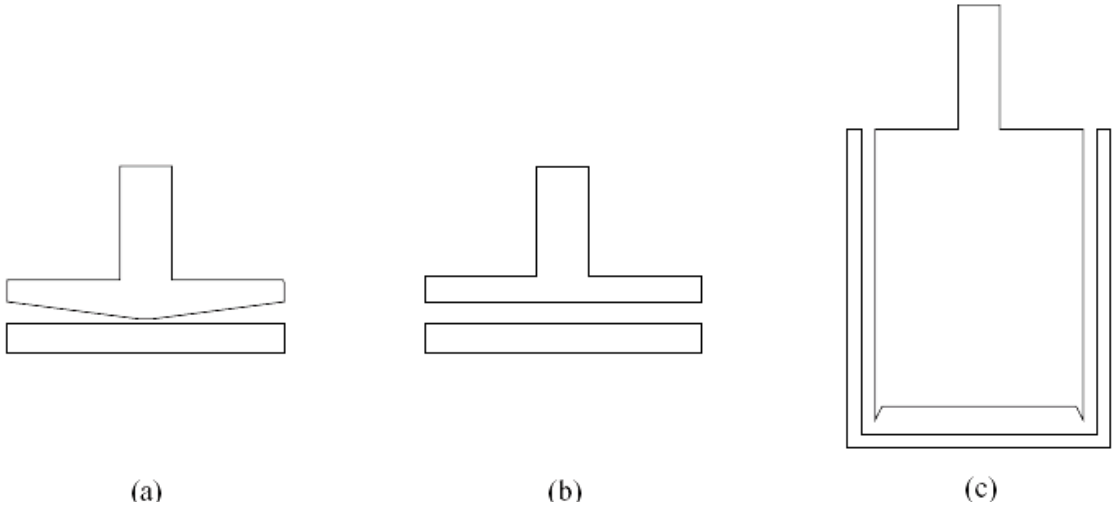

Figure 2.4 Three commonly used rheometer tool geometries. (a) Cone-and-plate; (b) parallel plates; (c) the Couette, or concentric cylinder, geometry. In all cases, one part of the tool is fixed and the other rotates about its axis.

In the parallel-plate geometry of Figure 2.4(b), the strain rate is simply given by

$$\dot{\gamma} = \frac{\Omega r}{h} \qquad 2.20$$

where h is the spacing between the plates and r the radial coordinate. While h can be varied, it should be small compared to the radius R of the plates and large compared to the scale of any structure in the material (for example, the size of any suspended particles). In this geometry, the deformation is not uniform: Equation (2.20) shows that the strain rate depends on r. The shear stress can be calculated in terms of the torque to be

$$\sigma = \frac{M}{2\pi R^3}\left(3 + \frac{d \ln M}{d \ln \dot{\gamma}_R}\right) \qquad 2.21$$

where $\dot{\gamma}_R$ is the strain rate the the edge of the plate [2]. Note that in principle the derivative in Equation (2.21) has to be measured to permit an accurate determination of the stress , while rheometer software typically calculates an effective stress based on an approximation to Equation (2.21) which assumes a particular value for d lnM/d ln $\dot{\gamma}_R$ [2]. One should, in general, be aware how the numbers produced by the software are actually determined! Despite this, parallel-plate tools are simple to use, and by making h small can be used for measurements at high strain rates. Measurements at

different values of h can also be used to check and correct for the presence of slip at the surfaces of the tool [21].

2.1.3 Former evaluation of bitumen rheology and current empirical tests.

The use of bitumen in paving applications has generated a lot of interests in its rheological properties, because of their importance in the manufacture and quality of bituminous pavements. But due to its highly viscous character at room temperature, giving rise to a confusing and somewhat imprecise description such as pasty or semi-solid, bitumen rheological behaviour remained hard to quantify. In the absence of simple test procedures, early evaluation of bitumen rheology for specification purposes was based on tactile observations or even chewing it. Dowrefined the penetrometre in 1903, using a set-up very similar to the current one [22] and nowadays, the penetration test (ASTMD5 – EN 1426) consists in measuring the depth (expressed in tenth of millimetres) at which a standard needle penetrates after 5 s loading time and with a 100 g load (Figure 2.5). Under these conditions, typical values for paving grade bitumen range between 15 and 200 1/10 mm.

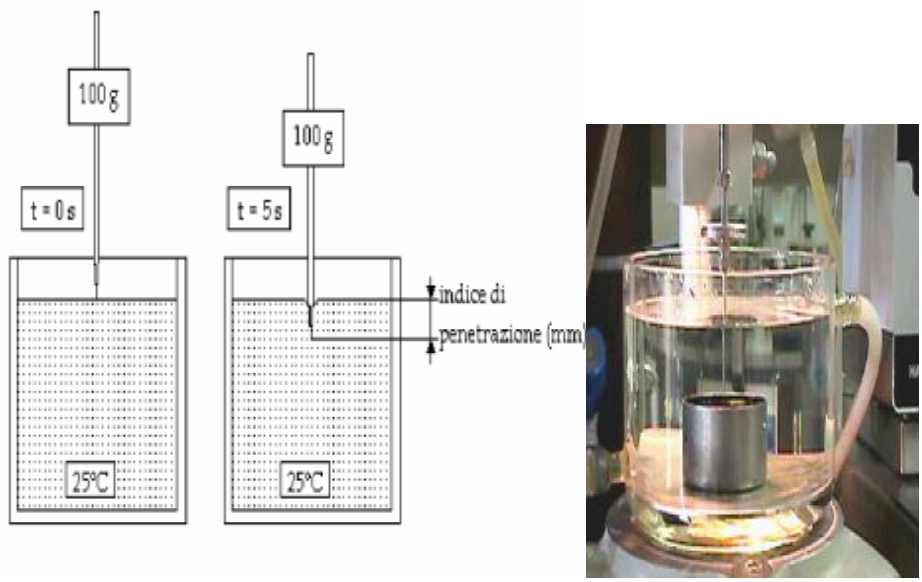

Figure 2.5. Penetration test

Figure 2.6 Penetrometer

For penetration less than 30 1/10 mm, the bitumen is generally said to be hard. On the contrary, penetration values higher than 100 1/10 mm correspond to soft bitumens. Penetration remains the basic test for paving grade specifications in Europe and European paving grades are labelled by their penetration grade. For example, a 70/100 penetration grade bitumen has a penetration value at 25 °C ranging from 70 to 100 in units 1/10 mm [23].

Softening point: ring and ball test.

Another consistency test that is still being used in the European specifications is the Ring & Ball softening temperature (TR&B). It was already proposed as a standard for ASTM in 1915 [186]. The experimental set-up for the current procedure (ASTM D36 – EN 1427) consists in preparing a 8-mm thick bitumen film inside a metal ring (average diameter close to 16 mm). The bitumen film is put inside a water bath at an initial temperature of 5 °C and a normalized 3.5 g steel-ball (9.5 mm diameter) is placed onto the bitumen. The temperature is then increased at a rate of 5 °C/min. The softening temperature is defined as the temperature at which the steel ball deforms the bitumen film to such an extent that it contacts the bottom of the vessel 25 mm below. Under these conditions, typical values for paving grade bitumen range between 35 and 65 °C.

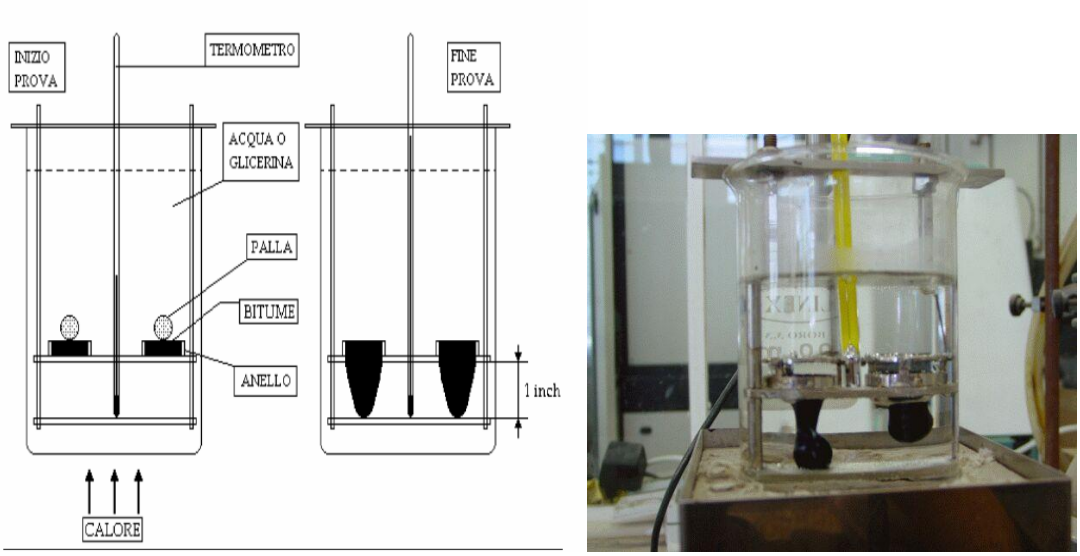

Figure 2.7 Ring and Ball test

Breaking point, FRAAS test.

The low temperature performance are associated with the loss of the elastic properties of the bitumen that then can cause phenomena of fragility. The fragility of a bitumen , it can be determined the lowest temperature at which it tolerates a given mechanical stress . It is , therefore , reference to the Fraass breaking point , that conventionally measure the temperature (TFraass) on which a film of bitumen, subjected to flexion, presents the first rupture phenomenon . Hence this test indicates the temperature to which a binder cooled gradually reaches a certain degree of fragility. The binder put on a plate is melted so that it can spread regularly , after it is left to cool at room temperature for at least one hour and subsequently the plate is inserted in the instrument where it is cooled using dry ice , lowering the temperature of 1 ° C per minute. Every 60 seconds, flexing the plate and record the temperature of the binder (Fig.2.8) . The measuring apparatus includes an air chamber , a cavity with acetone where the dry ice will be introduced and finally a chamber where equipment and the plate to be analyzed are inserted (Fig.2.8).

Figure 2.8 TFRAASS test

2.2 Nuclear Magnetic Resonance.

2.2.1 Basic Concepts

It is well known from elementary NMR theory [24] that a nucleus of spin I has 2I+1 energy levels, equally spaced with a separation

$$\Delta E = \mu H_0 / I, \tag{2.22}$$

where H_o is the applied magnetic field, and μ, the nuclear magnetic moment, is given by

$$\mu = \gamma h I / 2\pi. \tag{2.23}$$

Here *γ* is the magnetogyric ratio, a constant for a given nucleus, and *h* is Planck's constant. From the usual Bohr relation, the frequency of radiation that induces a transition between adjacent levels is

$$\nu_0 = \Delta E / h = \gamma H_0 / 2\pi \tag{2.24}$$

At equilibrium, nuclei are distributed among the energy levels according to a Boltzmann distribution. Following any process that disrupts this distribution (e.g., moving the sample into or out of the magnetic field, or absorption of rf energy), the nuclear spin system returns to equilibrium with its surroundings (the "lattice") by a first-order relaxation process characterized by a time T1 , the spin-lattice relaxation

time. To account for processes that cause the nuclear spins to come to equilibrium with each other, a second time T_2, the spin-spin relaxation time, is defined so that

$$\nu_{1/2} \approx 1/T_2 \qquad 2.25$$

with $\nu_{1/2}$ being a spectrum line of full width at half maximum intensity. If the magnetic field is not perfectly homogeneous, nuclei in different parts of the sample experience slightly different values of the field, hence by equation 2.24 resonate at slightly different frequencies. This leads to a contribution to the line width due to inhomogeneity (ΔH_o) of

$$\nu_{1/2}\ (\text{inhom}) = \gamma\ \Delta H_0/2\pi. \qquad 2.26$$

So we can define a time T_2* in terms of the observed line width as

$$\nu_{1/2}\ (\text{obsd}) = 1/\pi T_2^* \qquad 2.27$$

Thus T_2*includes contributions from both natural line width and magnetic field inhomogeneity :

$$1/T_2^* = 1/T_2 + (\gamma\ \Delta H_0/2) \qquad 2.28$$

It is easily shown by classical mechanics that the torque exerted on a magnetic moment by a magnetic field inclined at any angle θ relative to the moment (Figure 2.9) causes the nuclear magnetic moment to precess about the direction of the field with a frequency given by the well-known Larmor equation

$$\nu_0 = -\gamma \mathbf{H}_0/2\pi \qquad 2.29$$

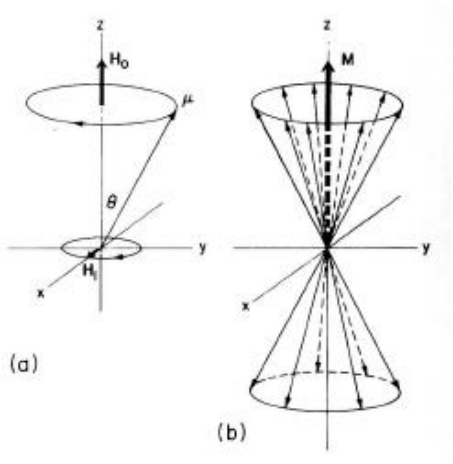

Figure 2.9 (a) Precession of a magnetic moment μ about a fixed magnetic field H_0 . The radio frequency field H1 rotates in the xy plane. (b) Precession of an ensemble of identical magnetic moments of nuclei with I = 1/2, The net macroscopic magnetization is oriented along H_0 (the z axis) and has the equilibrium value M_0 .

Free Induction Decay (FID).

Suppose a 90° pulse is applied along the x' axis in the frame rotating at the radiofrequency (rf). Following the pulse, M lies entirely along the y' axis, as indicated in Figure 2.10 a. Since the apparatus is normally arranged to detect signals induced in a coil along the fixed x or y axis , the magnitude of Mxy determines the strength of the observed signal (called a free induction signal, since the nuclei precess "freely" without applied rf). As transverse relaxation occurs, the signal decays. In a perfectly homogeneous field the time constant of the decay would be T_2 ; but, in fact, the free induction signal decays in a time T_2* that often is determined primarily by field inhomogeneity, since nuclei in different parts of the field precess at slightly different frequencies, hence quickly get out of phase with each other. Thus the signal decays with a characteristic time T_2* as defined in equation 2.28.

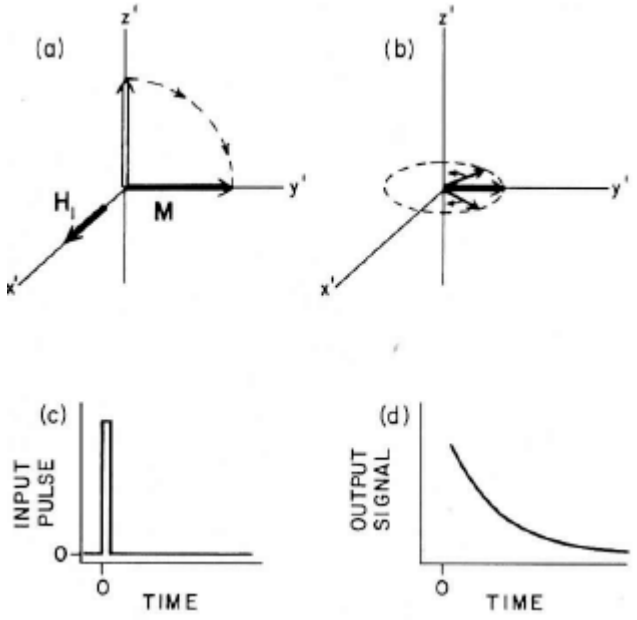

Figure 2.10. (a) A 90° pulse alongt z' rotates M from the equilibrium position to the y' axis. (b) M decreases as magentic moments dephase. (c) Input signal, at 90° pulse, corresponding to (a). (d) Exponential free induction decay, corresponding to {b).

2.2.2 Spin-Spin Relaxation time measurement: Spin Echo Sequences.

Unless $T_2 \ll (2/\gamma\,\Delta H_0)$;ee equation 2.28), the contribution of inhomogeneity in H_0 to the free induction decay precludes the use of this decay time, T_2* as a measure of T_2 . An ingenious method for overcoming the inhomogeneity problem was first, proposed by Hahn[25] who called it the spin-echo method. The method consists of the application of a 90°, τ, 18O° sequence and the observation at. a time 2 τ of a free induction "echo." The rationale of the method is shown in Figure 2.11, which depicts the behavior of the magnetization in the rotating frame.

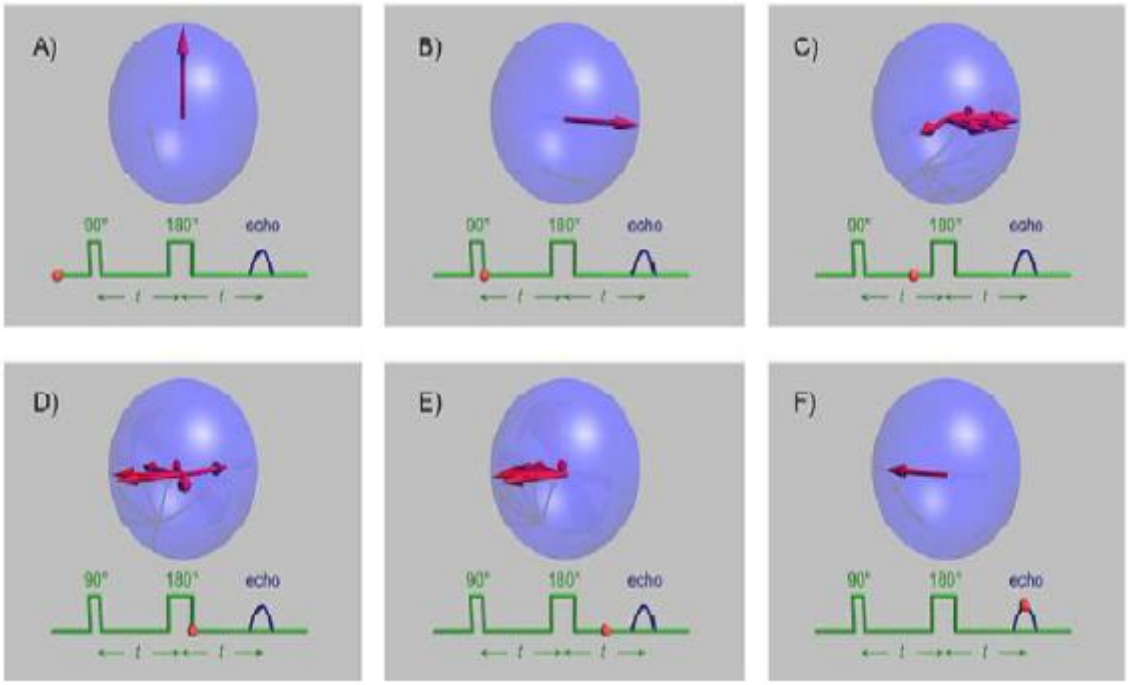

Figure 2.11. Behaviour of Magnetizazion during Hanh Pulse sequence.

In (b) M is shown being tipped through 90° by application of H_1 along the positive x' axis. The total magnetization M can be thought of as the vector sum of individual macroscopic magnetizations me arising from nuclei in different parts of the sample and hence experiencing slightly different values of the applied field, which is never perfectly homogeneous. There is thus a range of precession frequencies centered about ν_0 , which we have taken as the rotation frequency of the rotating frame. In (c) then, the m_i begin to fan out, as some nuclei precess faster and some slower than the frame. At a time τ after the 90° pulse, a 180° pulse is applied, also along the positive x' axis, as shown in(d). The effect of this pulse is to rotate each me by 180° about the x'

axis. Thus those m_i that are moving faster than the frame moving toward the observer or clockwise looking down the z' axis naturally continue to move faster, but in (e) their motion is now away from the observer. At time 2 all m_i come into phase along the negative y' axis, as shown in (f). Then the phase coherence is lost again. The rephasing of the m_i causes a free induction signal to build to a maximum at 2 τ but the signal is, of course, negative relative to the initial free induction decay since rephasing of the m_i occurs along the negative y' axis. If transverse relaxation did not occur, the echo amplitude might be just as large as the initial value of the free induction following the 90° pulse. However, each m_i decreases in magnitude during the time 2 τ because of the natural processes responsible for transverse relaxation in the time T_2. Thus the echo amplitude depends on T_2 , and this quantity may in principle be determined from a plot of peak echo amplitude as a function of τ. It is necessary to carry out separate pulse sequences at different τ and wait between pulse sequences an adequate time, at least $5T_1$.

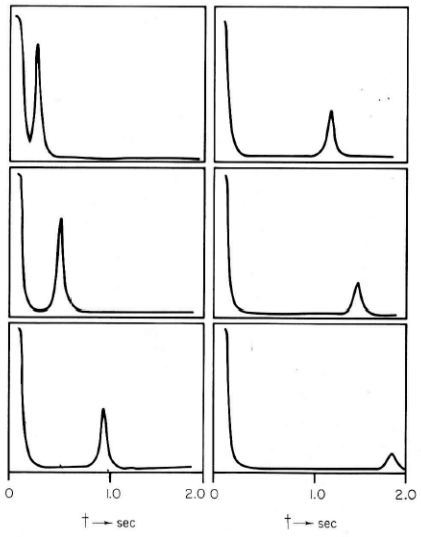

Figure 2.12. Typical Hahn experiment.

Carr and Purcell [26] showed that a simple modification of Hahn's spin-echo method reduces drastically the effect of diffusion on the determination of T_2 . This method may be described as a 90°, τ, 180°, 2 τ, 180°, 2 τ , 180°, 2 τ,…… sequence (or, more commonly, a Carr—Purcell sequence). As in the spin-echo method described previously, all pulses are applied along the positive x' axis. The result is the same as that shown in Figure 2.11 except that following the dephasing of the m_i another 180° pulse at time 3 τ after the initial 90°pulse causes a rephasing of the m_i along the

positive y’ axis at time 4 τ. Subsequent 180° pulses at 5 τ, 7 τ -, etc. cause echoes at 6 τ, 8 τ , etc., alternately positive and negative, as shown in Figure 2.13 (a).

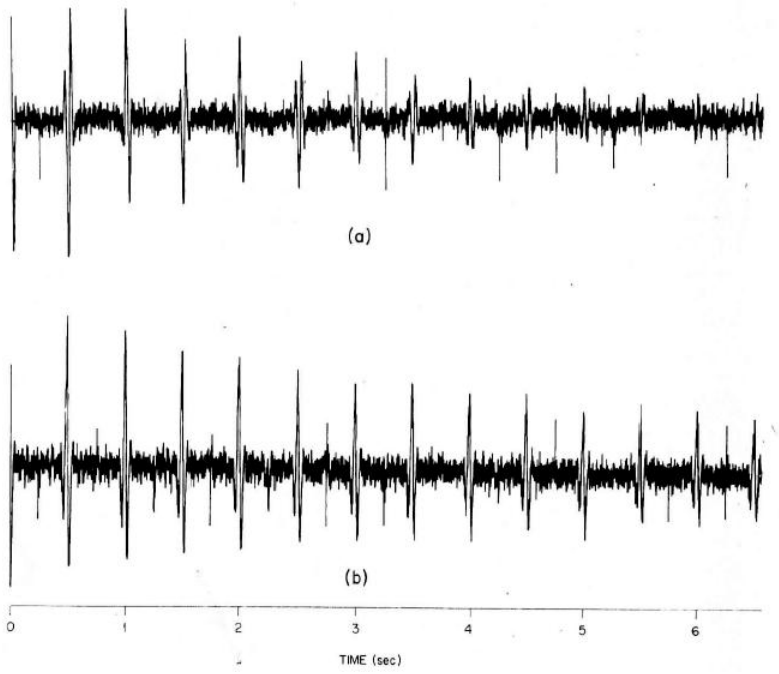

Figure2.13. (a) Carr-Purcell experiment. (b) Meiboom-Gill method.

Another method, which is often easier experimentally, was proposed by Meiboom and Gill [27].This method uses the same pulse sequence as the Carr-Purcell technique, but the 180° pulses are applied along the positive y' axis, i.e., at 90° phase difference relative to the initial 90° pulse. Hence, for pulses that are exactly 180° the m_i are rotated about the y' axis, and for all echoes focus along the positive y' axis, so that only positive echo signals are obtained, Figure 2.13 (b).

2.2.3 Inverse Laplace Transform of the echo decay.

In the previous paragraph it has been mentioned that the T_2 time can be obtained by plotting the peak echo amplitude as a function of τ. The envelope of the echo amplitudes give rise to an exponential decay of the signal. If the Carr-Purcell envelope has a mono-exponential decay, the relaxation time T_2 of the sample can be obtained by fitting the n data to the following equation:

$$A_n = A_0 e^{-2n\tau/T_2} \qquad 2.30$$

The Laplace transform is a powerful tool for solving ordinary and partial differential equations, linear difference equations and linear convolution equations. The Laplace transform F(s) of a function f (t) is defined by [28–30]

$$F(s) = \int_0^\infty f(t)\mathrm{e}^{-st}\mathrm{d}t \qquad 2.31$$

In the equation 2.30 A_n is the amplitude of the n^{th} echo in the echo train and A_0 is a constant depending on the sample magnetization, filling factor, and other experimental parameters. Usually the T_2 relaxation time varies all over the sample because of the sample heterogeneity or surface relaxation differences; then a multiexponential attenuation of the CP envelope should be observed. Hence, if inside the sample a continuous distribution of relaxation times exists, the amplitude of the n^{th} echo in the echo train is given by

$$A_n = A_0 \int_0^\infty P(T_2)\mathrm{e}^{-2n\tau/T_2}\,\mathrm{d}T_2 \qquad 2.32$$

In 2.32, $P(T_2)$ is the Inverse Laplace transform (ILT) of the unknown function that fit the plot of the echo amplitudes. Hence $P(T_2)$ can be understood as a distribution of rate constants, strictly, a probability density function, PDF. The ILT can give the answers required where it needs to face the inverse problem of estimating the desired function from noisy experiments. As an integration, the Laplace transform (eq. 2.31) is a highly stable operation, in the sense that small fluctuations (or errors) in f(t) are averaged out in the determination of the area under a curve. Furthermore, the exponential factor, e^{-st}, means that the behaviour of f(t) at large t is in practice unimportant, unless *s* is very small. As a result of these two aspects, a large change in f(t) at large t indicates a small (perhaps insignificant) change in F(s). On the contrary, the inverse transformation from F(s) to f(t) is a highly unstable process: a tiny change in F (s) may result in an uncontrolled variation of f(t) and all significant trends may disappear [31].
This kind of problems are known as ill-posed problems which means that errors in an unregularized inversion are unbounded. The problem was well faced by Provencher [32,33], who wrote down a computer program that uses numerical stable algorithms which are able to find regularized solution. In the present work a little adjustment of

this computational program has been made (unpublished data) on the basis of the Tikhonov regularization [34].

2.3 Atomic Force Microscopy (AFM).

The AFM, introduced in 1986 [35] , provides insight into the surface topography (nm resolution) and mechanical properties of bitumen. During AFM measurements, the specimen is scanned by a silica cantilever with a small tip placed near its free end (Figure 2.14). The deflection of the cantilever, *ws*, describing the interaction between the AFM tip and the sample surface, is monitored by an optical lever method. Based on the deflection *ws* and the stiffness *k* of the cantilever, the force acting at the tip is obtained as

$$F = k\, ws \qquad 2.33$$

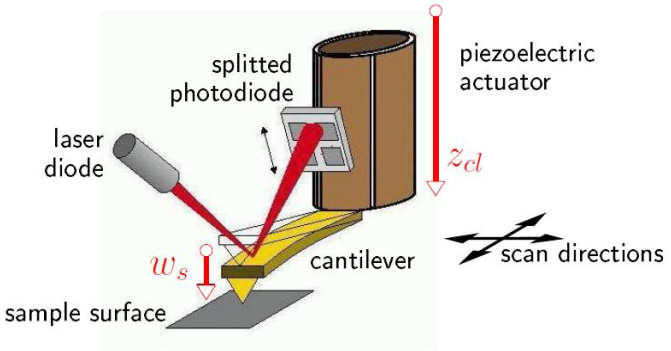

Figure 2.14 . AFM measurement

Non-contact mode (NCM)

During AFM measurements employing the NCM, the oscillation of the AFM cantilever, described by the amplitude corresponding to free oscillation A_0, is reduced by attraction/repulsive forces when approaching the bitumen surface. By enforcing a constant reduction of the amplitude, with e.g. $A_{sp}/A_0 = 0.5$, where A_{sp} represents the amplitude of the near-surface oscillation, an image of the surface topography is obtained.

Pulsed-force mode (PFM)

In contrast to the NCM, the tip located at the end of the cantilever is penetrating the specimen surface during PFM measurements, providing insight into mechanical properties of bitumen. By reducing the frequency f, the deflection of the cantilever, $_{ws}$ [nm], is recorded. Based on the deflection history, two output quantities are provided by the AFM.

Tapping Mode

Tapping mode has been used to explore the bitumen morphology for the present thesis. In tapping-mode AFM [36,37]an oscillating probe makes intermittent contact with a sample, and the associated change in the amplitude of oscillation is used for the feedback control. Tapping-mode AFM has been applied to a broad range of materials to examine surface topography, and its applicability to studying other surface properties such as stiffness, viscoelasticity and adhesion are being investigated [38-41]. When the tip and sample come into contact, the amplitude, resonance frequency and phase angle of the oscillating probe are affected by tip sample interactions. The minimization of these interactions is necessary to acquire accurate information about the surface topography, whereas images obtained at various applied forces can provide invaluable information about local variations of stiffness and adhesion [39-41]. An example of AFM micrography taken in tapping mode is given in Figure 2.15.

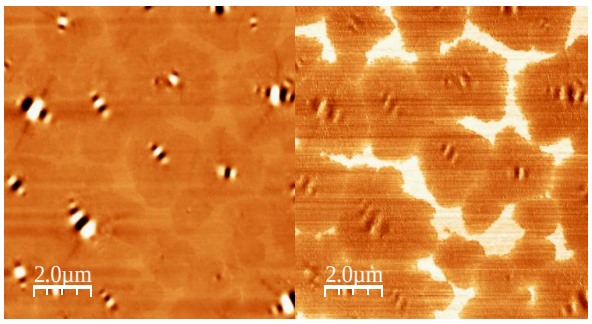

Figure 2.15. AFM of a bitumen sample. (left) topography. (right) phase contrast.

In early atomic force microscopy (AFM) work on bitumen, the bee-like structure, called catana phase, was attributed to asphaltene. The bee structure does not have a defined pattern but usually it can be visualized by AFM as composed of a series of aligned protrusions and depressions. They can be either isolated or in star shape. However more recent studies attributed to the presence of wax a substantial contribution to the bee-like structures [42].

REFERENCES.

[1] R. G. Larson, The Structure and Rheology of Complex Fluids (Oxford University Press, New York, 1999).

[2] C. W. Macosko, Rheology: Principles, Measurments, and Applications (Wiley-VCH, New York, 1994).

[3] F. A. Morrison, Understanding Rheology (Oxford University Press, New York, 2001).

[4] R. W. Whorlow, Rheological Techniques (Ellis Horwood, New York, 1992).

[5] F. C. MacKintosh and C. F. Schmidt, "Microrheology," Curr. Opin. Coll. Interf. Sci. 4, 300 (1999).

[6] M. L. Gardel, M. T. Valentine, and D. A.Weitz, "Microrheology," in K. Breuer (ed.), Microscale Diagnostic Techniques (Springer, New York, 2005).

[7] T. A. Waigh, "Microrheology of complex fluids," Rep. Prog. Phys. 68, 685 (2005).

[8] N. Willenbacher and C. Oelschlaeger, "Dynamics and structure of complex fluids from high frequency mechanical and optical rheometry," Curr. Opin. Colloid Interface Sci. 12, 43 (2007).

[9] C. Pipe and G. H. McKinley, "Microfluidic rheometry," Mech. Res. Comm. 36, 110 (2009).

[10] T. G. Mason and D. A. Weitz, "Optical measurements of frequency-dependent linear viscoelastic moduli of complex fluids," Phys. Rev. Lett. 74, 1250 (1995).

[11] M. T. Valentine, P. D. Kaplan, D. Thota, J. C. Crocker, T. Gisler, R. K. Prud'homme, M. Beck, and D. A. Weitz, "Investigating the microenvironments of inhomogeneous soft materials with multiple particle tracking," Phys. Rev. E 64, 061506 (2001).

[12] R. Bird, R. Armstrong, and O. Hassager, Dynamics of Polymeric Liquids, Volume 1: Fluid Mechanics (Wiley, New York, 1987).

[13] F. K. Oppong, P. Coussot, and J. R. de Bruyn, "Gelation on the microscopic scale," Phys. Rev. E 78, 021405 (2008).

[14] M. Wilhelm, "Fourier transform rheology," Macromol. Mater. Eng. 287, 83 (2002).

[15] R. H. Ewoldt, A. E. Hosoi, and G. H. McKinley, "New measures for characterizing nonlinear viscoelasticity in large amplitude oscillatory shear," J. Rheol. 52, 1427 (2008).

[16] J. C. Maxwell, "On the dynamical theory of gases," Phil. Trans. 157, 49 (1867).

[17] D. V. Boger and K. Walters, Rheological Phenomena in Focus (Elsevier, Amsterdam, 1993).
[18] P. Coussot, A. I. Leonov, and J.-M. Piau, “Rheology of concentrated dispersed systems in a low molecular weight matrix,” J. Non-Newtonian Fuid Mech. 46, 179 (1993).
[19] F. Pignon, A. Magnin, and J.-M. Piau, “Thixotropic colloidal suspensions and flow curves with minimum: identification of flow regimes and rheometric consequences,” J. Rheol. 40, 573 (1996).
[20] P. M. Chaikin and T. C. Lubensky, Principles of Condensed Matter Physics (Cambridge University Press, Cambridge, 1995).
[21] A. Yoshimura and R. K. Prud’homme, “Wall slip corrections for Couette and parallel disk viscometers,” J. Rheol. 32, 53 (1988).
[22] Halstead WJ,Welborn JY. History of the development of asphalt testing apparatus and asphalt specifications. Proc Assoc Asphalt Paving Techn ;43A:89–120 (1974).
[23] Read J, Whiteoak D. The Shell Bitumen Handbook. 5th Ed. London: Thomas Telford Publishing, (2003).
[24] Levitt MSpin dynamics : basics of nuclear magnetic resonance. 2nd Ed. N.York Wiley ed.(2008).
[25] Hahn, E.L. "Spin echoes". Physical Review 80: 580–594 (1950).
[26] Carr, H. Y.; Purcell, E. M., "Effects of Diffusion on Free Precession in Nuclear Magnetic Resonance Experiments". Physical Review 94: 630–638 (1954).
[27] S. Meiboom and D. Gill, “ Modified Spin-Echo Method for Measuring Nuclear Relaxation” Times Rev. Sci. Instrum. 29, 688 (1958).
[28] D.V. Widder, Advanced Calculus, 2nd ed. Prentice-Hall, Englewood Cliffs, (1947).
[29] R.E. Bellman and R.S. Roth, The Laplace Transform World Scientific, Singapore, (1984).
[30] D.A. McQuarrie, Mathematical Methods for Scientists and Engineers, University Science Books, Sausalito, (2003).
[31] R. Bellman, R.E. Kalaba. and JA. Lockett, Numerical Inversion of the Laplace Transform: Agglications to Biology, Economics. Engineering and Physics, Elsevier, New York, (1966).
[32] S.W. Provencher: A constrained regularization method for inverting data represented by linear algebraic or integral equations. Comput. Phys. Commun. 27, 213 (1982).
[33] S.W. Provencher: CONTIN: A general purpose constrained regularization program for inverting noisy linear algebraic and integral equations. Comput. Phys. Commun. 27, 229 (1982).

[34] Tikhonov, A. N.; Arsenin, V. Y. Solutions of Ill-Posed Problems; John Wiley & Sons: New York, (1977).

[35] Binnig, G., Quate, C., and Gerber, C. Atomic force microscope. Physical Review Letters, 56(9):930–933 (1986).

[36] Q. Zhong, D. Innis, K. Kjoller, V.B. Elings, Surf. Sci. Lett. 290 (1993).

[37] V. Elings, J. Gurley, U.S. Patents 5 412 980 and 5 519 212.

[38] P.K. Hansma, J.P. Cleveland, M. Radmacher, D.A. Walters, P. Hillner et al., Appl. Phys. Lett. 64, 1738 (1994) .

[39] A. Wawkuschewski, K. Crgmer, H.-J. Cantow, S.N. Magonov, Ultramicroscopy 58, 185 (1995).

[40] S.N. Magonov, V. Elings, M.-H. Whangbo, Surf. Sci. Lett. 375, L385 (1977) .

[41] M.-H. Whangbo, S.N. Magonov, H. Bengel, Probe Microsc. 1,23 (1997).

[42] Benjamin McCarron “The Investigation of ‘Bee-Structures’ in Asphalt Binders” Major Qualifying Project 2011-2012, Dept. of Physics, Worcester Polytechnic Institute, (2012).

3. Additives for Bitumen Recycling and bitumen modifiers.

3.1 Introduction.

The deterioration of road surfaces flexible , due to phenomena of cracking at fatigue or rutting , has become the object of study and investigation . Often such events are accelerated by water , which , in the absence of impermeable layers , reaches the lower layers of the superstructure going to affect the cohesive properties of the binder and adhesion between the bitumen and aggregates . Moreover, these problems ranging in damage to the road infrastructure , also causing environmental problems related to landslides , etc. . For these and other reasons, over the past few years, the recycling is a viable alternative to the disbursement of large sums of money for the maintenance and in some cases, the reconstruction of road networks , as well as the disposal of materials removed. The recycling of road surfaces as a measure of recovery is a concept relatively new , except for a series of technical documents on specific arguments in the recycling. Over the past few decades it has had a remarkable development infrastructure: transport road increased, particularly in the relative volume of heavy vehicles, which move the goods at faster speed and flexibility than a railway transport, the same type of vehicles has changed, and the load per axle of a truck, is enhanced. Hence the deterioration already present on our roads is increasing, making inevitable an increase of maintenance . These considerations are valid not only for Italy but also for the majority of European countries , which will devote a future budget every year higher for road maintenance : If , for lack of funds , the maintenance has not been intervened , with consequent and irreversible deterioration of the road network , you may need a total makeover the same pavements , with significantly higher costs . However, with the economic crisis that we are facing at this time , it is necessary increase the productivity of the reduced budget available by individual countries. We have also to consider the fact that this type of intervention involves considerable consumption of valuable and non-renewable resources , such as stone aggregates and bitumen, and which are simultaneously produced large quantities of waste materials , with both economic costs of disposal , and environmental pollution . Hence it is even more necessary to find a alternative solution to the problem [1]. This solution comes, with recycling. In the field of road pavement the term "recycle" means

any chance to recover and reuse the material crushed, for the production of a new asphalt.

3.2 Recycling.

In Italy, recycling of road pavements began in the '70s, thanks to the milling of the surface layers , and in conjunction with the oil crisis at that time. The first technique used was that of the hot- milling , obtained by a heating and a subsequent demolition of 5 or 6 cm of the pavement surface , with the use of special combs (Foschi , 2000) .

The success was immediate : considering the fact that many safety barriers had already been installed , the milling of the pavement did not result in an increase of their ground level . However, the presence of large gas containers on the road, for the hot-milling , and the low thickness of the road milling , have encouraged researchers to turn their studies towards technologies that are less dangerous and more productive[3].

In 1983 , in fact, the Rome- Civitavecchia began the first work of recycling in situ with mobile systems very similar to those permanent , with a productivity of 120 tons/ hour, which reached a depth of more than 10 cm with the use of cold milling machines , and they could recycle up to 80% of material , to be integrated with a 20 % of virgin aggregate , to adjust their mean size. the first recycling train in Italy was developed by the Pavimental, road construction company established in 1982 for the maintenance of the motorway network, along with the company Marini. The first permanent installation of recycling, however, was made at the beginning of the 80s, which allowed the creation of an important maintenance of the entire track number one of the Fiumicino Airport: In this type of system, the recycled material, obtained from the milling of bituminous pavements, was brought into the stationary implant and recycled, at an amount of around 40-50%. In 1983 the first steps were made to recover granular materials with a 100% reuse of the material milling (IRI-Highway stretch Magliano Sabina-Fiano) [2]. In 1989, Italy began the first attempts to recycling bituminous pavements, totally cold, both for milling and for the production, with bituminous emulsions, using a suitable recycling technology, at a production rate of 250 tons / hour. The only fault of the technology, was represented by long waiting

times for the re-opening to traffic, even 3-4 days, at which reasonably followed by new studies and experiments in the field. Expand this market and direct from point of view of environmental protection, primarily involves:

- design new road surfaces with the criterion for reuse across the resulting material, in all future maintenance cycles;
- make the utmost use of techniques that aim at the recovery of 100% of the material;
- adopt technologies that preserve as far as possible to the environment, and under all aspects.

Regarding the latter point, there is greater attention to those who are recycling processes in situ, with the aim to minimize not only the cost, but also environmental pollution and energy consumption, which would result from the continuous transport between construction and fixed installation.

3.2.1 Recycling methods.

As previously said, the recycling solutions can be divided into two categories namely recycling in fixed installation and recycling in situ. In the case of fixed installation recycling the material milled from the floor must be transported from the place of recovery then to be inserted into the production cycle and then reused. The main advantages of in-plant recycling are the high-quality technique of the recycling process , crushing, the sieve and the mixture of aggregates turn out to be the best , it also has the possibility to perform further laboratory analysis , and therefore quality checks , on the milled material and the final product . The final product results to be more homogeneous and it has the possibility of a temporary storage and a greater flexibility in the production of different blends. At the same time it is worth mentioning the shortcomings of in-plant recycling:

higher transportation costs , therefore it has higher costs of storage and material handling in the plant; mixtures that are formed in the plant , despite the homogeneity of the mixture , can not exceed percentage of reuse of RAP (Reclaimed Asphalt Pavement) of 50-60% .

In the on-site recycling , the costs of transport and management of the milled material are reduced, and the impact on traffic in the vicinity of the site is minimal and occasional, it can get to recycle 100 % of the RAP . These are the main advantages that make the recycling on-site one of the more attractive alternative policy. Both the recycling stationary plant and on-site , in turn, can be divided into two distinct subcategories for the temperature at which the RAP is worked

- hot recycling
- cold recycling

At these two types , a third process for bituminous mixtures has to be mentioned namely warm recycling , preferred to cold processes , but currently available only in fixed installations.

3.2.2 Cold recycling.

Although it is possible to cold recycle in the fixed plant, it would be better to recycle on-site to enhance as much as possible the advantages that this technology offers, because it offers significant environmental advantages: it has in fact the recovery of almost 100% of the material of the existing pavement, and an overall reduction of energy consumption thanks economy of transport operations. The material to be recycled is made of mineral aggregate covered with a thin film of bitumen. It is obtained from the grinding to blocks (scarification) or cold milling of asphalt concrete layers present in the road pavements. The process of cold milling (that is ambient temperature) is performed through a milling drum, which pulverizes the former pavement by striking vehemently the course that has to be removed. This process involves a variation in the grading distribution of the granulated material, compared with the mineral aggregates making the original mixture. The cold recycling process is characterized by the use of bituminous binders in a liquid state at ambient temperature, which provide an effective and durable binding action shortly after the application. Bituminous emulsions, bitumen dispersion in water with the addition of surfactants, were studied and improved in order to stabilize the cold recycled asphalt concrete. The asphalt is spread disguised as minute spherules, ranging from 1 to 3 μm, in a percentage varying from 50% to 69% according to the peculiar kind of emulsion

and the required viscosity. In order to avoid that the droplets of bitumen flocculate and a coalescence phenomenon occurs, their surface must be covered with an emulsifier. This emulsifier by settling at the interface bitumen-water, provides the droplets with an electrical charge with the same sign, keeping them spread. Different emulsions with exceptional performances were developed over the years, particularly by using modified bitumens or by adding polymers to the emulsions obtained with natural bitumens. The properties of RAP are almost completely supplied by the kind of material forming the old pavement. Also the means through which the RAP is milled, the rotation speed of the milling drum and the forward speed of the recycler influence its quality, determining the final grading distribution. In general the RAP shows, in comparison with the virgin mineral aggregate, a slight lower specific gravity. The bitumen covering the aggregates is moreover particularly friable, subjected to raveling and lacking in binding power because of its ageing due to oxidation processes and to the effect of ultraviolet ray.

3.2.3 Hot Recycling.

Hot mix recycling is the process in which reclaimed asphalt pavement materials are combined with new materials, sometimes along with a recycling agent, to produce hot mix asphalt mixtures. Just as in the case of conventional HMA, recycled mixtures must be designed properly to ensure proper performance. When properly designed, recycled mixtures can have properties similar to those of new conventional hot mix asphalt mixtures. There are four components in hot mix recycling: the reclaimed asphalt pavement (RAP), the virgin aggregate, the virgin asphalt binder and in some cases, a recycling agent [4]. The two steps in the mix design procedure are material evaluation and mix design. The objective of the material evaluation process is to determine the important properties of the component materials to come up with an optimum blend of materials to meet the mix requirements. The objective of the mix design step is to determine the type and percentage of asphalt binder with the help of results from compacted test mixes. The specific steps of the material evaluation and mix design process are as follows [5].

1. Obtain representative field samples of the reclaimed material.

2. Perform laboratory analysis:

1) determine composition and properties of the RAP

2) determine the proper amounts of virgin aggregates to be added

3) select the type and amount of the virgin asphalt binder

4) mix, compact and test trial mixes.

3. Select the optimum combination of mix components that meet the mix design criteria.

The RAP material needs to be evaluated before the actual mix design. This is because with aging and oxidation certain significant changes occur in the HMA (Hot Mix Asphalt, the former concrete product). For the binder, this includes loss of the lighter fractions and a corresponding increase in the proportions of the asphaltenes, hardening (increase in viscosity), and loss of ductility. The gradation of the aggregate may change due to degradation caused by traffic loads and the environment. Hence the composition of the RAP must be determined at the beginning. Most agencies determine aggregate gradation, asphalt content, and asphalt viscosity at 60°C for the reclaimed asphalt pavement. The aged asphalt binder must be extracted from a representative sample of the RAP to determine these properties. The following guidelines are suggested for aggregate and binder evaluation[6]. There are four basic purposes for using recycling agents [7]. These are: (1) to restore the aged asphalt binder characteristics to a consistency level appropriate for construction purposes and end use of the mix; (2) restore the recycled HMA mix to its optimum characteristics for durability; (3) provide sufficient additional binder to coat any virgin aggregate added to the recycled mix; and
(4) provide sufficient additional binder to satisfy mix design requirements. Recycling agents have been defined as organic materials with chemical and physical characteristics selected to restore aged asphalt to desired specifications.

In selecting the recycling agent, the viscosity characteristics of the combined aged asphalt binder and the recycling agent are the determining factors. These agents are also known as softening agents, reclaiming agents, modifiers, fluxing oils, extender oils, and aromatic oils [7]. A recycling agent it is defined as a hydrocarbon product with physical characteristics selected to restore aged asphalt binder to requirements of current asphalt binder specifications. Under this definition, softer asphalt and specialty products can be classified as recycling agents. Asphalt cements can be used when an increase in total binder content of the recycled mix is required and the specific grade can be blended with the aged asphalt binder in the RAP to yield an asphalt binder meeting the desired specifications. In general in hot mix recycling, soft grades bitumen binder are used and this is more prevalent in the U.S. compared to the use of

commercial recycling agents. If the aged asphalt binder has a very high viscosity (or low penetration) or the percentage of RAP in the recycled HMA is much greater than 50 percent, a relatively small amount of a commercial recycling agent can be used to modify the aged asphalt binder without altering the desired binder content. Then, if additional binder is required, the normal grade of asphalt for a virgin mix can be added, though this necessitates that the plant be capable of adding two binder materials [8]. Recycling agents in emulsion form have the potential advantages of improved fluxing, mixing and temperature control to prevent localized overheating in drum mixers. Furthermore, the formulation of the emulsion can be adjusted to provide the design end result viscosity of the binder in the recycled HMA mix. A disadvantage is that additional heat is required to remove the 30 to 35 percent water contained in the emulsion [9]. To ensure the proper function of the modifiers, the following properties are suggested for specification purposes:

1. Be easy to disperse in recycled mixture.
2. Capable of altering the viscosity of aged asphalt binder in the RAP to the desired level.
3. Be compatible with the aged asphalt binder to ensure that syneresis (exudation of paraffins from asphalts) will not occur.
4. Have the ability to redisperse the asphaltenes in the aged asphalt binder.
5. Improve the life expectancy of the recycled HMA mix.
6. Be uniform in properties from batch to batch.
7. Be resistant to smoking and flashing.

3.2.4 Warm Mix Asphalt.

Warm Mix Asphalt (WMA) is the process of using additives to reduce the mixing temperatures of HMA by 10°C to about 40°C [10]. These relatively new processes and products use various mechanical and chemical means to reduce the shear resistance of the mix at construction temperatures while reportedly maintaining or improving pavement performance [11].The reduction in temperature is beneficial because it reduces the amount of fuel used to heat the mix, minimizes the expulsion of greenhouse gasses, and minimizes the paving temperature necessary in the field. Energy reductions have been shown to be over 54% when heating temperatures were reduced from 150°C to 130°C [12]. However, the WMA process still uses 100% virgin materials so in general, Reclaimed Asphalt Pavement (RAP) uses recycled HMA pavement as the foundation for a new, re-graded, remixed pavement material. In

addition to the focus on WMA, there has also been an ever-increasing interest in using RAP with WMA technologies to decrease the environmental impacts by using less virgin material and reducing CO2 emissions. New industrial processes are treating the RAP as a WMA and thus, including additives to reduce the compaction and production temperatures. Nevertheless the use of Warm Mix Asphalt (WMA) technology for utilizing Reclaimed Asphalt Pavement (RAP) materials demands a complete understanding of WMA additives and their interaction with the asphalt binder.. According to Mallick et al. [13] , it is possible to manufacture mixes with 75% to 100% RAP with similar properties to HMA mixes through the use of additives . Higher mixing and compaction temperatures age the binder in the RAP which has negative effects on the entire mix. The use of WMA additives helps reduce temperatures while achieving desired workability, thus enabling HMA to contain higher percentages of RAP.

3.2.5 Additives.

A mix produced in the temperature range of 105°C to 135°C is considered to be WMA and the goal of such a mix is to obtain a strength and durability that is equivalent to or better than a HMA mix . Currently, a common way of achieving this is through the use of additives. All of the current WMA additives in use facilitate the lowering of production temperature by either lowering the viscosity and/or expanding the volume of the asphalt binder at a given temperature. By lowering the viscosity or expanding the volume of the asphalt binder, the aggregates are completely coated in asphalt binder at a lower than conventional temperature (approximately 150°C). Reductions in temperature decrease energy costs and emissions but the lowered temperatures are often criticized. Regardless of reduced energy costs, researchers are concerned that lower compaction temperatures used in WMA will reduce tensile strength, increase moisture damage, and increase the rutting potential [1.4]

RAP is an aggregate that contains aged bitumen. Therefore, in order to recover and reuse the entire milled material, with the technique of recycling either hot or cold, the lost chemical and physical properties of the binder need to be restored. On this purpose, specific additives for bitumen have been developed called ACF (Chemical

Functional Activators). The ACFs are employed to rejuvenate the characteristics of the aged bitumen in the asphalt conglomerate to be recycled and they must have the

Table 3.1

Chemical Functional Activators (Rejuvenators - ACF)

Parameter	*Law*	*Unit*	*Value*
Density at 25/25°C	ASTM D - 1298		0,900 - 0,950
Flammability point.	ASTM D - 92	°C	200
dinamic viscosity at 160°C, γ =10s^{-1}	SNV 671908/74	Pa s	0,03 - 0,05
tricloroetilene solubility	ASTM D - 2042	% weight	99,5
Neutralization Number	IP 213	mg/KOH/g	1,5-2,5
Water content	ASTM D - 95	% volume	1
Nitrogen content	ASTM D - 3228	% weight	0,8 - 1,0

chemical-physical characteristics shown in the table 3.1.

These additives, correct some properties of bitumen as the thermal susceptibility of the bitumen, the 'plasticity, cohesion, viscosity, its rheological behavior and the resistance to oxidation. They can regenerate the oxidized bitumen by re-introducing ne the more volatile fractions that are lost along time and thus improving the final quality of the conglomerate. The ACFs are mixed with fresh bitumen to be added to the aged bitumen and regenerated directly in the storage tank. The amount added is a function of the mass of milled used: 0.2% to 0.3% on the weight of new bitumen introduced every 5% of the milled material entered in the conglomerate (4% to 6% over 100% RAP). The addition of the ACF in the bitumen must be carried out with suitable equipment, such to guarantee the exact dosage and their perfect dispersion in the bituminous binder. The introduction of the milled involves indirectly difficulties due to the increase in viscosity of the mix, as the viscosity of the bitumen of the paving to be regenerated is very high.

- The milled only has a high viscosity, even undetectable at temperatures below 80 ° C, and its addition in a percentage of 30% significantly increases the viscosity of the final conglomerate;

- The addition of the ACF to bitumen, leads to a reduction of viscosity with consequent increase workability, adhesion to the aggregates, and compaction of the conglomerate, and a possibility to decrease the temperatures of mixing and paving compared to a conglomerate without ACF.

The adhesion promoters are complementary components that modify the conditions at the interface stone aggregate/binder, allowing the realization of a suitable and stable bituminous coating of the aggregates itself. The adhesion promoters, are additives used to improve the durability of the bituminous mixtures to water. They must possess the following properties: active adhesion so that to overcome the resistance that the film of water absorbed on the surface of the aggregate opposes to the bitumen surface and ensure a strong bond between the binder and the aggregate, whatever its mineralogical nature; passive adherence, that is enhancing the strength of the bond between the aggregate and the bituminous binder against the different agents that can cause the collapse of the system. The adhesion process is regulated by several mechanisms that involve, among other the following factors:

- The chemical reactions of neutralization between the acidic compounds of the bitumen and those basic possibly present on the surface of the aggregates;
- The presence of interfacial tensions between the asphalt binder and the stone surface (eg. vapor pressure in the mixing);
- The mechanical effects related to the degree of surface roughness and porosity of the aggregates .

The first two mechanisms are related to the phenomena of detachment and the pull out, and the third is related to that of the spontaneous retention.

Therefore the adhesion promoter act by improving the adhesiveness of the bitumen in two ways: by increasing chemical reactivity and by lowering the surface tension at the interface between bitumen and inert. These products are nitrogen compounds of different nature and complexity.

3.3 Bitumen Modifiers: Overview

Liquid petroleum bitumen (also called asphalt in the US) produced by refiners for use in road paving has been, historically, one of three primary products: asphalt cement (AC, or asphalt binder), cutback asphalt (AC liquefied with petroleum solvent diluents), and asphalt emulsion (AC mixed with an emulsifying agent and water) [15-17]. Over time, asphalt cement represented the greatest production volume compared with emulsions and cutbacks. In the production of liquid petroleum asphalt from petroleum refining, the aim is to produce a material that satisfies physical performance specifications for paving; the material does not necessarily have a specific chemical composition. Refineries may use a combination of production processes (e.g., atmospheric or vacuum distillation) to produce different grades of liquid petroleum asphalt that can be further processed or blended to make other grades of liquid petroleum asphalt at the refinery [18]. In addition, a variety of materials (additives and modifiers, Table 3.2) can be mixed with liquid petroleum asphalt binder at the refinery to enhance the performance of the material to meet standard specifications for road paving.

Table 3.2

TYPE OF MODIFIER	TYPE OF ADDITIVE
(1) Thermoplastic Elastomers	• Styrene – butadiene – styrene (SBS) • Styrene – butadiene – rubber (SBR) • Styrene – isoprene – styrene (SIS) • Styrene – ethylene – butadiene – styrene (SEBS) • Ethylene – propylene – diene terpolymer (EPDM) • Isobutene – isoprene copolymer (IIR) • Natural rubber • Crumb tyre rubber • Polybutadine (PBD) • Polyisoprene
(2) Thermoplastic Polymer	• Ethylene vinyl acetate (EVA) • Ethylene methyl acrylate (EMA) • Ethylene butyl acrylate (EBA) • Atactic polypropylene (APP) • Polyethylene (PE) • Polypropylene (PP) • Polyvinyl Chloride (PVC) • Polystyrene (PS)

(3) Thermosetting Polymers	• Epoxy Resin • Polyurethane Resin • Acrylic Resin

TYPE OF MODIFIER	TYPE OF ADDITIVE
Chemical Modifiers	• Organo-metallic compounds • Sulphur • Lignin
Fiber	• Cellulose • Alumino-magnesium silicate • Glass fiber • Asbestos • Polyester • Polypropylene
Adhesion improvers	• Organic amines • Amides
Antioxidants	• Amines • Phenols • Organo-zinc/organo-lead compounds
Natural asphalts	• Trinidad Lake Asphalt (TLA) • Gilsonite • Rock asphalt
Fillers	• Carbon black • Hydrated lime • Lime • Fly ash
Extender	• Sulphur

Table 3.2. List of possible bitumen modifiers.

Despite this great variety of substances only a few materials added consistently by industry. In the past, subjective reports indicated that experimentation occurred with many materials, but there is little to support widespread use of these materials in the refining sector, and also in the literature. The most common additives in recent years, including SBS, SBR, amine liquid anti-strips, are used in amounts typically less than 5% per unit weight of asphalt. Other asphalt materials produced in the past that would have had wide distribution, such as cutbacks, are now infrequently used. Additives such as sulfur, tall oils, or vacuum gas oils were used in such limited amounts for very

short periods of time. Crude sources vary as widely as they are available, which precludes any inferences regarding their distribution in asphalt.

3.3.1 Most Used Modifiers.

Hydrocarbons.

Hydrocarbons as bitumen modifiers may have been obtained from process streams within the refinery (kerosene, fuel oils) or from sources outside the refinery (natural asphalts, kerojet). Hydrocarbons are used primarily to produce cutback asphalts, which, historically, represented only a small proportion of asphalt products and, therefore, are an insignificant amount of the total produced. Kerosene is added to produce medium-cure cutback asphalts. “Asphalt flux” was historically and is currently added to certain asphalt products at concentrations up to 73%, depending on the asphalt end product. Diesel is also used in the production of slow-cure cutbacks. Other hydrocarbon materials that were reported either historically or currently to be added include Jet Fuel A and the residuum from the re-refining of used motor oil.

Adhesion improvers.

Currently or historically, some type of anti-strip compound was added to asphalt products before distribution, at either the refinery or the terminal. In general, anti-strip is added at an average reported concentration of approximately 0.6% by weight beginning in the early 1990s; the two most commonly used are polyamine and amine blends at concentrations ranging between 0.25 and 1%. Other anti-strip agents that were currently or historically added to asphalt at the participating facilities included fatty amidoamine, imidazoline, and fatty amine.

Polymers.

Six different elastomers are currently the most employed polymer modifiers: styrene butadiene (SB), styrene butadiene styrene (SBS), styrene butadiene rubber latex (SBR), polychloroprene latex, reactive ethylene terpolymer (RET), or crumb rubber. The most commonly added elastomer is SBS, incorporated at a concentration ranging between 1% and 10% by weight. Use of SBS typically began in the early to mid-1990s, SBR, RET, and crumb rubber are also used by a good part of refineries. Addition of plastomers, i.e., ethylene vinyl acetate (EVA), low-density polyethylene (LDPE), and

functionalized polyolefin to asphalt products. Plastomers typically were added to asphalt starting in the late 1990s and at concentrations of approximately 2% by weight. Currently the addition of plastomers is not so common.

Various.

Of the materials that could not be otherwise classified, silicone defoamers (siloxane compounds) are the most commonly used, averaging 0.5 kg per thousand barrels. Also the addition of poly phosphoric acid (PPA) to asphalt products is still in use, with concentrations ranging between 0.1% and 1%. The earliest dates of use were the 1990s.

3.3.2 Polyphosphoric Acid (PPA) as bitumen modifier.

Among the polymers added to bitumen as modifier, polyphosphoric acid (PPA) is often used to improve both high and low temperature performances. It reduces the polymer content leading to improved processing conditions, high temperature viscosity and storage stability. However, the mechanism of chemical modification of bitumen with PPA depends on the base bitumen and is to a great extent still unknown [19]

3.3.3 Synthesis, composition and PPA dissociation

In general PPA is a reactive oligomer of H_3PO_4. High-purity material is produced either from the dehydration of H_3PO_4 at high temperatures or by heating P_2O_5 dispersed in H_3PO_4.

Figure 3.1 illustrates the equilibria for these reactions, which produce different chain lengths and distributions. The dehydration method tends to produce short chains, whereas the dispersion method usually produces chains with more than 10 repeat units.

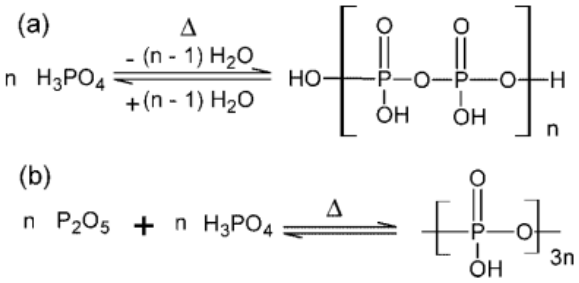

Figure 3.1. Production of PPA from the (a) dehydration and (b) dispersion methods. n is an integer.

PPA is available in various grades, the naming of which can be confusing because the percentage can exceed 100% (Table 3.3). The 100% phosphoric acid contains 72.4% P_2O_5 as calculated from the formula weight ratio P_2O_5/H_3PO_4. Similarly, pyrophosphoric acid ($H_4P_2O_7$) contains 79.8% P_2O_5 as calculated from the ratio $P_2O_5/H_4P_2O_7$. The ratio of these P_2O_5 contents provides a relative phosphoric acid content, which for pyro-phosphoric acid is 79.8%/72.4% 110%. Other examples are provided in Table 3.3.

PA	formula 1	formula 2	formula 3	designation	P_2O_5 (%)	PA (%)	P_2O_5/H_2O[a]
ortho	H_3PO_4	$P_2O_5 \cdot 3H_2O$	$HO(HPO_3)H$	solid anhydrous	72.4	100	0.33
		$P_2O_5 \cdot 2.35H_2O$		super-PA	75.9	105	0.40
pyro	$H_4P_2O_7$	$P_2O_5 \cdot 2H_2O$	$HO(HPO_3)_2H$		79.8	110	0.50
tri	$H_5P_3O_{10}$	$3P_2O_5 \cdot 5H_2O$	$HO(HPO_3)_3H$		82.6	114	0.60
meta	$H_2P_2O_6$	$P_2O_5 \cdot H_2O$	$(HPO_3)_n$	meta-PA	88.8	123	1.00

[a] Molar ratio.

Table 3.3 Grades and Designations of Phosphoric Acids (PA)

The 105% PA grade contains for the most part short mono- and dimeric segments, ortho- and pyrophosphoric acids. In contrast, the 110% grade has the same dimeric content but little monomer, converted to segments with n > 3. In the higher 114% grade, little monomer is left. They have all been converted to chains with 2-14 units. This increase in chain length leads to chain entanglements and explains the increased viscosity of the higher grades.

It is noteworthy that PPA may be a very weak acid when mixed with bitumen. For PPA to dissociate into PPA^- and H^+, the medium must be of sufficiently high dielectric constant (ε).

Water is very polar. It has the highest dielectric constant of all solvents, closely followed by H_3PO_4, as shown in Table 3.4

name	structure	ε
water	HOH	79
phosphoric acids	HOP(O)(OH)OH	61[a]
ethanol	$HOCH_2CH_3$	24
ethyl ether	$CH_3CH_2OCH_3CH_2$	4
bitumen	hydrocarbon mixture	3
benzene	C_6H_6	2
hexane	C_6H_8	2

[a] From ref 47.

Table 3.4 Dielectric Constants of Some Compounds

Consequently, a hydration sphere can stabilize the charges of dissociated anions and cations. This stabilization is gradually lost when water protons are replaced with nonpolar alkyl groups. The reduced potential for charge stabilization is shown, for example, by the reduced dielectric constant for ethanol and ether in Table 3.4. Below a dielectric constant of 15, it is generally considered that charge stabilization is not possible. Consequently, in nonpolar bitumen (ε =3), PPA is unlikely to dissociate to its charged moieties, PPA^- and H^+ . Any dissociation of PPA and reaction with bitumen would have to be localized to bitumen enclaves with high dielectric constant, the existence of which is speculative, but not incompatible with the grouping of several amphoteric groups and nanodomains.

3.3.4 Polyphosphoric acid modified bitumen: proposed mechanisms

Orange et al. (2004) hypothesized that PPA protonates basic sites, inducing a loss of hydrogen bonding and the disaggregation of asphaltenes [20]. The result is a greater dispersion of smaller asphaltene domains. Baumgardner performed Gel-permeation Chromatography (GPC) measurements of modified bitumens and he observed a decrease of mean molecular weight of asphaltenes, consequently he agreed with Orange assuming that PPA disperses associated asphaltenes into smaller domains in solution. Then, conducting a deeper characterization by Atomic Force Microscopy, he observed that the addiction of PPA induced a greater association of polar material and the fall in saturates in the modified bitumens by SARAs analysis.

All these aspects could not be explained by the simple Orange reaction hypothesis, therefore other mechanisms must also act.

Table 3.5 summarized all possible chemical reactions of PPA with bitumens [19].

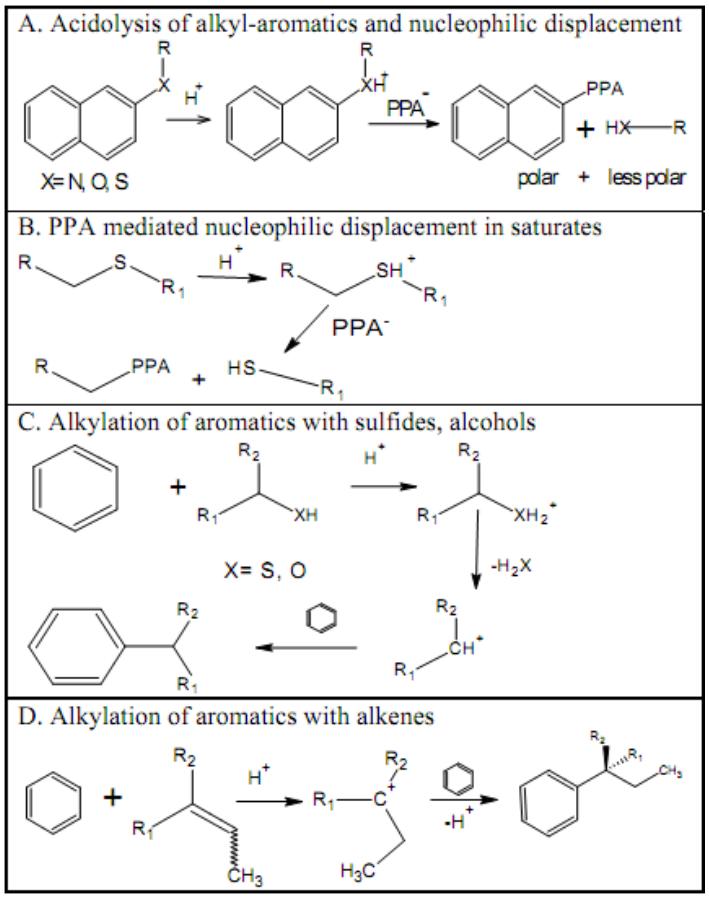

Table 3.5 Possible mechanisms of PPA reaction with bitumen

The acidolysis of alkyl-aromatics (scenario A) would explain both the reduction in asphaltenes molecular weight and the greater dispersion of smaller asphaltenes. The PPA-adduct would also be consistent with the presence of phosphorus in the asphaltenes as obtained by 31P-NMR.

Scenario B, which also leads to polar PPA adduct, would explain the loss of saturates and the increase in the size of the associated polar domains through the association of all the PPA containing material. The increase in asphaltenes (heptanes insoluble) may result from the co-precipitation of asphaltenes with polar and insoluble PPA-adducts. These two scenarios are not entirely satisfactory, as PPA adduct would contain CO-P bonds that have not been detected in asphaltenes . The co-precipitation of a physical mixture of asphaltenes and neat PPA, rather than adducts, could also explain the presence of phosphorus in asphaltenes.

Table 3.5 also shows scenarios C and D, which represent the alkylation of aromatic rings. These reactions could explain the increase in asphaltenes and the loss of saturates through coupling reactions.

However, Baumgardner [19] highlighted that all the experimental results were strongly dependent on the bitumen sources. In conclusion, the reaction mechanisms between PPA and bitumen are not fully understood yet due to the complexity of the bitumen system.

3.3.5 Crumb rubber modified bitumen.

Waste rubber products are dominant among solid waste materials, the annual amount of waste rubber products is more than 12 million tons in the world. So how to make use of waste rubber rapidly and effectively is an important project. Now, waste rubber has been used to produce reclaimed rubber, which is used as fuel or the materials for civil engineering. But more than 50 percent of them are used as fuel. For fully utilizing natural resources and protecting environment, many countries give priority to the reuse of waste rubber in recent ten years [21] . Waste rubber has come into use in construction of roads and highways because crumb rubber made of waste rubber can be used as a modifier of bitumen. Crumb rubber modified bitumen can improve the heat-resistance, the crack-resistance at low temperature and the durability of bitumen [22] . Compared with an unmodified bitumen roadway, the service life of a crumb rubber modified bitumen roadway will be prolonged largely.

Crumb rubber modified bitumen is made by mixing crumb rubber with bitumen at high temperature for several hours. As is known to all, however, crumb rubber in the sulfurization can not be dissolved and can only be swelled. But, in fact, because the viscosity of the blend of crumb rubber and bitumen is very low at high temperature, which results in that the shearing force produced by stirring is small and weak, the swelling of crumb rubber in bitumen is also difficult and a perfect elastic network can not be formed in the crumb rubber modified bitumen. For these reasons, the elasticity and the stability of crumb rubber modified bitumen are inferior to that of other rubber modified bitumens, such as SBS modified bitumen, SBR modified bitumen [23] . But because of the cheap price of waste crumb rubber and the

enormous contribution of its reuse to protecting environment, crumb rubber modified bitumen has attracted a close attention of many countries in the world [24-27]. Reclaimed rubber is produced as follows [28] . Firstly, waste rubber is ground into crumb rubber and then desulfurated to destroy S - S and S - C bonds in rubber by means of heating, machanical force or other action after adding some activator. Lastly, the desulfurized crumb rubber is plasticized into reclaimed rubber with two rollers. Obviously, the desulfurized crumb rubber has a larger swelling capacity in bitumen because the cross bonding structure of the crumb rubber has been destroyed during desulfuration. So it is believed that the properties of bitumen modified with desulfurized crumb rubber will be superior to that with general crumb rubber. However, few research on the desulfurized crumb rubber modified bitumen has been reported.

REFERENCES.

[1] J. Shen, S. Amirkhanian, and J. A. MillerJournal of Materials in Civil Engineering, Vol. 19, No. 5, May 1, (2007).

[2] Foschi R., " Demolizione e riciclaggio delle pavimentazioni stradali", Il nuovo Cantiere,No. 5. (1998).

[3] Nik.D. Oikonomou, "Recycled concrete aggregates", Cement and Concrete Composites, Vol. 27, Issue 2, Pages 315–318, (2005).

[4] J.A. Epps, D.N. Little, R.J. O'Neal, and B.M. Gallaway, " Mixture Properties of Recycled Central Plant Materials" American Society for Testing and Materials (ASTM), STP 662, Philadelphia,(1977.)

[5] Pavement Recycling Guidelines for Local Governments - Reference Manual, Report No. FHWA-TS-87-230, FHA, U.S. Department of Transportation, Washington, DC, (1987).

[6] Asphalt Hot-Mix Recycling, The Asphalt Institute Manual Series No. 20 (MS-20), 2nd Ed.(1986.)

[7] J.A. Epps, D.N. Little, R.J. Holmgreen, and R.L. Terrel. Guidelines for Recycling Pavement Materials, NCHRP Report No. 224, TRB, National Research Council, Washington, DC, (1980).

[8] Pavement Management Systems Limited. Study of Hot Mix Recycling of Asphalt Pavements, Roads and Transportation Association of Canada (RTAC), Ottawa, Ontario, (1983).

[9] C.F. Potts, B.E. Ruth, H.E. Schweyer, and K.H. Murphy. Asphalt Emulsion Recycling Project: Analysis and Development of Guidelines, Proceedings of the AAPT, Volume 50, (1981).

[10] Warm Mix Asphalt, Retrieved January 2009, from http://www.warmmixasphalt.com, (2009).

[11] Newcomb, D. “An Introduction to Warm-mix Asphalt”. National Asphalt Pavement Association. (2006).

[12] Pakula, M., & Mallick, R. “CO2 Emission Reductions Through the Use of Warm Mix Asphalt”,. (2007).

[13] Mallick, R., Kandhal, P., & Bradbury, R. “Using Warm Mix Asphalt Technology to Incorporate High Percentage of Reclaimed Asphalt Pavement (RAP) Material in Asphalt Mixtures. Worcester Polytechnic Institute, Transportation Research Board, Transportation Research Record 2051, (2008).

[14] L., J., Saboundjian, S., Li, P., Connor, B., and Brunette, B. J. Mater. Civ. Eng. 23, SPECIAL ISSUE: Energy Efficient and Environmentally Friendly Paving Materials, 1498–1505. (2011).

[15] Roberts, F.L., P.S. Kandhal, E.R. Brown, D.-Y. Lee, and T.W. Kennedy: Hot Mix Asphalt Materials, Mixture Design and Construction, 2nd ed. Lanham, Md.: National Asphalt Paving Association Research and Education Foundation, (1996).

[16] “Asphalt Paving,”, Available at http://www.epa.gov/ttn/chief/eiip/techreport/volume03/iii17apr2001.pdf (Accessed sept 20, 2013).

[17] “DRAFT Periodic Emissions Inventory of Ozone Precursor Emissions for the Washington DC-MD-VA Ozone Nonattainment Area.” [Online] Available at http://www.mwcog.org/uploads/committeedocuments/pF5XXl420040513102231.pdf (Accessed sept 20, 2013).

[18] The Asphalt Institute (AI): The Asphalt Handbook, 1989 ed. College Park, Md.: The Asphalt Institute, (1988).

[19] Baumgardner GL, Masson JF, Hardee JR, Menapace AM, Williams AG., “Pholyphosphoric acid modified asphalt-proposed mechanisms; Association of asphalt paving technologists, annual meeting and technical sessions, Long Beach, California;. p. 1–19. (2005).

[20] Orange G., D. Dupuis, J. V. Marin, F. Farcas, C. Such, B. Marcant, “Chemical Modification of Bitumen through Polyphosphoric Acid: Properties-Microstructure Relationship”, 3rd Euraphalt & Eurobitume Congress, Vienna, Paper 334, book 1, p. 733-745. (2004).

[21] Qiou Qinghua, Jia Diming, Wang Feidi. Development on Using of Crumb Rubber. Rubber Industry, ,44,11, 691 – 695. (1997)

[22] Cheng Yuan. Prospect for Application of Waster Rubber Powder. China Synthetic Rubber Industry, ,24, 2, 65 – 66. (2001)

[23] Wang Shifeng, Wang Dizhen. Rubber Modified Bitumen for Highways. Rubber Indnsuy, ,47,8, 503 – 506. (2000).

[24] Heitnaaan M. Design and Construction of Asphalt Paving Malerials with Crumb Rubber Modifier. Transportation Research Record, 1, 8, 1339 – 1345. (1992).

[25] Tao Guoliang, Yang Jibe, Wang Zhanhua. A Study on the Fine Rubber Powder Modified Bitumen Material. J Jiangsu Institute Petrochemical Technology, 12,3, 16 – 19. (2000)

[26] Hussain U, Robert D. Effect of Crumb Rubber Modifiers (CRM) on Performance-related properties of Asphalt Binders. Asphalt Pavement Technology, 63, 414 – 440. (1994)

[27] Magdy A, Abdelrahman. Engineering Characterization of the Interaction of Asphalt with Crumb Rubber Modifier (CRM). Science & Engineering, 57,8, 5197 – 5208. (1997).

[28] He Yongfeng, Liu Yuqing. Production and Application of Crumb Rubber-New Technology on Utilization of Waster Rubber. Beijing: China Petrochemical Press. (2001)

4. Results part I - Analysis of the effects of bitumen modifiers and additives for bitumen recycling: Published Data.

Molecular Crystals and Liquid Crystals
Publication details, including instructions for authors and subscription information:
http://www.tandfonline.com/loi/gmcl20

Rheological and ^{1}H-NMR Spin-Spin Relaxation Time for the Evaluation of the Effects of PPA Addition on Bitumen

Luigi Gentile [a], Luigi Filippelli [a], Cesare Oliviero Rossi [a], Noemi Baldino [b] & Giuseppe A. Ranieri [a]

[a] Dipartimento di Chimica, Università della Calabria, 87036, Arcavacata di Rende (CS), Italy

[b] Department of Engineering Modeling, University of Calabria, 87036, Arcavacata di Rende (CS), Italy

Published online: 18 Apr 2012.

To cite this article: Luigi Gentile, Luigi Filippelli, Cesare Oliviero Rossi, Noemi Baldino & Giuseppe A. Ranieri (2012) Rheological and ^{1}H-NMR Spin-Spin Relaxation Time for the Evaluation of the Effects of PPA Addition on Bitumen, Molecular Crystals and Liquid Crystals, 558:1, 54-63, DOI: 10.1080/15421406.2011.653679

To link to this article: http://dx.doi.org/10.1080/15421406.2011.653679

Mol. Cryst. Liq. Cryst., Vol. 558: pp. 54–63, 2012

ISSN: 1542-1406 print/1563-5287 online
DOI: 10.1080/15421406.2011.653679

Rheological and ^{1}H-NMR Spin-Spin Relaxation Time for the Evaluation of the Effects of PPA Addition on Bitumen

LUIGI GENTILE,[1,*] LUIGI FILIPPELLI,[1] CESARE OLIVIERO ROSSI,[1] NOEMI BALDINO,[2] AND GIUSEPPE A. RANIERI[1]

[1]Dipartimento di Chimica, Università della Calabria,
87036 Arcavacata di Rende (CS) Italy
[2]Department of Engineering Modeling, University of Calabria,
87036 Arcavacata di Rende (CS) Italy

Bitumens are currently modelled as a colloidal system and are the most used materials for road paving. Despite this large application, asphalts are still affected by some inconveniences that bring to road deterioration. This is prevalently due to temperature cycling which is related to the given local climate conditions and to the incident traffic load. In the last decades bitumen performances have been improved by means of different types of additives in order to match various expectations. This improvement is often the result of the indications given by traditional empirical standardized tests like penetration grade, temperature ductility and Fraas breaking point. The comprehension of the chemical mechanism that regulates the action of the used additives can greatly help in designing new and better performance materials. By means of a Stress Controlled Rheometer we present a laboratory evaluation of the rheological properties of a 70/100 bitumen which has been doped by different percentage of Polyphosphoric acid (PPA). In addition ^{1}H-NMR measurements of proton transverse relaxation time (T_2) have been exploited in order to corroborate the rheological data. As a novel approach to the knowledge of bitumen macro-structures, we applied an Inverse Laplace Transform (ILT) to the measured echo decay. The results show the effect of PPA addition on bitumen mechanical behaviour.

Keywords Bitumen; asphaltenes; rheology; NMR; Inverse Laplace Transform

Introduction

Bitumens are commonly employed as binders in road construction and roofing systems because of their thermoplastic nature, water resistance and adhesion properties.

Asphaltenes and maltenes are two of the major constituents in the bituminous materials, with asphaltenes as the dispersed phase and maltenes as the continuous phase [1]. Asphaltenes are formed by condensed polyaromatic structures containing alkyl chains, hetero-aromatic compounds with sulphur present in benzothiophene rings and nitrogen in pyrrole and pyridine rings. In addition, asphaltenes may contain polyfunctional molecules

*Address correspondence to L. Gentile, Dipartimento di Chimica, Università della Calabria, 87036 Arcavacata di Rende (CS) Italy. E-mail: luigi.gentile@inucal.it

with nitrogen, as amines and amides; oxygen, nickel and vanadium metals complexed with pyrrole nitrogen atoms in porphyrin rings [1,2]. Considering their chemical composition, asphaltenes are the rigid portion of the material [3]. Maltenes are the soft part of the material and they are constituted by resins, aromatic hydrocarbons, olefins, cyclic saturated hydrocarbons and straight or branched chain saturated hydrocarbons (paraffins) [1]. The presence of both rigid and soft portions in the bitumen structure is at the basis of its liquid crystalline behavior [4].

Bitumens rheological behaviour is governed by the chemical-physics interactions of the individual constituents and it is strongly dependant on the temperature [5]. During the last years researchers focused their attention on the performances of bituminous materials. This is because of bituminous binders play a crucial role in the performance of the corresponding asphalt mix [6]. A frequent indication of the asphalt road deterioration is the occurrence of different types of cracks, such as those caused by traffic loading or temperature cycling, induced by frost heaving, and fissures formed at low temperature [7].

Generally bitumen composition is variable depending on its provenience and this strongly influences the rheological properties. For example, a bitumen that have a high waxes content is more sensitive to cracking or create plastic deformations of the paved asphalt [8] due to the crystal nature of these components. In order to reduce this phenomenon, bitumens should be able to relax the applied stress and at the same time their rigidity should not exceed a given value especially at low temperature [9]. In convenient applications, different types of additives, like waxes, polymers and acids (poly-phosphoric acid, PPA, as an example) are added to bitumens or to mixtures in order to improve their mechanical properties, with particular attention to the operative temperature conditions. To achieve good performance at both high and low temperatures, small quantities of PPA are used as a doping substance in bitumen formulation [8]. As matter of fact it was found that PPA can increase the stiffness of the material at intermediate and high temperatures. Unfortunately the asphalt mixture containing PPA showed an increased sensitivity to permanent deformation compared to mixture without the additive [8]. Besides the conventional tests, new approaches for the characterization of bituminous materials are developing [10–13]. Different rheological techniques are demonstrated to be a valuable and more sensitive way to asses bitumen properties [14]. Furthermore a deeper knowledge of the chemical composition as well as the morphology of the bituminous binder is essential to design new additives and the relative obtained materials. In this frame we performed rheological tests and exploited nuclear magnetic resonance trying to find new analytical approaches and a correlation between molecular organisation and mechanical behaviour. In the present work we have investigated straight and modified bitumen with different PPA content. Moreover for the first time we applied an inverse Laplace transform to the measured echo decays. This procedure allowed to distinguish different spin-spin relaxation times (T_2) that we can attribute to different macro-aggregates.

Experimental

Materials

The straight bitumen that we used in this study, has been produced in Venezuela and it has a 70/100 penetration grade. Polyphosphoric acid, 83.3% P_2O_5, or otherwise stated 115% H_3PO_4 equivalent [15], has been provided by ICL Performance Product LP (St. Louis, MO, USA).

Sample Preparation

The appropriate amount of PPA has been added to bitumen, at 120°C, to reach a level of 1 and 2% by weight. After mixing, the system has been heated up to 160°C (ARE, Velp Scientifica, Italy) and maintained at this temperature, under stirring at 600 rpm (RW 20 Digital, IKA, Germany), for 30 minutes in a sealed beaker to avoid any oxidation process. Afterwards, the resulting bitumen has been poured into a small sealed can and then stored in a dark chamber thermostated at 25°C to retain the obtained morphology. The samples for rheological tests have been rightly prepared; the bituminous material has been taken to the liquid status, increasing the temperature in a controlled way, then it has been poured directly on the plate of the rheometer preheated at 130°C. For the ^{1}H-NMR T_2 measurements, the samples have been introduced in a 5mm NMR tube, then heated up to 130°C and successively observed in cooling.

Methods

To explore the structural changes induced by temperature, a rheological characterization has been performed. In particular temperature-ramp test experiments have been performed on the bitumen. Rheological measurements have been conducted using a shear stress controlled rheometer SR5 (Rheometrics, USA) equipped with plate-plate geometry (gap 2.0 mm, diameter 25 mm). The temperature has been controlled by a Peltier system (±0.1°C). All the experiments have been performed in cooling. All the experiments have been carried out by using dynamic shear technique. The small amplitude dynamic tests provided information on the linear viscoelastic behavior of materials through the determination of the complex shear modulus [16].

$$G^*(\omega) = G'(\omega) + iG''(\omega) \tag{1}$$

where $G'(\omega)$ is the in phase (or storage) component, and $G''(\omega)$ is the out-of-phase (or loss) component.$G'(\omega)$ is a measure of the reversible, elastic energy, while $G''(\omega)$ represents the irreversible viscous dissipation of the mechanical energy. The rheological behaviour at different temperatures has been investigated by a time cure test (temperature-ramp test) at 1 Hz with a cooling ramp rate of 1°C/min. The applied shear stress of 100 Pa ensures to perform the dynamic rheological tests within the linear visco-elastic region.

NMR Measurement

For the ^{1}H spin-spin measurements a homemade NMR instrument has been used. It operates at a proton frequency of 15 MHz. Measurements have been performed at different temperatures ranging from 130 to 25°C with an error of ±0.1°C. A classic Carr-Purcell pulse sequence has been used to record the echo decay [17]. The applied width of $\pi/2$ pulse was 5.9 μs and that of π pulse was 11.8 μs. The τ delay time was 0.06 ms. In a basic NMR concept, at equilibrium, nuclei are distributed among the energy levels according to a Boltzmann distribution. Following any process that disrupts this distribution (e.g. absorption of radiofrequency energy), the nuclear spin system returns to equilibrium with its surroundings (the "lattice") by a first-order relaxation process characterized by a time T_1 called the spin-lattice relaxation time. To account for processes that cause the nuclear spins to come to equilibrium with each other, a second time T_2 is required. The T_2 is called the spin-spin relaxation time, because the relaxation is concerned with the exchange of energy

between spins via a flip-flop type mechanism. It is defined according to:

$$v_{\frac{1}{2}} \approx \frac{1}{T_2} \tag{2}$$

where $v_{\frac{1}{2}}$ is the linewidth at half height of a resonance line. In a perfectly homogeneous field the time constant of the decay would be T_2. However the real experiment is often characterized by field inhomogeneity. As a consequence, nuclei in different parts of the field precess at slightly different frequencies and quickly get out of phase with each other, causing the signal to decay with a different characteristic time T_2^*. This decay directly measures the decrease in the transverse magnetization M_{xy}, but due to the contribution of the magnetic field inhomogeneity it cannot be taken as a measure of T_2 [17].

A method for overcoming the inhomogeneity problem is to apply the Carr–Purcell technique [18]. This method may be described as a 90°, τ, 180°, 2τ, 180°, 2τ, 180°, 2τ, ... sequence (Fig. 1). The 180° pulses are applied along the positive y′ axis, i.e., at 90° phase difference relative to the initial 90° pulse. The main advantage of such a multiple echo technique is its fastness as compared with other techniques based on single echoes. Consequently, it allows multiple accumulations of the echoes train signal which is an important issue in low-field experiments where the detection sensitivity is strongly reduced relative to the high-field experiments.

If the CP envelope, has a mono exponential decay, the relaxation time T_2 of the sample can be obtained by fitting the data to the following equation:

$$A = A_o e^{-\frac{2\pi\tau}{T_2}} \tag{3}$$

where A is the amplitude of the nth echo in the echo train and A_0 is a constant depending on the sample magnetization, filling factor and other experimental parameters. Usually the relaxation time varies all over the sample because of the sample heterogeneity or surface relaxivity differences, then a multi-exponential attenuation of the CP envelope should be observed. Hence if inside the sample, a continuous distribution of relaxation times exists, the amplitude of the nth echo in the echo train is given by:

$$A = A_o \int_o^\infty P(T_2) \exp\left(\frac{-2\pi\tau}{T_2}\right) dT_2 \tag{4}$$

where $P(T_2)$ is the T_2 relaxation time probability density. The last Equation suggests that the analysis of the experimental data using an Inverse Laplace Transform (ILT) might provide the relaxation time probability function. The ILT have been performed using an homemade software based on CONTIN [19, 20]. This is an iterative fitting software and

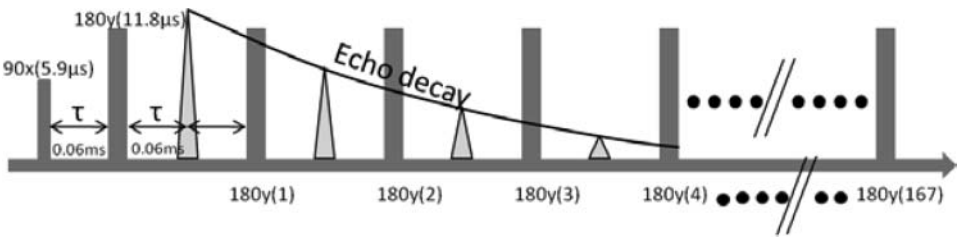

Figure 1. The echo detection pulse sequence used in the present paper.

it has been improved in order to extrapolate the data from the experimental T_2 decay. For a given CP decay, there are a certain different number of possible combinations of times which fit well the solution, especially in presence of signal noise. Therefore, the numerical ILT must be used with caution when interpreting the experimental results. As a matter of fact we cross-linked the ILT numbers with other experimental techniques.

Discussion

The present paper deals with the possibility of a more accurate description of the mechanical properties of bitumen if compared to the traditional standard empirical tests. These mechanical properties are the result of the chemical composition and phases arrangement of the molecular structures. So far, bitumen producers neglected, to a certain extent, the correlation of the molecular level with the macro-behaviour of the material. However there is a growing customer expectations in terms of given application performances. Hence bituminous materials are currently and always doped through substances that make the performance better for a given employment. On the other hand not always the mechanisms by which some additives act to dope bitumen are known. This is the case of PPA which is currently used by bitumen industry but it is still controversial its way to improve material performances. It is believed to reduce the size of the macro-polymers inside material leading to improved processing conditions, high temperature viscosity and storage stability. However, the mechanism of the chemical modification induced by PPA depends on the base bitumen. Here we investigated the effect of two different percentage of PPA onto a Venezuelan straight bitumen. Samples of pure materials have been added with a 1% and 2% of polyphosphoric acid. Rheology temperature-sweep experiments have been exploited to have some information on the structural changes induced by temperature, trying to better define a transition temperature range. In fact, in this experiment, the evolution of the storage and loss moduli is continuously monitored during a temperature ramp, at a constant cooling rate (1°C/min) and at a frequency of 1 Hz. Figure 2 shows the time-cure of the straight bitumen. No crossover between G′ and G″ is observed, but the elastic modulus G′ have

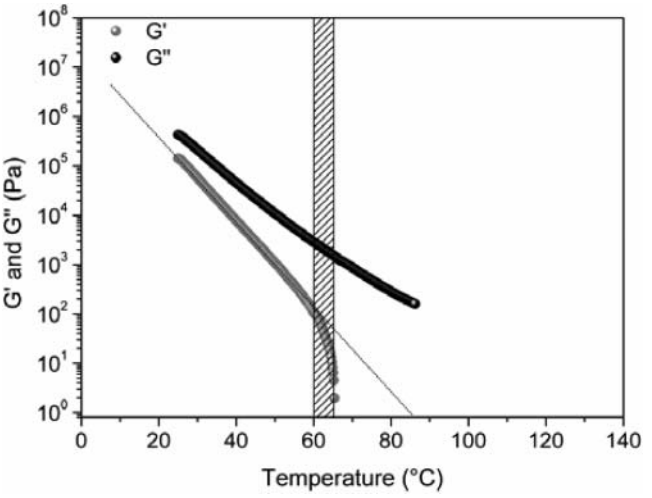

Figure 2. Time cure test at 1 Hz in the range 30–90°C of the straight bitumen. The two vertical lines define the temperature transition region.

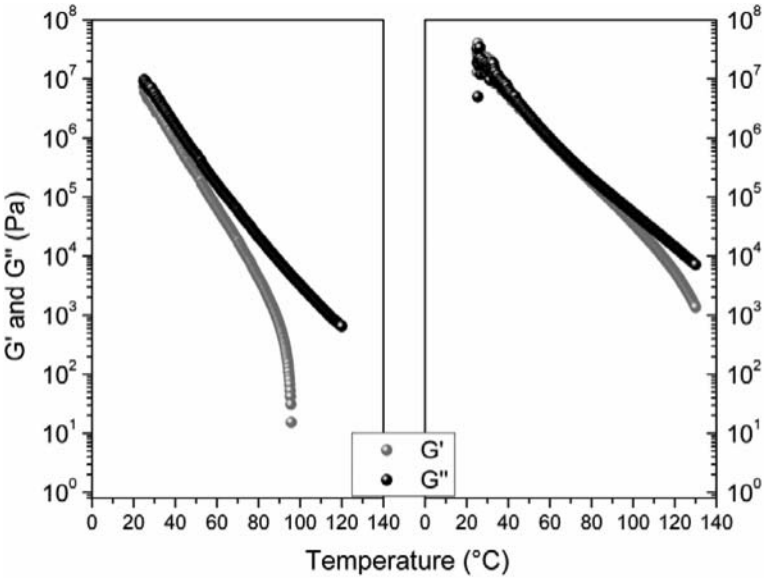

Figure 3. Time cure test at 1 Hz in the range 30–90°C of the bitumen modified with 1% and 2% PPA respectively.

a non-linear behaviour after 60°C. The starting point of the non-linear region of G′ can be considered as the beginning of the transition temperature region. The whole transition process from viscous to liquid regime ends when G′ modulus is no longer detectable.

Figure 3 shows the time-cure experiments for the 1% and 2% PPA modified bitumen. They show a similar behaviour of G′ and G″ in comparison with the straight bitumen. It is worthy to note that G′ and G″ of the modified bitumens, are higher than those of the straight bitumen and in addition G′ is closer to G″. This indicates that the doped material is more elastic. Moreover for the sample containing 2% PPA it can be observed a crossover between G′ and G″ along temperature. This behaviour is the result of a structural modification that occurs passing from a gel-like to a viscous material through a large visco-elastic region.

Table 1 reports the softening range temperatures for the three investigated bitumen. The addition of PPA shifts the transition range to higher temperatures.

The same samples have been investigated by means of ^{1}H-NMR spectroscopy. T_2 relaxation times were measured for all of the samples at different temperatures. The T_2 time can be used as a measure of the softness of a given material. The relaxation process, in fact, is more efficient when the material is more rigid, that corresponds to shorter relaxation times. As matter of fact, higher temperatures correspond to longer T_2 times,

Table 1. Temperature range transition of the straight, 1% and 2% PPA modified bitumen

	Starting Temperature	Final Temperature
Straight Bitumen	60.1	65.4
Bitumen + 1% of PPA	87.0	95.6
Bitumen + 2% of PPA	121.8	129.8

bitumen is not an exception. As mentioned above the T_2 time is usually extracted from an exponential decay which is the envelope of the recorded echo signals. When the material is not homogeneous, the measured T_2 is averaged over all of the contributions of the different macro-structures. Considering bitumen models, one can roughly distinguish between a rigid (asphaltenes) and a soft fraction (maltenes) inside the substance. These two parts have a different intra-molecular arrangement and interactions and it is reasonable to think that they relax-back to the equilibrium in different times, contributing to the measured echo envelope differently.

A sophisticate mathematical process to extract the T_2 distribution times is to apply an Inverse Laplace transform (ILT) to the measured echo envelope. Figure 4 shows the echo decay and the ILT results for the straight bitumen at 25°C and 65°C.

It is worthy to note that at 25°C two very close T_2 distribution times can be observed. The first distribution corresponds to the "rigid" part while the second to the "soft" one. However these times distributions (peaks) are really close each other and this means that the whole structure is quite homogeneous with a mutual exchange of spin energy between the soft and rigid fractions. At the transition temperature of 65°C, the ILT reveals that the T_2 distribution times are longer, as we expected for temperature effects, but now the two macro structures can be absolutely differentiated. We attributed the largest T_2 peak to the oil phase inside bitumen (maltenes fraction). This result falls into the transition temperature range obtained by rheology.

The same experiments have been conducted for the two modified bitumens. Figure 5 shows the obtained results for the sample containing 1% PPA. The trend and the shape

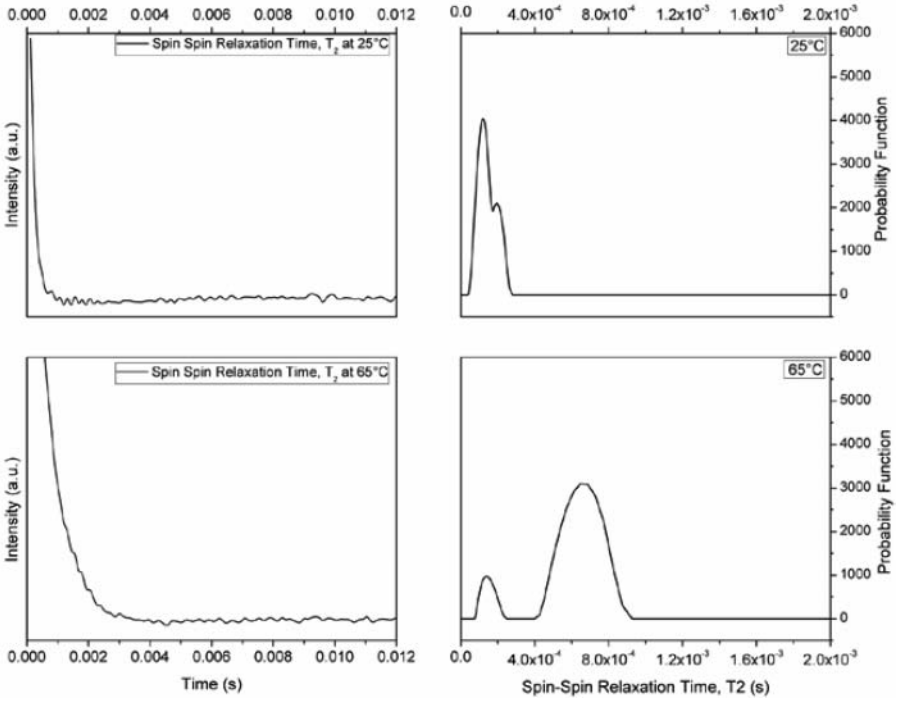

Figure 4. a) The echo intensity envelope versus time in a CP relaxation experiment in the case of straight bitumen at 25°C and 65°C. b) Relaxation times distribution of straight bitumen at 25°C and 65°C obtained by ILT.

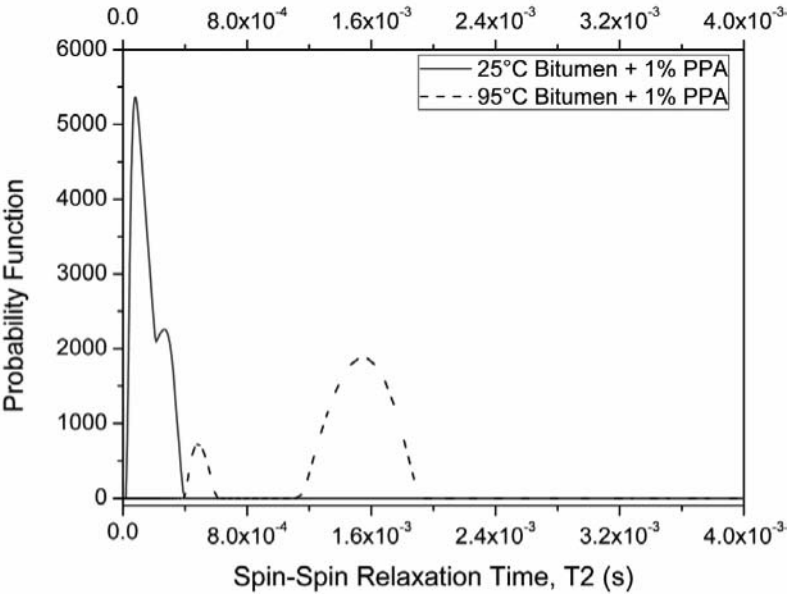

Figure 5. Relaxation time distribution of bitumen 1% PPA modified at 25°C (solid line) and 95°C (dashed line) obtained by ILT.

of the extracted peaks are very similar to those of the straight bitumen. However the transition temperature is shifted towards higher values (about 95°C, dashed line). Also for this modified sample we can say that there is good homogeneity at room temperature while at the transition temperature we attribute the largest T_2 peak centred at 1.6×10^{-3} s, to the soft part of the material. The calculated spin-spin relaxation times are shorter than the T_2 times of the straight bitumen. This is due to the enhanced rigidity after the addition of 1% PPA. The transition temperature as measured by applying the ILT is still in agreement with the rheology findings.

For the last sample, which contains 2% PPA (Fig. 6), we have registered the largest transition temperature deviation from the straight bitumen (Fig. 4). Indeed the sample turned from gel to liquid phase at a temperature around 130°C. Also in this case the transition temperature observed by NMR analysis is similar to that determined by rheological measurements. However we can make some new and interesting considerations. At room temperature we can clearly recognize three peaks underlying the echo envelope fitting. This means that the highest PPA content might induce the formation of a third macro-structure inside the material. As a matter of fact, the third peak indicates a inhomogeneity of the material that can cause processing and application problems. This macro-structure is a relatively soft component and it is evidenced by the smallest peak shown in Fig. 6. Indeed this peak falls into the same times region at both low and high temperatures. This indicates that the new structure seems not to be affected by temperature. On the other hand at high temperatures only two peaks are found, similarly to the straight and 1% PPA modified bitumens. In addition for the bitumen added with 2% PPA at 125°C, we observed that the T_2 peak centred at 2.6×10^{-3} s is wider and shorter than the correspondent peak for the 1% PPA sample (Fig. 5). This is probably due to a more fragmented structure as relaxation times are spread throughout a larger time range.

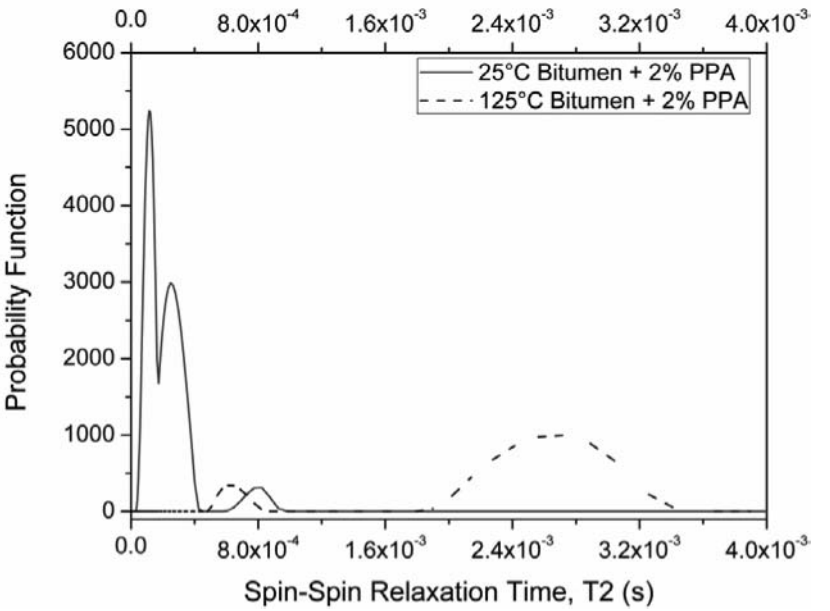

Figure 6. Relaxation distribution times of bitumen 2% PPA modified at 25°C (solid line) and 125°C (dashed line) obtained by ILT.

Conclusions

Commercial bitumen classification is still based on empirical standardized tests. Also the effects of doping substances on bituminous materials are evaluated by conventional methods. Here we reported a new analytical approach to improve the usual bitumen classification and the evaluation of the chemical changes caused by a given additive.

A common modifier, PPA, has been added to a Venezuelan 70/100 straight bitumen. Two PPA percentage were used to evaluate the effects of an excess of doping substance along temperature. Rheology and ^{1}H-NMR spin-spin relaxation times were used to assess the softening point of the three materials and their response to specific solicitations. Results were in agreement to what expected and to literature. It was found that a 1% of PPA can shift the transition temperature towards higher values and the systems remain stable. The sample containing 2% of PPA showed a huge transition temperature shifting as it was found around 130°C. However the last sample resulted more heterogeneous because of new structures appeared after the modifier addition, precluding practical application. In addition the Inverse Laplace Transform revealed itself as a valuable way to study the macrostructure of bitumen when this technique is supported by other methods.

Further investigations are needed to clarify the nature the nature of the interaction between PPA and the bitumen network.

Acknowledgments

We thank StarAsphalt S.p.A., S.P. Piana Loc. Garga, 87010-Saracena (CS) - Italy.

References

[1] Yen, T. F., & Chilingarian, G. V. (2000). *Asphaltenes and Asphalts*, Elsevier Science: New York, USA.

[2] Silva Ramos, A. C., Haraguchi, L., Notrispe, F. R., Loh, W., & Mohamed, R. S. (2001). *Journal of Petroleum Science and Engineering*, *32*, 201.

[3] Mullins, O. C., et al. (2007). *Asphaltenes, Heavy Oils and Petroleomics*, Springer: New York, USA.

[4] Bagheri, S. R., Bazyleva, A., Gray, M. R., McCaffrey, W. C., & Shaw, J. M. (2010). *Energy Fuels*, *24*, 4327.

[5] Loeber, L., Muller, G., Morel, J., & Sutton, O. (1998). *Fuel*, *77*, 1443.

[6] Soenen, H., De Visscher, J., Tanghe, T., Vanelstraete, A., & Redelius P. (2006). *Journal of the Association of Asphalt Paving Technologists*, *75*, 165.

[7] Isacsson, U., & Zeng, H. (1998). *Journal of Materials Science*, *33*, 2165.

[8] Edwards, Y., Tasmedir, Y., & Isacsson, U. (2006). *Fuel*, *85*, 989.

[9] Lu, X., Isacsson, U., & Ekblad, J. (2003). *Materials and Structures*, *36*, 652.

[10] Bernard, C. H. F., & Phillips, C. R. (1979). *Fuel*, *58*, 557.

[11] Zhao, B., & Shaw, J. M. (2007). *Energy Fuels*, *21*, 2795.

[12] Zhang, Y., Takanohashi, T., Sato, S., Saito, I., & Tanaka, R. (2004). *Energy Fuels*, *18*, 283.

[13] Zhang, Y., Takanohashi, T., Shishido, T., Sato, S., Saito, I., & Tanaka, R. (2005). *Energy Fuels*, *19*, 1023.

[14] Ala, B., Bazyleva, M. D., Hasan, A., Fulem, M., Becerra, M., & Shaw J. M. (2010). *J. Chem. Eng. Data*, *55*, 1389.

[15] Masson, J.-F. (2008). *Energy & Fuels*, *22*, 2637.

[16] Ferry, J. D. (1980). *Viscoelastic Properties of Polymers*, 3rd ed, Wiley: New York, USA.

[17] Bakhmutov, Vladimir I. *Practical NMR Relaxation for Chemists*, John Wiley & Sons: England.

[18] Carr, H. Y., & Purcell, E. M. (1954). *Phys. Rev.*, *94*, 630.

[19] Provencher, S. W. (1982). *Comp. Phys. Comm.*, *27*, 229.

[20] Ranieri, G. A., Coppola, L., Celebre, G., & Oliviero, C. (2002). *Molecular Crystals and Liquid Crystals*, *372*, 121.

Molecular Crystals and Liquid Crystals
Publication details, including instructions for authors and subscription information:
http://www.tandfonline.com/loi/gmcl20

Structural Characterization of Bitumen System by Prony-Like Method Applied to NMR and Rheological Relaxation Data

Luigi Filippelli [a], Cesare Oliviero Rossi [a], Manuela Carini [b], Francesco Chiaravalloti [c] & Luigi Gentile [a]

[a] Department of Chemistry, University of Calabria, Cosenza, Italy

[b] Department of Mathematics, University of Calabria, Cosenza INFN Group, Cosenza, Italy

[c] Department of Physics, University of Calabria, Cosenza, Italy

Published online: 02 Apr 2013.

To cite this article: Luigi Filippelli, Cesare Oliviero Rossi, Manuela Carini, Francesco Chiaravalloti & Luigi Gentile (2013) Structural Characterization of Bitumen System by Prony-Like Method Applied to NMR and Rheological Relaxation Data, Molecular Crystals and Liquid Crystals, 572:1, 50-58, DOI: 10.1080/15421406.2012.763210

To link to this article: http://dx.doi.org/10.1080/15421406.2012.763210

Mol. Cryst. Liq. Cryst., Vol. 572: pp. 50–58, 2013

ISSN: 1542-1406 print/1563-5287 online
DOI: 10.1080/15421406.2012.763210

Structural Characterization of Bitumen System by Prony-Like Method Applied to NMR and Rheological Relaxation Data

LUIGI FILIPPELLI,[1,*] CESARE OLIVIERO ROSSI,[1] MANUELA CARINI,[2] FRANCESCO CHIARAVALLOTI,[3] AND LUIGI GENTILE[1]

[1]Department of Chemistry, University of Calabria, Cosenza, Italy
[2]Department of Mathematics, University of Calabria, Cosenza INFN Group, Cosenza, Italy
[3]Department of Physics, University of Calabria, Cosenza, Italy

In order to characterize colloidal structures, T_2-nuclear magnetic resonance (NMR) and rheological relaxation times are used. NMR Car–Purcell sequence and mechanical stress relaxation experiments have been performed on a bitumen system at different temperatures. The rheological relaxation times spectra are fingerprints of the aggregates that constitute the system. These typical relaxation times have been obtained from an exponential fitting of the experimental data, based on a Prony-like method. The unknown parameters are estimated on the basis of a linear regression equation that uses altered signals obtained directly from the NMR and rheological measurements. This approach uses the derivative method in the frequency domain, yielding exact formula in terms of multiple integrals of the signal, when placed in the time domain. These integrals are explicitly solved by projecting signal on some set of orthogonal basis functions or, more in general, by using a polynomial that fits data in the least-squares sense. The method is able to deal with the case of nonuniform sampled signal.

Keywords Bitumen structure; NMR; rheology; Prony method; relaxation time

1. Introduction

A bitumen is a complex system of different chemical constituents, mainly hydrocarbons and, to a lesser extent, heteroatoms. After bitumen fractionation by specific solvents, four main chemical families are obtained, i.e., saturates, aromatics, resins, asphaltenes [1–4]. Asphaltene sheets are essentially highly polycondensed pseudomonomers with a carbon backbone, chemical functions, and heteroatoms surrounded by aliphatic chains. The aggregation of asphaltenes within the oily medium maltenes leads to formation of macrostructures so that the system is similar to a micellar arrangement.

To obtain structural information about bitumens, microscopy and diffusion techniques have to be implemented. As matter of fact, the presence of an oil phase disturbs normal observation through microscopy and the bitumen has to endure preparation to exclude the

*Address correspondence to Luigi Filippelli, Department of Chemistry, University of Calabria, Via P. Bucci, Cubo 14/D - 87036 Arcavacata di Rende, Cosenza, Italy. Tel.: 00390984493381. E-mail: l.filippelli@unical.it

oil phase. Clearly, this creates artifacts as the original structure is lost. Diffusion techniques always have to be performed in very diluted systems; hence, changes in the concentration of the components can change the structures and structural properties because bitumens behave as colloidal systems.

To preserve the bitumen structure, a freeze-fracturing method can be used. Dickie et al. [5], by means of spraying/evaporation techniques of diluted (0.1%) Boscan asphalt, found associated asphaltene particles with a length of 15–30 nm, and 2–3 nm for individual polyhedral particles. Donnet et al. [6] used scanning electron microscopy (SEM), and observed that pure asphalt consists of a network structure. Loeber et al [7] compared three different microscopy techniques, namely SEM, atomic force microscopy (AFM), and fluorescence microscopy. They found comparable results for the bitumen they studied and concluded that pure gel bitumen forms a network structure made of small spherical particles, the asphaltenes, with a diameter of about 100–200 nm and a network porosity of about 6 μm.

According to the colloidal picture, asphaltenes form micelles that are dispersed in an oily medium and stabilized by resins [8]. The nature of the interactions between asphaltene micelles decides the sol (Newtonian) or gel (non-Newtonian) character of a given bitumen. Structurally, the sol type occurs when the asphaltenes micelles are fully dispersed and noninteracting each other. The non-Newtonian behavior is due to a gel arrangement resulting from the interconnected asphaltene micelles [9]. The sol–gel structure is a coexistence of sol-type micelles and a gel structure. The role of the resins as stabilizers of asphaltenes was confirmed, and it was demonstrated that the asphaltenes would precipitate from the oily bitumen components if resins are not present [10].

New methods for the characterization of bituminous materials are developing [11–16]. Many rheological techniques are demonstrated to be a valuable and more sensitive way to assess bitumen properties than the conventional tests [17]. In addition, a deeper knowledge of the chemical composition as well as the morphology of the bituminous binder is essential to design new additives and the relative obtained materials.

Hence, we performed rheological tests and exploited nuclear magnetic resonance (NMR) to find new analytical approaches and a correlation between molecular organization and mechanical behavior. In the present work, we have investigated pure bitumen, and the morphological characterization was performed by means of stress relaxation rheology and ^{1}H-NMR spin-spin relaxation (T_2) [18].

We assumed that the NMR and rheological relaxation times spectra are fingerprints of the structures present in the system [19,20]. We have obtained these typical relaxation times from a multiexponential fitting of the experimental data, based on a Prony-like method.

Additionally, for the first time, we commented on a possible a correlation between NMR and rheological relaxation spectra. In fact, the interaction nature of the NMR T_2 relaxation times is strongly related to the rigidity of the system, and consequently, to the rheological relaxation times.

2. Experimental Section

2.1. Material and Samples

As fresh standard, a 70/100 penetration-grade bitumen made in Saudi Arabia was used. Samples were simply produced by warming up the material to 120°C and pouring it onto the rheometer plate and into the NMR tube.

2.2. Rheological Measurements

The rheological study in this contribution was performed using a strain-controlled rheometer (Rheometrics RFS III; Rheometrics Inc., Piscataway, NJ) equipped with parallel plates ($\varphi = 25$ mm) in the temperature range 20°C–120°C ± 0.1°C (by a Peltier temperature system). Stress relaxation experiments were performed. For all experiments, a strain value of $\gamma_0 = 10\%$, within the linear viscoelastic region, was applied (chosen by preliminary strain sweep tests).

Stress relaxation experiments were conducted by applying a constant strain throughout the experiment and recording the stress decay $\sigma(t)$ versus time. The transient shear modulus, $G(t)$, was obtained as $G(t) = \sigma(t)/\gamma_0$, where γ_0 is the applied strain. The sample was loaded at 100°C, giving a liquid phase. Then, the temperature was cooled to 20°C and kept for 10 minutes, which were sufficient to reach the micellar equilibrium phase. Successively, the sample was heated to the desired temperature to be investigated. This procedure guarantees to have the same initial structure and to observe reproducible $G(t)$ decays.

2.3. NMR Relaxation Experiments

For the ^{1}H spin-spin relaxation measurements, a home-made NMR instrument has been used. It operates at a proton frequency of 15 MHz. Measurements have been performed at different temperatures ranging from 100°C to 40°C, with an error of ±0.1°C. A classic Carr–Purcell (CP) pulse sequence has been used to record the echo decay [21]. The applied width of $\pi/2$ pulse was 5.9 μsec. The delay time was 0.05 msec. In a basic NMR concept, atom nuclei are excited by absorbing a specific radiofrequency. To relax back to equilibrium, nuclei follow two mechanisms, which correspond to characteristic times of the systems, namely T_1 and T_2. The first accounts for the so-called spin-lattice relaxation process. The second is called the spin-spin relaxation time, because the relaxation is concerned with the exchange of energy between spins via a flip-flop-type mechanism.

In a perfectly homogeneous field, the NMR time constant of the decay would be T_2, but, in fact, the signal decays in a time $T_2{}^*$, which often is determined primarily by field inhomogeneity. A method for overcoming the inhomogeneity problem is to apply the CP technique [21]. If the CP envelope has a mono-exponential decay, the relaxation time T_2 of the sample can be obtained by fitting the data to the following equation:

$$A_n = A_0 e^{-\frac{2n\tau}{T_2}}, \tag{1}$$

where A_n is the amplitude of the nth echo in the echo train and A_0 is a constant depending on the sample magnetization, filling factor, and other experimental parameters. Since the T_2 relaxation time varies all over the sample, a multiexponential attenuation of the CP envelope should be observed.

3. Discussion

In general, decaying experimental data in various scientific fields can be interpreted as combination of decreasing exponential functions, according to an expression of the type

$$y(t) = A \int_0^\infty P(\tau)\, e^{-\frac{t}{\tau}} dt, \tag{2}$$

where $P(\tau)$ is the probability density function of the decaying time τ [15]. This τ assumes different physical-chemical meanings and notations depending on whether it represents the spin-spin relaxation time (T_2) or the rheological stress relaxation time.

If $P(\tau)$ is significantly different from zero only around a finite number N of discrete values, as we expect in our case, it is possible to approximate (2) as weighted discrete sum of exponential functions:

$$y(t) \cong \sum_{i=1}^{N} A_i e^{-\frac{t}{\tau_i}}, \tag{3}$$

with

$$A > 0 \text{ and } \tau > 0, \tag{4}$$

where τ_i represents the local ith maximum of the related $P(\tau)$. This exponential sum model is frequently used in heat diffusion, diffusion of chemical compounds, time series in medicine, physical sciences, and technology [22].

However, the use of (3) to fit experimental data is a notoriously ill-conditioned problem, very sensitive to the presence of noise [23], and already with only two or three exponentials, small changes in experimental data can lead to dramatic fluctuations in fitting parameters. Also, the determination of the correct number of terms to be used in the fit is an open question [24].

Then, it is crucial to find a good method for the evaluation of parameters in exponential sums (5). In this work, a Prony-like method for noisy and nonuniform sampling [25] is used to perform an exponential fitting in the form:

$$y(t) = \sum_{i=1}^{N\text{exp}} R_i \cdot e^{t \cdot p_i}, \tag{5}$$

with

$$R_i,\ p_i \in \mathbf{C}. \tag{6}$$

Clearly, $A_i = R_i$ and $\tau_i = -\frac{1}{p_i}$.

In general, Prony's method is a noniterative parametric technique for modeling damped signals with a linear combination of decaying exponentials. In its original version, it is based on two separate least-squares solutions, each of order N, with the first least-squares solution resulting in the frequencies of the signal, and the second yielding the weighting terms (or residues) in the summation. Various changes to the original procedure have been introduced to increase the performance of the method, especially in the case of experimental data with noise. In particular, the fitting method in [25], based on the algebraic derivative method in the frequency domain [25,26], uses a new linear regression equation that utilizes filtered signals obtained directly from the experimental measurements. More in detail, multiple integrals of $y(t)$ in the regression equation give a very robust estimation even in the case of large measurement noise superimposed on the signal.

While in the classical Prony's method, the roots of the regression equation are expressed in terms of the elementary symmetric functions [27] on $e^{t_s \times p_i}$ ($i = 1, \ldots, N_{\text{exp}}$), where t_s is the sampling time ($s = 1, \ldots, k$), in the method [25], the roots contain the elementary symmetric functions on $p_i, i = 1, \ldots, N_{\text{exp}}$. Furthermore, this method does not require that the experimental data are sampled at a constant time interval.

In this work, for each series of experimental data $y_{\exp}(t) = \{y_{\exp}(t_1), y_{\exp}(t_2), \ldots, y_{\exp}(t_K)\}$, the fitting function (5) has been calculated for $1 \leq N_{\exp} \leq 4$. For each fitting function $y_{\exp}^{(N)}$ thus obtained, the "distance" from the experimental data has been calculated as

$$d_N = \sqrt{\sum_{j=1}^{K} \left(y_{\text{fit}}^{(N)}(t_j) - y_{\exp}(t_j)\right)^2}. \tag{7}$$

The choice of the optimal number N of terms in the exponential fit (5) was performed according to the minimum value of (7), also taking into account the "behavior" of the Prony-like method used in this work, varying N. The adopted method obeys the conditions (6), which are more general than (4), which, however, guarantee the physical sense of the problem under discussion.

If therefore, increasing N, R_i and p_i do not satisfy (4), this result is rejected, even if the distance (7) between the experimental data and the new fitting function is improved.

Another possible situation occurs if N increases: two pairs of complex conjugated values (R_l, p_l) and (R_m, p_m) appear [25]. In this case, if $R_l = a + ib$, $p_l = \alpha + i\beta$, and $R_m = a - ib$, $p_m = \alpha - i\beta$ are the complex values obtained, the contribution to the (5) of the two terms in l and m is

$$\begin{aligned} R_l \cdot e^{t \cdot p_l} + R_m \cdot e^{t \cdot p_m} &= (a + ib) \cdot e^{t \cdot (\alpha + i\beta)} + (a - ib) \cdot e^{t \cdot (\alpha - i\beta)} = \cdots \\ \cdots &= 2e^{t\alpha} \left(a \cos t\beta - b \sin t\beta\right). \end{aligned} \tag{8}$$

Therefore, in the case of complex conjugate values for R_l and p_l, instead of having two exponentials, a single exponential function multiplied by an oscillating factor is obtained.

In conclusion, to determine the number N in (5), the minimum value of (7) is considered, excluding, however, the cases in which there are fit parameters that do not satisfy (4) or that are in the form (8). This mathematical treatment has been applied to the practical case of the bitumen as it is a colloidal system trying to extrapolate the relaxation times that correspond to the given aggregates within the material.

The relaxation behavior for bitumen in the temperature range 40°C–100°C was examined by mechanical stress relaxation and NMR echo-decay experiments. Figure 1 shows the modulus decay and the NMR echo decay versus time at 50°C and 80°C.

Relaxation times greater than recording time ($\gg$700 seconds), contained in this stress decay, were excluded by removing the offset on $G(t)$ before the Prony-like method application.

At low temperature, the rheological decay reaches the equilibrium time slowly, while the NMR echo decay goes quickly to zero. In fact, the more rigid is the system (gel-like system), the less is the dissipative stress. Furthermore, if the system is rigid, dipole interactions are more efficient.

This can be appreciated in Figs. 2 and 3, where the τ_i relaxation times obtained by the application of the Prony-like method to the rheological and NMR experiments are shown. For each temperature that was investigated, two relaxation times were found. This indicates that the material is made of two macroaggregates, denoted as asphaltenes and maltenes in Fig. 2, that have different characteristic relaxation times. In other words, in order to extrapolate the typical relaxation times in a general decay experiment, a mono-exponential fitting is usually performed. However, this practice results in an averaged relaxation time that

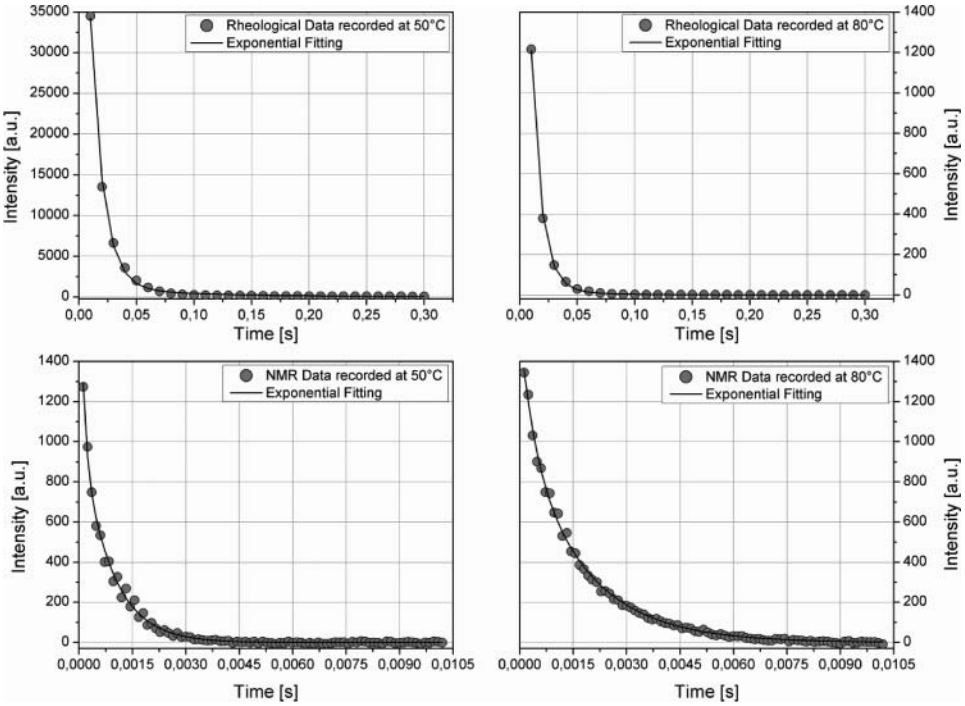

Figure 1. Rheological stress relaxation measurement (upper graphs) and ^{1}H-NMR echo decay for the spin-spin relaxation measurements (lower graphs).

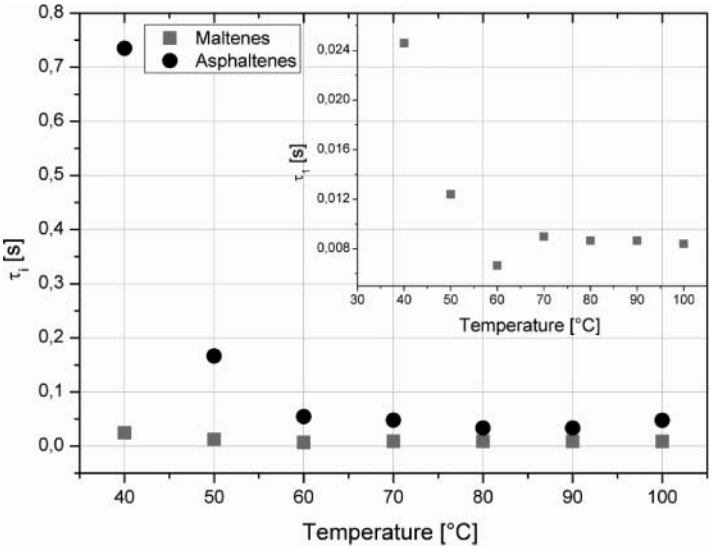

Figure 2. Temperature evolution of the rheological relaxation times obtained by applying the Prony-like method to the stress relaxation decay. The inset shows the enlarged representation of the maltenes τ_1 to remark the exponential decay.

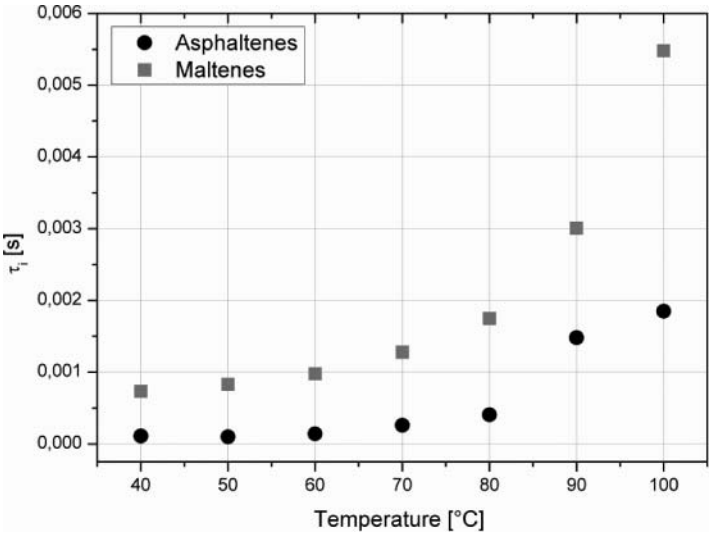

Figure 3. Temperature evolution of the NMR relaxation times obtained by applying the Prony-like method to the exponential echo decay.

does not allow distinguishing the different molecular aggregates that eventually contribute to the decay envelope.

A multiexponential fitting may provide further information on the system, allowing to discriminate between different contributions of the diverse aggregates to the experimental decay. As for the NMR measurement, the shorter relaxation times are due to the asphaltene aggregates, as they are more rigid than the maltenes dispersing oil. Also, rheological

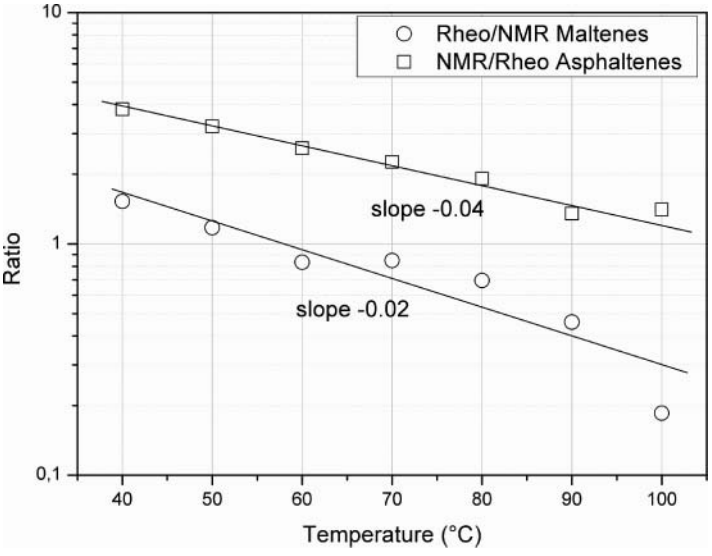

Figure 4. Ratio between rheological stress and NMR relaxations signals in function of the temperature. The line is the linear fitting in semilogarithmic scale.

measurements found two relaxation times, but in this case, the longer times correspond to the asphaltenes fraction. Despite the apparent discrepancy, the results obtained from both techniques are similar if we compare the NMR highest relaxation time to the rheological lowest time at a given temperature.

Data also indicate the occurrence of a complex stress relaxation process characterized by short and long time scales. The relaxation processes relative to the fast times (<1 second) can be attributed to the disruption and formation of aggregates [28,29]. The long relaxation times probably correspond to the progressive orientation loss of the aggregates in order to reach an equilibrium structure within a sample.

Figure 4 shows rheological/NMR relaxation time ratios as a function of the temperature, and it is worth noting that the trend is linear. This may indicate that a correlation between the two relaxation processes exists.

4. Conclusions

This work reports on the application of Prony-like method to the rheological and NMR decay experiments performed on a bitumen binder. This method has been described and implemented here, and it revealed itself as efficient in allowing the identification of two different mean relaxation times, which correspond to the maltenes and asphaltenes fractions of the investigated bitumen. We observed also the relaxation times' temperature dependence and found also the typical sol–gel transition for this system. By comparing data from the two experimental techniques we used here, we also conclude that a correlation between the rheological and the NMR relaxation times could be observed, which although deducible, was never shown before.

References

[1] Barth, E. J. (1962). *Asphalt: Science and Technology*, Gordon and Breach Science Publishers: New York.
[2] Witherspoon, P. A., & Winniford, R. S. (1967). *The Asphaltic Petroleum Geochemistry*, Elsevier: Amsterdam.
[3] Yen, T. F., Erdman, J. G., & Pollack, S. (1962). *Anal. Chem.*, *33*, 1587.
[4] Baldino, N., Gabriele, D., Oliviero Rossi, C., Seta, L., Lupi, F. R., & Caputo, P. (2012). *Constr. Build. Mater.*, *36*, 592.
[5] Dickie, J. P., HaUer, M. N., & Yen, T. F. (1969). *J. Colloid Interface Sci.*, *29*, 47518.
[6] Donnet, J. B., Ducret, J., Papirer, E., & Kennel, M. (1973). *J. Microsc.*, *17*, 139.
[7] Loeber, L., Sutton, O., Morel, J., Valleton, J., & Muller, G. (1996). *J. Microsc.*, *182*, 32.
[8] Speight, J. G. (1991). *The Chemistry and Technology of Petroleum*, Marcel Dekker: New York.
[9] Pfeiffer, J. P., & Saal, R. N. J. (1940). *J. Phys. Chem.*, *44*, 139.
[10] Koots, J. A., & Speight, J. G. (1975). *Fuel*, *54*, 179.
[11] Bernard, C. H. F., & Phillips, C. R. (1979). *Fuel*, *58*, 557.
[12] Zhao, B., & Shaw, J. M. (2007). *Energy Fuels*, *21*, 2795.
[13] Zhang, Y., Takanohashi, T., Sato, S., Saito, I., & Tanaka, R. (2004). *Energy Fuels*, *18*, 283.
[14] Zhang, Y., Takanohashi, T., Shishido, T., Sato, S., Saito, I., & Tanaka, R. (2005). *Energy Fuels*, *19*, 1023.
[15] Gentile, L., Filippelli, L., Oliviero Rossi, C., Baldino, N., & Ranieri, G. A. (2012). *Mol. Cryst. Liq. Cryst.*, *558*, 1.
[16] Filippelli, L., Gentile, L., Oliviero, Rossi C., Ranieri, G. A., & Antunes, E. F. (2013). *Industr. Eng. Chem. Res.*, *51*, 16346.
[17] Ala, B., Bazyleva, M. D., Hasan, A., Fulem, M., Becerra, M., & Shaw, J. M. (2010). *J. Chem. Eng. Data*, *55*, 1389.

[18] Bakhmutov, V. I. (2004). *Practical NMR Relaxation for Chemists*, John Wiley & Sons: Chichester.
[19] Abhijit, P., Deshpande, J., Murali Krishnan, P. B., & Sunil, K. (2010). *Polymer Rheology in Rheology of Complex Fluids*, Springer: New York.
[20] Farrar, T. C., & Becker, E. D. (1971). *Pulse and Fourier Transform NMR*, Academic Press: New York.
[21] Carr, H. Y., & Purcell, E. M. (1954). *Phys. Rev.*, *94*, 630.
[22] Holmstrom, K., & Petersson, J. (2002). *Math. Comput.*, *126*, 31.
[23] Bromage, G. E. (1983). *Comput. Physics Commun.*, *30*, 229.
[24] Holt, J. N., & Antill, R. J. (1977). *Math. Biosciences*, *36*, 319.
[25] Coluccio, L., Eisinberg, A., & Fedele, G. (2007). *Signal Process.*, *87*, 2484.
[26] Fedele, G. (2009). *J. Franklin Inst.*, *346*, 1.
[27] Eisinberg, A., & Fedele, G. (2005). *Calcolo*, 42.
[28] Gentile, L., Silva, B., Balog, S., Mortensen, K., & Olsson, U. (2012). *J. Colloid Interface Science*, *372*, 32.
[29] Coppola, L., Gianferri, R., Oliviero Rossi, C., & Ranieri, G. A. (2003). *J. Colloid Interface Science*, *264*, 554.

I&EC research
Industrial & Engineering Chemistry Research

Article

pubs.acs.org/IECR

Structural Change of Bitumen in the Recycling Process by Using Rheology and NMR

Luigi Filippelli,*[,†] Luigi Gentile,[†] Cesare Oliviero Rossi,[†] Giuseppe A. Ranieri,[†] and Filipe E. Antunes[‡]

[†]Department of Chemistry, University of Calabria, 87036 Arcavacata di Rende (CS), Italy

[‡]Department of Chemistry, University of Coimbra, 3004-535 Coimbra, Portugal

ABSTRACT: The mechanical properties of bitumen are the result of the chemical composition and arrangement of the molecular structures (phases present). The loss of elasticity of the bitumen with aging is mainly due to the oxidation of aromatic compounds and resins. This work deals with the recycling process of bitumen, by following the changes in the bitumen structure. Fresh, aged, and doped recycled bitumens were investigated. Rheology and nuclear magnetic resonance were used to monitor the differences between the bitumens and the role of the additives. As a novel approach to the understanding of the colloidal nature of the bitumen, an inverse Laplace transform of the NMR spin-echo decay (T_2) was applied. The results indicate that the rejuvenating additives have little influence on the solid−liquid transition. However, they help to restructure the aged bitumen, thus facilitating workability at a lower temperature. Two-dimensional maps of the structure distributions were reconstructed.

1. INTRODUCTION

In the bitumen recycling method, doping substances play a crucial role to ensure a more efficient industrial process. The study of the action of these chemicals can give information on the understanding of the supramolecular arrangement of bitumen structure, thus contributing to the expansion of knowledge about the colloidal nature of the bitumen. Many researchers have devoted their efforts to understanding the influence of the colloidal arrangement of bitumen on its modification and usage for different applications.[1−8] In this bitumen depiction, asphaltenes and maltenes represent two of the major constituents in the bituminous materials, with asphaltenes as the dispersed phase and maltenes as the continuous phase. Asphaltenes are formed by condensed polyaromatic structures containing alkyl chains and hetero-aromatic compounds with sulfur present in benzothiophene rings and nitrogen present in pyrrole and pyridine rings. In addition, asphaltenes may contain polyfunctional molecules with nitrogen, such as amines and amides, oxygen, and nickel and vanadium metals complexed with pyrrole nitrogen atoms in porphyrin rings. Considering their chemical composition, asphaltenes are considered the rigid portion of the material. Maltenes are the soft part of the material and are constituted by resins, aromatic hydrocarbons, olefins, cyclic saturated hydrocarbons, and straight or branched chain saturated hydrocarbons (paraffins).[1−8]

Nowadays, the majority of the global production of bitumen each year is for the road paving industry, where it is employed as binders for mineral aggregates to produce asphalt mixes or what are usually called "asphalts". Once the asphalt has been laid to build the roads, bitumen has to become sufficiently rigid at the highest pavement temperature to oppose rutting. At the same time, it must stay flexible enough at the lowest pavement temperature to resist cracking. However, after a certain operative time, several degradation phenomena, such as aging effects and adverse climatic events, cause a high demand for pavement replacement. Today, there is much attention paid to the environmental impact of the production processes of bitumens, and at the same time special attention is devoted to energy cost saving. On those grounds, road paving companies remove and recycle deteriorated aged asphalt (RAP, reclaimed asphalt pavement) that is scratched out from roadways by huge mechanical tools.[9]

Scheme 1. Sketch of Possible Supramolecular Arrangement[a]

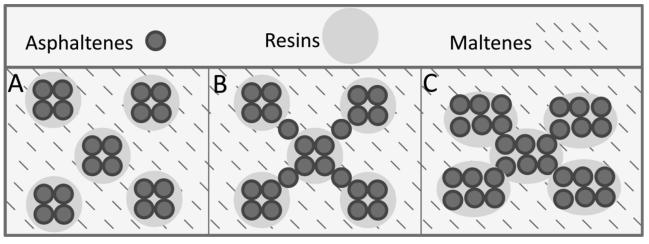

[a](A) Sol-like bitumen. (B) Gel-like bitumen. (C) Oxidized bitumen.

In general, aged bitumens have higher reprocessing temperatures because some of their aromatic components and resins, which are responsible for a certain grade of mobility, are oxidized to asphaltenes and reduced to saturates. Hence asphaltene micelles became larger so that the fluidity of the system is reduced (Scheme 1).[10] In order to regenerate used bituminous materials, currently a doping step utilizing substances that make bitumen performance suitable for a reuse is performed. The mechanical properties of bitumen are strongly dependent on the chemical−physical interactions between different phases within the material. So far, the correlation between the supramolecular level and the macro-behavior of the material is still poorly described. Indeed, the

Received: July 17, 2012
Revised: November 20, 2012
Accepted: November 20, 2012
Published: November 20, 2012

characterization of bituminous materials for their application is still made by empirical standardized tests. The reason for this is because the bitumen chemistry is very complex, since this material contains many different chemical entities. Indeed, bitumen mainly consists of carbon (80−88 wt %) and hydrogen atoms (8−12 wt %), with a hydrogen-to-carbon molar ratio H/C around 1.5. The H/C ratio is midway between those of aromatic structures (benzene has H/C = 1) and saturated alkanes (H/C < 2).[11] Sulfur is the polar atom mostly found in bitumen and is present as sulfides, thiols, and sulfoxides. Ketones, phenols, and, to a lesser extent, carboxylic acids are the chemicals containing oxygen, while nitrogen is present in pyrrolic and pyridinic structures. This huge amount of chemicals varies a lot depending on the source of production, and overall their supramolecular arrangement is still a matter of controversy. Indeed, two different views are still oppose each other: the "homogeneous" and the "inhomogeneous" models.[12] The first describes bitumen as a disperse polar fluid, DPF, and explains asphalt microstructure as a continuous association of polar molecules (asphaltenes) dispersed in a fluid of nonpolar or relatively low polarity molecules. The monotonic time dependence of bitumen viscoelasticity was taken as a key argument in support of the DPF model.[12,13] However, the inhomogeneous view has received much more scientific validation, and currently the colloidal picture of bitumen is the most credited model.[14−16] In this representation, asphaltenes form micelles that are dispersed in an oily medium and stabilized by resins.[17] The nature of the interactions between asphaltene micelles determines the sol (Newtonian) or gel (non-Newtonian) character of a given bitumen (Scheme 1). Structurally, the sol type occurs when the asphaltene micelles are fully dispersed and noninteracting. The non-Newtonian behavior is due to a gel arrangement of interconnected asphaltene micelles.[18] The sol−gel structure consists of a coexistence of sol-type micelles and a gel structure. The role of the resins as stabilizers of asphaltenes was confirmed, and it was demonstrated that the asphaltenes would precipitate from the oily bitumen components without the resins.[19] At least 75% of the original resin content is necessary to avoid asphaltene precipitation.[19] According to this view, resins are able to mediate the differences in polarity between the asphaltenes and the maltenes, and stabilize the system.[20] It is usually established that the main chemical consequences induced by bitumen aging is the loss of aromatics that leads to the formation of asphaltenes.[21−23] The result is a harder bitumen that needs to be brought to higher temperatures to be reprocessed. However, the temperature can be reduced by using suitable additives.

In the present study, we focus on understanding the physical−chemical interactions between two regenerating commercial substances and bitumen. To reach this goal, we performed rheological tests and exploited nuclear magnetic resonance by applying the inverse Laplace transform to the spin-echo decay (T_2). We also contribute to supporting the colloidal view of the bitumen structure.

2. MATERIALS AND METHODS

2.1. Materials. As a fresh standard, a 70/100 penetration grade bitumen produced in Saudi Arabia was used. The 70/100 is a standard bitumen usually employed for paving roads. This penetration grade indicates that a standard needle loaded with 100 gr on top traveled into the bitumen specimen for a length comprised between 7 and 10 mm. Aged bitumen was obtained directly from roads by means of the UNI EN 12697/35 procedure. The inert materials were heated to 200 °C and fresh bitumen (4 wt % of the mixture) was warmed to 160 °C, while the asphalt removed directly from roads (30 wt % of the mixture) was left at room temperature. A Infratest Laboratory 30 L mixer was used to prepare the conglomerate, and after 120 s it was poured into a metallic container. After that, a 5 kg sample was distilled to 1 kg by means of a Tecnotest bitumen extractor with a Pyrex jar, using perchloroethylene as solvent. To separate the filler from the perchloroethylene/bitumen solution, a Tecnotest steady flow centrifuge was used. The solvent was evaporated by means of a Tecnotest cut-back electric distiller, and then a rotavapor procedure removed all the solvents. To make the conglomerate reprocessable, two commercial additives were used to obtain two different materials. StarDope ACF20 (ACF20) was added in a 0.9 wt % ratio to the recycled conglomerate. ACF20 is a mixture of aromatic oils and a mix of amidic surfactants. This additive is considered an adhesive promoter for the bitumen to the inert materials.[24] The benzosulfonamide WarmMix-L (WML) was added in a 0.4 wt % ratio in order to lower the temperature of the fresh inert materials in the reprocessing procedure to make new asphalt mix.[25] The benzosulfonamide molecule is supposed to act as a organosurfactant on the surface tension of the bituminous mixture.

All the products and their preparation were obtained in collaboration with StarAsphalt S.p.A., S.P. Piana Loc. Garga, 87010 Saracena (CS), Italy.

2.2. Empirical Characterization. Asphaltenes were isolated from bitumens according to the procedure described by Altgelt and Boduszynski.[26] A 2−3 g sample of bitumen was dissolved in a volume (in milliliters) of toluene numerically equal to the weight of the sample. A volume of pentane equal to 40 times the toluene was added. The mixture was shaken and then kept in the dark during precipitation for 2 h with occasional shaking. Asphaltenes were collected on a Büchner funnel filter, washed with pentane until the filtrate was colorless, dried, and weighed; the asphaltenes received additional "purification" by repetition of the reprecipitation procedure.

The ring and ball test [ASTM Standard D36-D36M, 2009] was used to determine the bitumen softening temperature (R&B). The test was performed by the ring and ball apparatus B530 (Tecnotest, Italy). A bitumen sample was poured into two standard brass rings, and the obtained specimens were kept at room temperature for 30 min. The samples were then placed in a support provided of two guides for centering two steel balls, one for each ring, and finally they were immersed in a thermostatted bath at 5 °C. After a conditioning period, to guarantee a uniform sample temperature, the steel balls were put on the bitumen specimens. The temperature was then increased at a rate of 5 °C/min. When the balls reached a plate positioned on the first level under the rings, the softening temperature was recorded. According to the standard procedure (ASTM D946), the bitumen consistency was evaluated by measuring the penetration depth (PN) (531/2-T101, Tecnotest, Italy).

2.3. Rheological Characterization. To explore the structural changes induced by temperature, a rheological characterization has been performed. In particular, temperature-ramp test experiments have been performed on the bitumen. Rheological measurements have been conducted using a shear stress controlled rheometer SR5 (Rheometrics, USA) equipped with plate−plate geometry (gap 2.0 mm,

diameter 25 mm). The temperature has been controlled by a Peltier system (±0.1 °C). All the experiments have been performed in cooling ramps and were carried out by using dynamic shear technique. The small amplitude dynamic tests provided information on the linear viscoelastic behavior of materials through the determination of the complex shear modulus[27,28]

$$G^*(\omega) = G'(\omega) + iG''(\omega) \quad (1)$$

where $G'(\omega)$ is the in-phase (or storage) component and $G''(\omega)$ is the out-of-phase (or loss) component. $G'(\omega)$ is a measure of the reversible, elastic energy, while $G''(\omega)$ represents the irreversible viscous dissipation of the mechanical energy. The loss tangent, $\tan(\delta)$, is a measure of the ratio of energy lost to energy stored in a deformation cycle.

$$\tan(\delta) = \frac{G''(\omega)}{G'(\omega)} \quad (2)$$

The rheological behavior at different temperatures has been investigated by a time cure test (temperature-ramp test) at 1 Hz with a cooling ramp rate of 1 °C/min. The applied shear stress of 100 Pa was selected to allow for dynamic rheological tests within the linear viscoelastic region.

2.4. NMR Measurement and Inverse Laplace Transform. For the ^{1}H spin−spin relaxation measurements, a homemade NMR instrument has been used. It operates at a proton frequency of 15 MHz. Measurements have been performed at different temperatures from +120 to +25 °C with an error of ±0.1 °C (Eurotherm temperature controller). The applied width of $\pi/2$ pulse was 5.9 μs. In a basic NMR concept, at equilibrium, nuclei are distributed among the energy levels according to a Boltzmann distribution. Following any process that disrupts this distribution (e.g., absorption of radio frequency energy), the nuclear spin system returns to equilibrium with its surroundings (the "lattice") by a first-order relaxation process characterized by a time T_1 called the spin−lattice relaxation time. To account for processes that cause the nuclear spins to come to equilibrium with each other, a second time T_2 is required. T_2 is called the spin−spin relaxation time, because the relaxation is concerned with the exchange of energy between spins via a flip-flop type mechanism.

In a perfectly homogeneous field the NMR time constant of the decay would be T_2, but, in fact, the signal decays in a time T_2* that often is determined primarily by field inhomogeneity, since nuclei in different parts of the field precess at slightly different frequencies and hence quickly get out of phase with each other. Thus the signal decays with a characteristic time T_2*. This decay directly measures the decrease in the transverse magnetization M_{xy}. The contribution of the magnetic field inhomogeneity to the free induction decay precludes the use of this decay time, T_2* as a measure of T_2. A method for overcoming the inhomogeneity problem is to apply the Carr−Purcell technique (CP).[29] This method may be described as a 90°, τ, 180°, 2τ, 180°, 2τ, 180°, 2τ, ... pulse sequence. The 180° pulses are applied at 90° phase difference relative to the initial 90° pulse, and the τ time delay was 0.05 ms. The main advantage of such a multiple echo technique is its quickness compared with other techniques based on single echoes. Consequently, it allows multiple accumulations of the echo train signal, which is an important issue in low-field experiments where the detection sensitivity is strongly reduced relative to the high-field experiments. If the CP envelope has a monoexponential decay, the relaxation time T_2 of the sample can be obtained by fitting the n data to the following equation:

$$A_n = A_0 e^{-2n\tau/T_2} \quad (3)$$

where A_n is the amplitude of the nth echo in the echo train and A_0 is a constant depending on the sample magnetization, filling factor, and other experimental parameters. Usually the T_2 relaxation time varies all over the sample because of the sample heterogeneity or surface relaxation differences; then a multiexponential attenuation of the CP envelope should be observed. Hence, if inside the sample a continuous distribution of relaxation times exists, the amplitude of the nth echo in the echo train is given by

$$A_n = A_0 \int_0^\infty P(T_2) e^{-2n\tau/T_2}\, dT_2 \quad (4)$$

where $P(T_2)$ is the T_2 relaxation time probability density. Equation 4 suggests that the analysis of the experimental data using an inverse Laplace transform (ILT) might provide the relaxation time probability function. The ILT is a well-known mathematical tool,[30] and it can give the answers required in several fields (spectroscopic techniques, digital electronics, and so on) where it needs to face the inverse problem of estimating the desired function from the noisy measurements of experimental data. Anyway, for convenience, we will shortly recall the definition of the problem.

Let $f(t)$ be a function defined for $t \geq 0$; the function $F(s)$ introduced by means of the expression

$$F(s) = L\{f(t)\} = \int_0^\infty e^{-st} f(t)\, dt \quad (5)$$

is the real Laplace transform of $f(t)$. The inverse process, indicated by the notation $f(t) = L^{-1}[F(s)]$, is termed the inverse Laplace transform (ILT). In the present work a nonnegative, linearly regularized ILT on experimental T_2 decay has been performed. To obtain numerical ILT, we developed a homemade software based on the Tikhonov regularization method[31] by means of Matlab code (release 6.5, The Mathworks Inc., Natick, MA, USA). This is an iterative fitting software, and it has been improved in order to extrapolate the data from the experimental T_2 decay.

3. RESULTS AND DISCUSSION

In the present work we investigated four types of samples based on a 70/100 penetration grade bitumen: fresh, extracted from deteriorated aged asphalt, and recycled with two different doping substances. We first performed an empirical standard characterization by measuring the penetration depth (PN), the softening point (R&B) of the samples, and the temperature interval at which the viscoelastic−liquid transition occurs. Looking at the values reported in Table 1, we see, as expected, that the extracted bitumen is harder than the fresh bitumen: PN is lower while the transition and the R&B temperatures are higher in the extracted bitumen. This is due to the presence of oxidized aged bitumen in the recycled material and to a partial oxidation of the fresh plain bitumen after reaching the temperature of production. The two extracted samples, to which the doping substances were added, have very close values of PN and R&B compared to that of the extracted bitumen without additives (Table 1). However, the additives make the regenerated conglomerate (bituminous mixture) processable at lower temperatures, about 40 °C lower than the ordinary

Table 1. Standardized Tests

sample	PN[a] (mm)	R&B[b] (°C)	SCR-ΔT[c] (°C)	X_A[d] (wt %)
fresh bitumen	72	48	60−64	10.5
extracted bitumen	31	59	98−105	19
extracted + 0.9% ACF20	29	62	95−101	18
extracted + 0.4% WML	33	59	92−98	18.5

[a]Penetration depth. [b]Softening point. [c]Viscoelastic to liquid transition. [d]Asphaltene content.

process temperature. This is of great importance in terms of saving energy costs of production and has also a lower environmental impact.

The values obtained from the SCR-ΔT (Stress Controlled Reometry transition temperature) method and from the R&B procedure are not the same. This is explained by considering that the SCR-ΔT analysis is performed in the linear region of the material response, i.e., it is a nonperturbative observation, and then it shows the intrinsic behavior of the material. Nevertheless, the penetration depth and the R&B tests are nonlinear/perturbative measurements; hence they cannot be related to the structure of the material. In addition, the R&B test is a measure of softness rather than an estimation of the viscoelastic to liquid transition point. Rheological temperature-sweep experiments have been exploited to have some information on the structural changes induced by temperature, to better define a transition temperature range. Figure 1 shows the time cure for all of the investigated samples. The temperature at which the elastic modulus G' shows an inflection point can be considered as the beginning of the transition temperature region, and the whole transition process, from viscous to liquid regime, ends when the G' modulus is no longer detectable. It can be confirmed that the addition of the doping substances slightly reduces the transition temperature (solid to liquid). Fresh bitumen has a higher loss modulus (G'') than the storage modulus (G') along the considered temperature range, while oxidized (aged) samples (with or without additive) show closer moduli values, and even similar at low temperatures. These data are indicative of the higher fluidity in the fresh bitumen. For all samples both moduli decrease with heating. The thermal effects are more evident on the elastic component. At a critical temperature, G' falls sharply, becoming lower than the minimum detectable value and evidencing the complete transition from a viscoelastic to a viscous liquid regime. This rheological behavior is often described by a colloidal model, considering bitumen as a multidisperse micellar system with a rather complex internal structure based on asphaltene micelles dispersed within a maltene phase.[32,33] According to this model, the bitumen can be described as a weak gel made by asphaltene aggregates interacting each other and entrapping the liquid maltene phase.[33] Hence the specific rheological properties should depend on the asphaltene content and particle−particle interactions.

The transition is better evidenced when the loss tangent (tan δ) is plotted as a function of temperature. The initial trend is almost linear with temperature, when the material mainly behaves like a viscoelastic system. The subsequent sharp increase occurs in correspondence of the transition toward a liquidlike behavior. Even though the typical trend is quite similar for the different samples, a discrepancy in transition temperatures and in the numerical values of the moduli is clearly observed. The extracted and recycled materials have

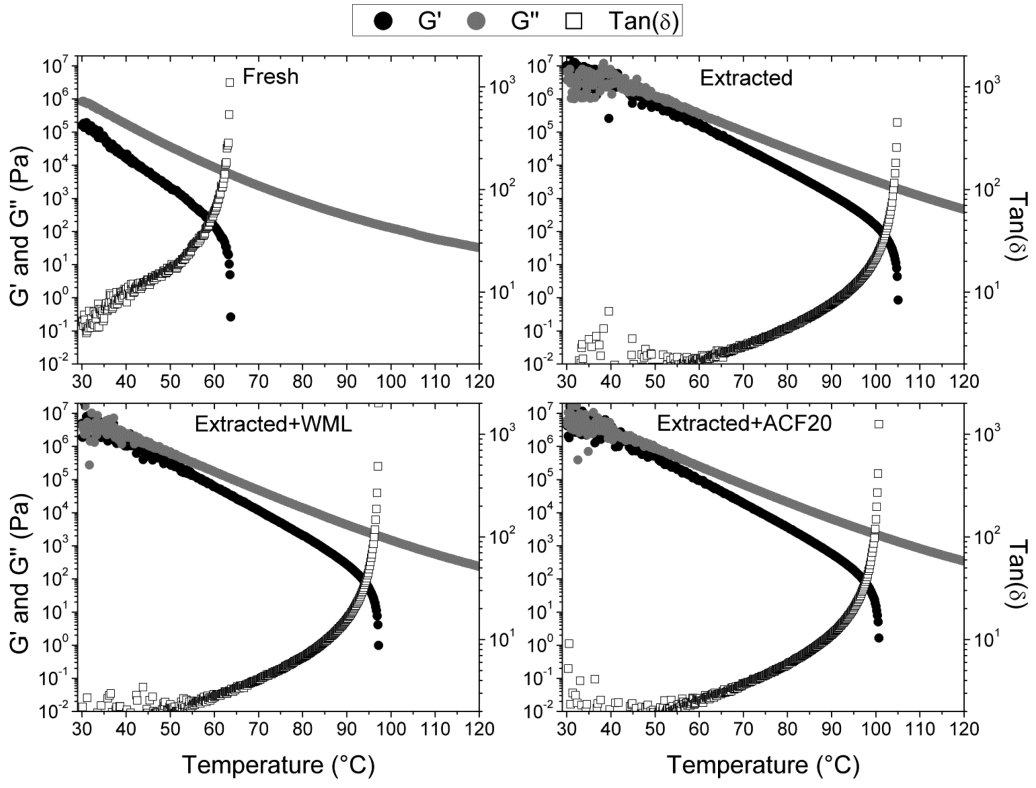

Figure 1. Semilog plots of time cure tests at 1 Hz in the range 30−120 °C for all of the bitumen samples. Black dots represent G', gray dots represent G'', and square symbols represent tan(δ).

dx.doi.org/10.1021/ie301899v | Ind. Eng. Chem. Res. 2012, 51, 16346−16353

much higher transition temperatures than the fresh material. Most likely this effect is the result of an increased fraction of asphaltenes due to the oxidation processes of the soft resinous materials. This asphaltene enrichment might cause a stronger rigidity and connectivity, if compared to the less dense network of the plain bitumen where the asphaltene domains are poorly connected to each other. Both ACF20 and WML induce a slight shift toward lower transition temperatures from the viscoelastic to liquid regime (Table 1). They also reduce the values of G' and G'' moduli, thus making the system less viscous than the simply extracted product. The additive WML seems to have a greater effect in terms of loss of rigidity. As already mentioned, this additive has an amphiphilic nature. We believe that this behavior might reduce the associative interactions between the asphaltene particles by interposing itself between the asphaltenes and the maltenes. This phenomenon might be similar to the one found in the deactivation of hydrophobic cross-links in hydrophobically modified polymers by surfactants.[34,35] This effect results in a weakening of the colloidal network, which in turn may give rise to a lowering of the transition temperature. In order to better clarify the description at a supramolecular level to the oxidized extracted bitumen and the correspondent products with additives, we performed a ^{1}H NMR analysis by measuring the T_2 relaxation times through a monoexponential fitting of the echo decay in a classic Carr−Purcell pulse sequence at different temperatures (Figure 2).

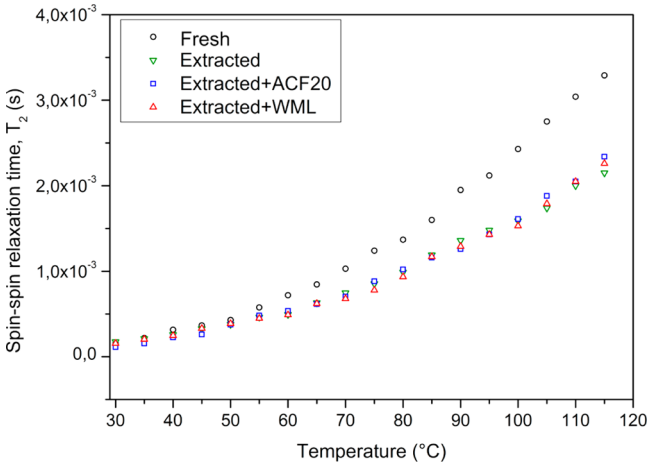

Figure 2. Dependence of ^{1}H NMR T_2 relaxation time on temperature for the investigated bitumens.

Considering the description given under Materials and Methods, the spin−spin relaxation time (T_2) of a material can be a measure of the molecular mobility under certain conditions. The relaxation process is, in fact, more efficient when the material is more rigid; that corresponds to shorter relaxation times. As matter of the fact, higher mobility corresponds to longer T_2 times. Hence, the proton T_2 time along temperature was measured for all the samples. The results, shown in Figure 2, indicate that the fresh bitumen has the greatest mobility (softest). When the material is not homogeneous, the measured T_2 is averaged over all the contributions of the different macrostructures due to their own characteristic mobility. Each macrostructure has its own intramolecular arrangement and interactions, and it is reasonable to think that they relax back to the equilibrium at different characteristic T_2 times, contributing to the measured echo envelope differently. A sophisticated mathematical process to obtain the T_2 distribution times corresponding to the different molecular aggregates regards the application of an inverse Laplace transform (ILT) to the measured echo envelope. Figure 3 shows the ILT at 90 °C of the investigated samples.

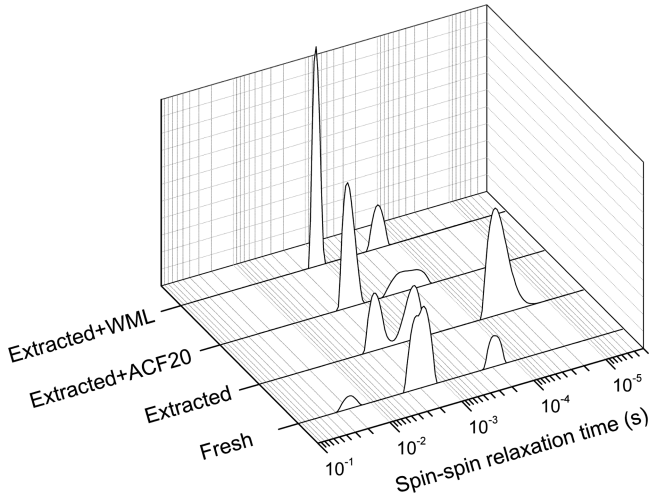

Figure 3. Inverse Laplace transform of the measured ^{1}H NMR echo decay at 90 °C for all of the samples.

The peaks reported in Figure 3 represent the distribution of the spin−spin relaxation times for the bituminous materials. Each peak corresponds to the T_2 time distribution of a given macroaggregate inside the material, where shorter T_2 times correspond to more rigid fractions. This finding weakens the DPF description of bitumen structure. Indeed, if the polar fluid model was valid for our system, the ILT result would have been a single broad peak referred to a continuous T_2 time distribution. Hence, in the frame of the colloidal model of bitumen, shorter T_2 times should correspond to the asphaltene fraction while longer spin−spin relaxation times should correspond to the maltene fraction. Intermediate T_2 times should represent resins, which are expected to have an intermediate mobility between asphaltenes and maltenes. The ILT of the echo signal decay for the fresh bitumen at 90 °C (Figure 3) shows that three macroaggregates constitute the material. The peak centered at 2×10^{-2} s represents a distinct soft fraction, referable to the maltenes that have the greatest mobility inside the material, while the other two peaks centered at 2×10^{-3} and 2×10^{-4} s represent the resins and the asphaltene fractions, respectively. In Figure 3, the extracted bitumen is the only material that presents a peak that falls at T_2 time 5×10^{-5} s. This peak is attributable to the very rigid and well-connected asphaltene fraction, which very likely comes from the oxidized aged road pavement. On the other hand, it is clear that the addition of ACF20 and WML to the extracted bitumen makes the asphaltene peaks shift to longer T_2 times, around 2×10^{-4} s. This picture, for the samples at 90 °C, becomes clearer and very interesting when the ILT results are plotted along the investigated temperature range. Figure 4 is a two-dimensional representation of the T_2 time distributions for the fresh bitumen at temperatures ranging from +25 to +120 °C. The upper temperature limit has been chosen to avoid further oxidation processes.

dx.doi.org/10.1021/ie301899v | Ind. Eng. Chem. Res. 2012, 51, 16346−16353

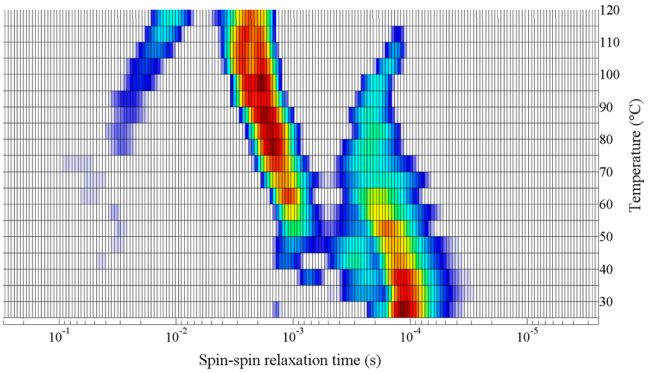

Figure 4. Two-dimensional plot of the T_2 time distributions for fresh bitumen in the temperature range 25−120 °C. Colors represent the intensities of the peaks in arbitrary units, taking white as the baseline and dark red as the highest intensity.

This representation can be considered as the map of the distribution of the different aggregates at the different temperatures. Colors represent the intensities of the peaks in arbitrary units, with white being the baseline and dark red being the highest intensity. It can be seen that at low temperatures the T_2 times are concentrated and centered around 10^{-4} s, and this indicates that the material is quite homogeneous. However, by progressively raising the temperature, there is a clear differentiation between the asphaltene (on the right of the map), resins (in the middle of the map), and the softest fraction (maltenes), which is visible between 10^{-1} and 10^{-2} s. If we look at the T_2 distribution map of the extracted bitumen (Figure 5),

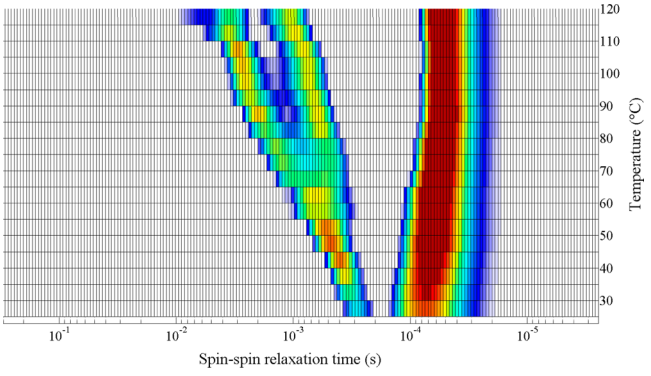

Figure 5. Two-dimensional plot of the T_2 time distributions for extracted bitumen in the temperature range 25−120 °C. Colors represent the intensities of the peaks in arbitrary units, taking white as the baseline and dark red as the highest intensity.

this maltene fraction appears to have a lower mobility as a consequence of the recycling procedure and of the oxidative processes. The harder feature of this oxidized bitumen is evident from the compact peaks that fall at T_2 times between 10^{-4} and 10^{-5} s (the red line on the right of Figure 5), being almost unchanged along temperatures. This is due to the enrichment of the very rigid asphaltene component.[15] At lower temperature the extracted bitumen shows two distribution peaks. Raising the temperature, the mobile component splits (on the left in Figure 5), highlighting also the resins.

The T_2 distribution map of the extracted bitumen with the ACF20 additive (Figure 6) shows that the asphaltene fraction is no longer compact and rigid as it was in the one just extracted. This can be deduced by the longer T_2 times that reflect a better

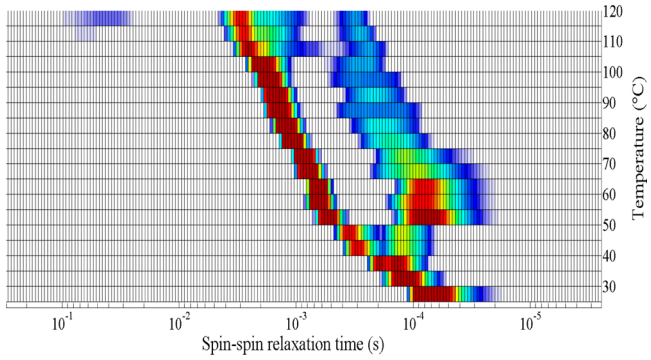

Figure 6. Two-dimensional map of the T_2 time distributions for extracted bitumen + ACF20 in the temperature range 25−120 °C. Colors represent the intensities of the peaks in arbitrary units, taking white as the baseline and dark red as the highest intensity.

mobility of the asphaltenes. This is probably due to a better dispersion of the asphaltene particles promoted by the aromatic oils and to the lowering of the surface tension, induced by the amidic component of the ACF20. Furthermore, at 120 °C a very light fraction appears (T_2 times close to 1×10^{-1}), as a consequence of the rejuvenated oily medium.

In the case of the system containing WML (Figure 7), the T_2 distribution map also reveals that the asphaltene fraction is less

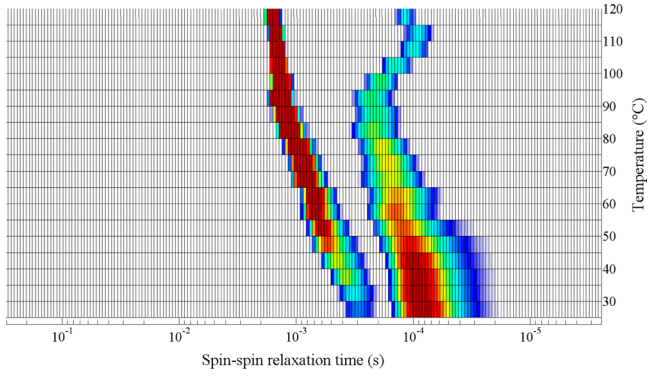

Figure 7. Two-dimensional map of the T_2 time distributions for extracted bitumen + WML in the temperature range 25−120 °C. Colors represent the intensities of the peaks in arbitrary units, taking white as the baseline and dark red as the highest intensity.

rigid. In addition, the material seems to be structured in a better defined network with asphaltene micellar phase well dispersed into the maltene−resin oily medium. This can be deduced by the net compartmentalization of the two components; i.e., the peaks are quite sharp and differentiated along the temperature range. This seems consistent with the fact that this additive has the greatest effect in lowering the transition temperature of the extracted bitumen (Table 1).

4. CONCLUSIONS

Fresh, extracted, and recycled bitumen were characterized by NMR and rheology. We reported a new analytical approach to improve the usual bitumen classification and to evaluate the structural changes caused by aging and the given additives in the recycling procedure. On a 70/100 penetration grade bitumen, we performed standard empirical tests, rheology analysis, spin−spin proton relaxation time measurements, and the inverse Laplace transform to draw a map of the

dx.doi.org/10.1021/ie301899v | Ind. Eng. Chem. Res. 2012, 51, 16346−16353

macroaggregates inside bitumen at different temperatures. In order to compare the natural aging and the recycling procedure effects, the same experiments were performed on the bitumen extracted from a real aged road asphalt mix, to which was afterward added two commercial doping substances working as rejuvenating agents. Our findings are in agreement with a colloidal depiction of the macromolecular organization of bitumen with an enhanced occurrence of asphaltenes in the aged and recycled bitumens. ILT provided the suggestion that the asphaltene−asphaltene interactions are much greater in the aged and recycled bitumens and gave also indications of the possible modification introduced by the additives ACF20 and WML. Both doping substances, added to the aged bitumen, induced a slight lowering of the temperature transition from the viscoelastic to liquid regime. Additives had a low impact on G' and G'' moduli. However, the doping substances made the asphalt conglomerate workable at 160 °C, well below the standard 200 °C required in the recycling process of RAP. This is probably due to the restructuring of the recycled bitumen conglomerate by promoting a more ordered asphaltene network. WML seems to have a better impact on the restructuring of the asphaltene network. This last observation needs to be further investigated, due to potential benefits of understanding the details of this phenomenon to improve the recycling process.

AUTHOR INFORMATION

Corresponding Author

*E-mail: l.filippelli@unical.it. Tel.: +39.0984.49.33.81.

Notes

The authors declare no competing financial interest.

ACKNOWLEDGMENTS

We thank StarAsphalt S.p.A., S.P. Piana Loc. Garga, 87010 Saracena (CS), Italy, for supporting this work.

REFERENCES

(1) Carrera, V.; Partal, P.; García-Morales, M.; Gallegos, C.; Páez, A. Influence of Bitumen Colloidal Nature on the Design of Isocyanate-Based Bituminous Products with Enhanced Rheological Properties. *Ind. Eng. Chem. Res.* **2009**, *48*, 8464.

(2) Johnson, S. E.; Svrcek, W. Y.; Mehrotra, A. K. Viscosity prediction of Athabasca bitumen using the extended principle of corresponding states. *Ind. Eng. Chem. Res.* **1987**, *26*, 2290.

(3) Knotnerus, J. Bitumen Durability—Measurement by Oxygen Absorption. *Ind. Eng. Chem. Prod. Res. Dev.* **1972**, *11*, 411.

(4) Long, J.; Zhang, L.; Xu, Z.; Masliyah, H. J. Colloidal Interactions between Langmuir−Blodgett Bitumen Films and Fine Solid Particles. *Langmuir* **2006**, *22*, 8831.

(5) Kotlyar, L. S.; Sparks, B. D.; Woods, J. R.; Chung, K. H. Solids Associated with the Asphaltene Fraction of Oil Sands Bitumen. *Energy Fuels* **1999**, *13*, 346.

(6) Liu, J.; Xu, Z.; Masliyah, J. Studies on Bitumen−Silica Interaction in Aqueous Solutions by Atomic Force Microscopy. *Langmuir* **2003**, *19*, 3911.

(7) Baldino, N.; Gabriele, D.; Oliviero Rossi, C.; Seta, L.; Lupi, F. R.; Caputo, P. Low temperature rheology of polyphosphoric acid (PPA) added bitumen. *Constr. Build. Mater.* **2012**, *36*, 592.

(8) Gentile, L.; Filippelli, L.; Oliviero Rossi, C.; Baldino, N.; Ranieri, G. A. Rheological and H-NMR spin-spin relaxation time for the evaluation of the effects of PPA addition on bitumen. *Mol. Cryst. Liq. Cryst.* **2012**, *558*, 1.

(9) Karlsson, R.; Isacsson, U. Material-Related Aspects of Asphalt Recycling—State-of-the-Art. *J. Mater. Civ. Eng.* **2006**, *18*, 81.

(10) Illston, J. M.; Domone, P. *Construction Materials: Their Nature and Behaviour*; Taylor & Francis e-Library: New York, 2010.

(11) Branthaver, J. F.; Petersen, J. C.; Robertson, R. E.; Duvall, J. J.; Kim, S. S.; Harnsberger, P. M.; Mill, T.; Ensley, E. K.; Barbour, F. A.; Scharbron, J. F. *Binder Characterization and Evaluation*; National Research Council: Washington, DC, 1994; Vol. 2.

(12) Petersen, J. C.; Robertson, R. E.; Branthaver, J. F.; Harnsberger, P. M.; Duvall, J. J.; Kim, S. S.; Anderson, D. A.; Christiansen, D. W.; Bahia, H. U. *Binder Characterization and Evaluation*; National Research Council: Washington, DC, 1994; Vol. 1.

(13) Christensen, D. W.; Anderson, D. A. Rheological evidence concerning the molecular architecture of asphalt cements. *Proceedings of the Chemistry of Bitumen*; Rome, 1991; Vol. 2, p 568.

(14) Yen, T. F. The colloidal aspect of a macrostructure of petroleum asphalt. *Fuel Sci. Technol. Int.* **1992**, *10*, 723.

(15) Loeber, L.; Muller, G.; Morel, J.; Sutton, O. Bitumen in colloid science: a chemical, structural and rheological approach. *Fuel* **1998**, *77*, 1443.

(16) Espinat, D.; Rosenberg, E.; Scarsella, M.; Barre, L.; Fenistein, D.; Broseta, D. Colloidal structural evolution from stable to flocculated state of asphaltene solutions and heavy crudes. In *Structures and Dynamics of Asphaltenes*; Mullins, O., Sheu, E. Y., Eds.; Plenum Press: New York, 1998.

(17) Nellensteyn, F. J. The constitution of asphalt. *J. Inst. Pet. Technol.* **1924**, *10*, 311.

(18) Pfeiffer, J. P.; Saal, R. N. J. Asphaltic bitumen as colloid systems. *J. Phys. Chem.* **1940**, *44*, 139.

(19) Koots, J. A.; Speight, J. G. Relation of petroleum resins to asphaltenes. *Fuel* **1975**, *54*, 179.

(20) Murgich, J.; Rodriguez, J. M.; Aray, Y. Molecular recognition and molecular mechanics of micelles of some model asphaltenes and resins. *Energy Fuels* **1996**, *10*, 68.

(21) Moschopedis, S. E.; Speight, J. G. Influence of metal salts on bitumen oxidation. *Fuel* **1978**, *57*, 235.

(22) Siddiqui, M. N.; Ali, M. F. Studies on the ageing behavior of the Arabian asphalts. *Fuel* **1999**, *78*, 1005.

(23) Farcas, F. *Étude d'une méthode de simulation du vieillissement des bitumes sur route*; LCPC Research Report CR21; LCPC: Paris, France, 1998.

(24) StarDope ACF20; Star Asphalt S.p.A, Saracena (CS), Italy. http://starasphalt.com/STARDOPEACF20_engl.PDF (accessed Nov 20, 2012).

(25) WML; Star Asphalt S.p.A, Saracena (CS), Italy. http://www.starasphalt.com/additivi1F_engl.asp (accessed Nov 20, 2012).

(26) Altgelt, K. H.; Boduszynski, M. M. *Composition and Analysis of Heavy Petroleum Fractions*; Marcel Dekker Inc.: New York, 1994.

(27) Ferry, J. D. *Viscoelastic Properties of Polymers*; Wiley: New York, 1980.

(28) Coppola, L.; Gentile, L.; Nicotera, I.; Oliviero Rossi, C.; Ranieri, G. A. Evidence of Formation of Ammonium Perfluorononanoate/^2H_2O Multilamellar Vesicles: Morphological Analysis by Rheology and Rheo-^2H NMR Experiments. *Langmuir* **2010**, *26*, 19060.

(29) Carr, H. Y.; Purcell, E. M. Effects of Diffusion on Free Precession in Nuclear Magnetic Resonance Experiments. *Phys. Rev.* **1954**, *94*, 630.

(30) Ranieri, G. A.; Coppola, L.; Celebre, G.; Oliviero, C. The Structural Fingerprint in Lyotropic Mesophases by the Use of Inverse Laplace Transform Applied to PGSE NMR Data. *Mol. Cryst. Liq. Cryst.* **2002**, *372*, 121.

(31) Tikhonov, A. N.; Arsenin, V. Y. *Solutions of Ill-Posed Problems*; John Wiley & Sons: New York, 1977.

(32) Provencher, S. W. CONTIN: A general purpose constrained regularization program for inverting noisy linear algebraic and integral equations. *Comput. Phys. Commun.* **1982**, *27*, 229.

(33) Lesueur, D. The colloidal structure of bitumen: Consequences on the rheology and on the mechanisms of bitumen modification. *Adv. Colloid Interface Sci.* **2009**, *145*, 42.

(34) Holmberg, K.; Jönsson, B.; Kronberg, B.; Lindman, B. *Surfactants and Polymers in Aqueous Solution*; John Wiley & Sons: New York, 2002.
(35) Antunes, E. F.; Marques, E. F.; Miguel, M. G.; Lindman, B. Polymer−vesicle association. *Adv. Colloid Interface Sci.* **2009**, *147−148*, 18.

5. Results part II - Analysis of the effects of bitumen modifiers and additives for bitumen recycling: Data to be published.

Quantitative evaluation of the restructuring effect of a Warm Mix additive on bitumen recycling production as revealed by atomic force spectroscopy and Inverse Laplace transform of NMR relaxation time.

Luigi Filippelli, Maria P. De Santo, Filipe E. Antunes, Luigi Gentile, Giuseppe A. Ranieri and Cesare Oliviero Rossi

Department of Chemistry and Chemical Technologies, University of Calabria, 87036 Arcavacata di Rende (CS), Italy

Department of Physics, University of Calabria, 87036 Arcavacata di Rende (CS), Italy

Department of Chemistry, University of Coimbra, 3004-535 Coimbra, Portugal

Abstract.

Warm mix asphalt (WMA) is a promising technique that allows the production of asphalt at an noticeably lower temperature. One of the methods in use is to add small quantities of specific organic compounds to the asphalt conglomerate. Although it is well established that this procedure leads to an effective reduction of the temperature of asphalt production, there is still a lacking in the comprehension and description of the real mechanism of the additive action. In this work tridimensional micro-scale atomic force microscopy images (AFM) of fresh, aged and doped bitumen were taken to characterize and study the and interaction of a commercial WMA additive with bitumen. We also combined the AFM results with the inverse Laplace transform (ILT) of the nuclear magnetic resonance (NMR) relaxation times. Results revealed that the temperature lowering in the WMA recycling procedure is due to the restructuring action of the additive that leads to a re-organization of the colloidal network of bitumen.

Introduction.

Recycling asphalt pavement has undoubted environmental and economic advantages as the material can be 100% recycled. Reclaimed Asphalt Pavement (RAP) is none other than the material removed from aged worn out road pavements which contains mineral aggregates and bitumen binder [1]. In order to reuse RAP the hot mixing protocol (HMA) has been used since the 1970s [2]. In the HMA procedure for fresh made asphalt mix, temperatures are around 160 °C. However since aged bitumen become less fluid as some of their organic components are oxidized, the temperature for the RAP recycling has to be raised around 200 °C. It is clear that a noticeably higher amount of energy has to be spent to raise the temperatures with environmental and economic consequences. In addition, at these temperatures the asphalt can emit dangerous substances like polycyclic aromatic

hydrocarbons (HPAs) [3] so that asphalt workers are exposed to enhanced health risks. Alternatively the warm mix asphalt (WMA) refers to technologies which allow a significant reduction of mixing and compaction temperatures . Although there are different technologies and different additives for the production of WMA mixtures, the functionality of the WMA technology is based on the reduction of bitumen binder viscosity within the limits of certain temperature è [4-6] . If the technologies of WMA are incorporated into the mixes containing RAP, optimum mixing and compaction temperatures of the mixes are expected to decrease by at least 30 °C without adversely affecting the asphalt performances. Considering the colloidal nature of the bitumen binder, the WMA-RAP mixes are often chemically supported by small quantity of substances that are used as adhesion promoters, may act on surface tension of the bituminous mixture or used as asphaltenes dispersant agents [7,8]. A rheological description of the effects of the additives on the mechanical performances of some WMA-RAP mixes is commonly given as one have to test the mechanical properties of the asphalt mix for the convenient use [9,10]. Conversely there is still lacking of information on how some WMA additives, used to recycle bitumen binder, affect the molecular structure and arrangement of the bituminous colloidal network. In a previous work we investigated the chemical action of two regenerating commercial substances, StarDope ACF20® and WarmMix-L® (WML), [11,12] exploiting rheology, nuclear magnetic resonance and an innovative approach by applying the inverse Laplace transform to the echo decay of the T2 proton relaxing time [13]. We concluded that especially the WarmMix-L has a restructuring effect on the oxidized-altered colloidal network of the aged bitumen binder so that the temperature of the recycling process was lowered significantly. In the present study we have quantitatively evaluated this restructuring effect combining the NMR and ILT measurements with tridimensional micro-scale atomic force microscopy.

2. MATERIAL AND METHODS

2.1 Materials.

As fresh standard, a 70/100 penetration grade bitumen produced in Saudi Arabia was used. The 70/100 is a standard bitumen usually employed for paving roads. This penetration grade indicates that a standard needle loaded with 100 gr. on top, travelled into the bitumen specimen for a length comprised between 7 and 10 mm. Aged bitumen was obtained directly from roads by means of the UNI EN 12697/35 procedure. The inert materials are heated up to 200 °C, fresh bitumen (4 wt% of the mixture) is warmed up to 160°C, while the asphalt

removed directly from roads (30 wt% of the mixture) is left at room temperature . A Infratest Laboratory mixer 30 l, has been used to prepare the conglomerate and after 120 seconds it has been poured into a metallic container. After that, a 5Kg sample was distilled to 1 kg by means of a Tecnotest bitumen extractor with pyrex jar, using perchloroethylene as solvent. To separate the filler from the perchloroethylene/bitumen solution, a Tecnotest steady flow centrifuge has been used. The solvent was evaporated by means of a Tecnotest cut-back electric distiller, then a rotavapor procedure removed or all the solvents. To make the conglomerate re-processable two commercial additives were used to obtain two different materials. The benzosulfonamide WarmMix-L® (WML) was added in a 0.4 wt% ratio in order to lower the temperature of the fresh inert materials in the re-processing procedure to make new asphalt mix [12]. The benzosulfonamide molecule is supposed to act as a organo-surfactant on the surface tension of the bituminous mixture, hence as an adhesion promoter.
All the products and their preparation were obtained in collaboration with StarAsphalt S.p.A., S.P. Piana Loc. Garga, 87010 - Saracena (CS) – Italy.

2.2 Empirical Characterization.

Asphaltenes were isolated from bitumens according to the procedure described by Altgelt and Boduszynski. A 2 to 3 g sample of bitumen is dissolved in a volume (in ml) of toluene numerically equal to the weight of the sample. A volume of pentane equal to forty times the toluene is added. The mixture is shaken and then kept in the dark during precipitation for 2 h with occasional shaking. Asphaltenes are collected on a Buchner funnel filter, washed with pentane until filtrate is colourless, dried and weighed; in addition the asphaltenes received additional "purification" by repetition of the re-precipitation procedure.
The ring and ball test [ASTM Standard D36-D36M, 2009] was used to determine the bitumen softening temperature (R&B). The test was performed by the ring and ball apparatus B530 (Tecnotest, Italy). A bitumen sample is poured into two standard brass rings and the obtained specimens are kept at room temperature for 30 minutes. The samples were then placed in a support provided of two guides for centring two steel balls, one for each ring, and finally they were immersed in a thermostated bath at 5°C. After a conditioning period, to guarantee a uniform sample temperature, the steel balls are put on the bitumen specimens. The temperature is then increased at a rate of 5°C/min. When the balls reach a plate positioned on the first level under the rings, the softening temperature is recorded. According to the standard procedure (ASTM D946), the bitumen consistency was evaluated by measuring the penetration depth (PN) (531/2-T101, Tecnotest, Italy).

2.3 NMR measurement and Inverse Laplace Transform.

For the ^1H spin-spin relaxation measurements (T_2), a homemade NMR instrument has been used. It operates at a proton frequency of 15 MHz. Measurements have been performed at different temperatures at 30 °C with an error of ± 0.1°C (Eurotherm Temperature Controller). A classic Carr-Purcell pulse sequence (CP) has been used to record the echo decay [15]. The applied width of $\pi/2$ pulse was 5.9 μs. The $\tau 1$ delay time was 0.05 ms. This set-up allows multiple accumulations of the echoes train signal which is an important issue in low-field experiments where the detection sensitivity is strongly reduced. The relaxation time T_2 of the sample can be obtained by fitting the data to the following equation,

$$A_n = A_0 e^{-\frac{2n\tau}{T_2}} \qquad (3)$$

where A_n is the amplitude of the n^{th} echo in the echo train and A_0 is a constant depending on the sample magnetization, filling factor and other experimental parameters. The T_2 relaxation time varies all over the sample due to the sample heterogeneity or surface relaxation differences, then a multi-exponential attenuation of the CP envelope should be observed. If we perform the numerical Inverse Laplace Transform of the NMR echo decay, we may provide the relaxation time probability functions each of which account for the different macro-structures that compose the bitumen binder [17,18]. In the present work a non-negative, linearly regularised ILT on experimental T_2 decay has been performed [19]. To obtain numerical ILT we developed a home-made software based on an iterative fitting software in order to extrapolate the data from the experimental T_2 decay [unpublished data].

2.4 Atomic Force Microscopy.

Atomic Force Microscopy (AFM) has been used to image the surface morphology in tapping mode. In this method the cantilever oscillates up and down close to its resonance frequency, so that the tip enters in contact with the sample surface periodically. When the tip is brought close to the surface, the vibration of the cantilever changes due to the tip-sample interaction. Shifts in the phase angle of vibration when the oscillating tip interacts with the sample surface are related to surface properties as stiffness [20], viscoelasticity and adhesion. An MFP-3D (Asylum Research, CA) has been used for the AFM characterization of the different specimen in air. Silicon probes with resonance frequency 200–400 kHz, nominal tip radius of curvature 10 nm and cantilever length 125 μm, were used. Phase images have been acquired simultaneously with the topography. Materials with different viscoelasticity are clearly

distinguishable [21]. The softer domains appear dark (PB) while the stiffer ones appear bright (PS) in the phase images [23].

2. RESULTS AND DISCUSSION

The rheological behaviour of bitumen binder is currently described by a colloidal model, consisting of a multidisperse micellar system with a composite internal structure of asphaltene micelles dispersed into a maltene phase [24,25]. This model, describes bitumen as a weak gel where asphaltene aggregates interact each other and entrap the liquid maltene phase. Hence the mechanical and rheological properties should depend on the asphaltenes amount and particle-particle connections.

In the present work samples based on a 70/100 penetration grade bitumen were investigated: fresh, extracted from RAP and recycled with WML as rejuvenating agent. Firstly the penetration depth (PN) and the softening point (R&B) were determined with standardized tests (TABLE 1) . As expected, the bitumen extracted from RAP has a harder consistency than the fresh bitumen. This is due to the oxidized aged bitumen present into the recycled material. The penetration depth, the softening point and the asphaltene content is very similar for the extracted and doped bitumen. However, the additive allows to work the recycled conglomerate (asphalt mixture) at about 40 °C lower than the ordinary process temperature. This also allows to lower energy costs production and to have a lower environmental impact.

Table 1. Standardized tests.

SAMPLE	**PN (mm)** Penetration depth	**R&B (°C)** Softening point	**X_A (wt%)** Asphaltene content
Fresh bitumen	78	48	15.5
Extracted bitumen	34	61	18
Extracted+0.4%WML	35	60	17.5

This temperature lowering is due to the presence of the additive in the warm mix recycled conglomerate. The employed benzosulfonamide is considered an adhesion promoter, but the real mechanism through which the additive acts is still to be revealed. In a previous work we investigated a similar system and we supposed that the WML is able to restructure the colloidal network that is deteriorated in an aged bitumen as it is the one extracted from RAP[13]. In order to clarify the role of the WML in the recycling process and to verify the previous we made an atomic force microscopy investigation of the samples. Figure 1 shows the topographic 3D image (left) and the corresponding phase contrast image (right) on a

micro-scale level of the fresh bitumen. In the phase contrast image we can appreciate the asphaltene aggregates corresponding to the white regions. A pseudo-asphaltene network can be noted. The brown regions are attributed to the maltenes phase which is the dispersant of asphaltenes in the colloidal view. Are also clearly visible the characteristic bee-like structures that can be better appreciated in the 3D topography on the left. They are present as protrusion or depression of the surface and very likely are related to the presence of waxes in the bitumen network [26].

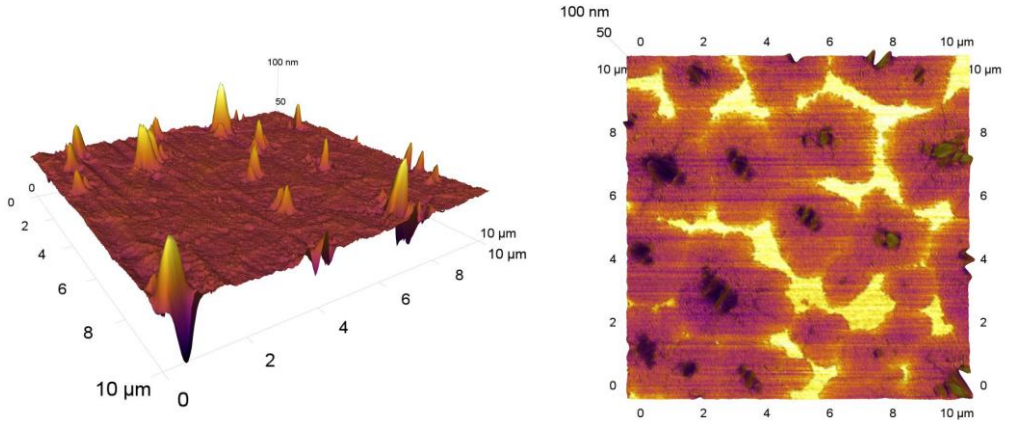

Figure 1. AFM images: (left) 3D topography of the fresh bitumen. (right) AFM Phase contrast of the same specimen.

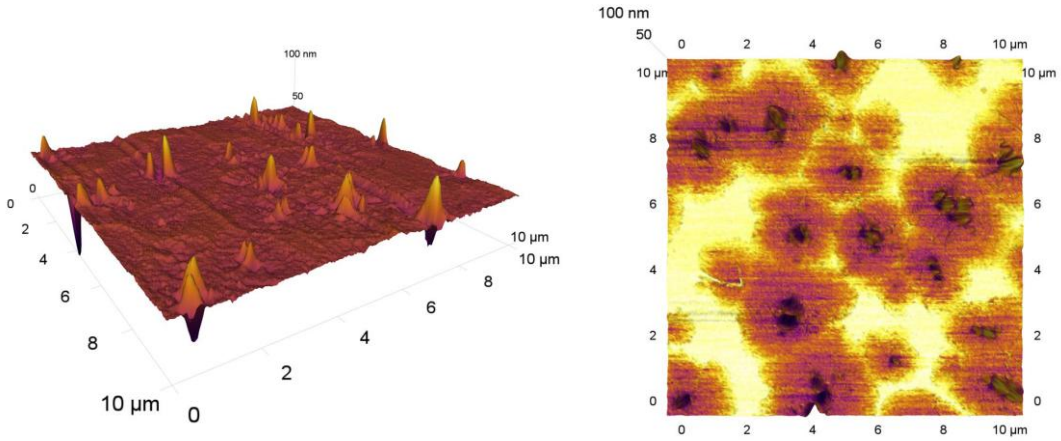

Figure 2. AFM images: (left) 3D topography of the bitumen extracted from RAP. (right) AFM Phase contrast of the same specimen.

Looking at the AFM images of the bitumen extracted from RAP (Figure 2) the differences with the fresh sample are immediately observable. The white region in the phase contrast image are extended. This means that the rigid portions of the material, the asphaltenes, are now more connected each other and this makes the material harder (see table 1) and subject to cracking. The bee-like structures are less prominent, probably the waxes are also more constricted in the asphaltenes network.

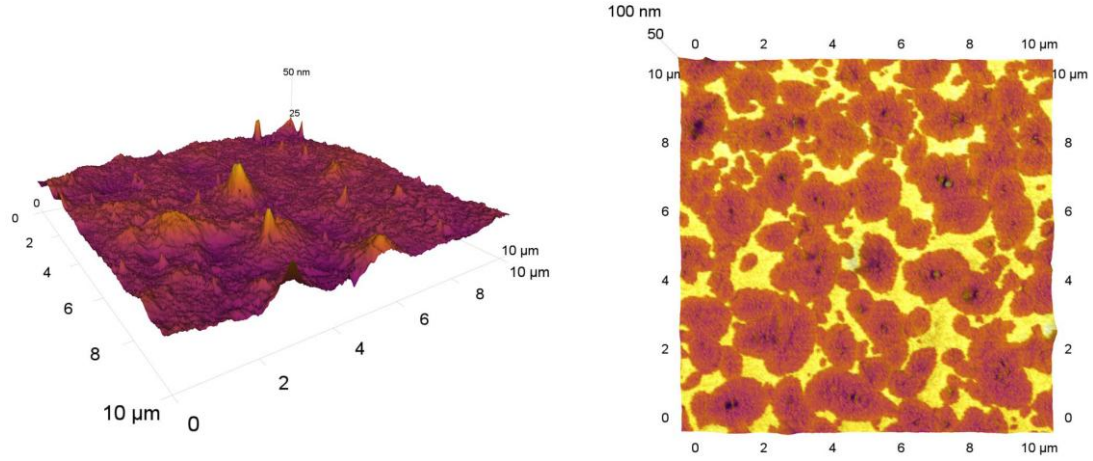

Figure 3. AFM images: (left) 3D topography of the bitumen extracted from RAP+0.4WML. (right) AFM Phase contrast of the same specimen.

When the WML is added to the extracted bitumen the AFM images are that of Figure 3. It can be noted that now the asphaltene particles (white regions) are smaller and uniformly distributed in the sample. As a consequence a ordered but weaker asphaltene network compared to the extracted from RAP (figure 2), is restored. Now the bee-like structures appear smaller and looking at the 3D topography they also appear smoothed. We also have performed the inverse Laplace transform of the echo decay in some T_2 NMR relaxation experiments at room temperature. As previously mentioned, this techniques allows to find the distribution of probability density functions, or in other words we can obtain different relaxation times that correspond to different molecular aggregates inside the samples. Results are shown in figure 4. The plots correlate the distribution as a function of the relaxation time. The shorter is this relaxation time more rigid is the corresponding molecular aggragates. In other words for the system that we are investigating, shorter times are attributed to asphaltene fraction and longer times to maltenes fraction. The ILT for the fresh bitumen present three peaks. The peak that falls around 10^{-4} s is due to asphaltenes; the one centred at 10^{-4} s corresponds to maltenes and the last one falling between 0.01 and 0.10 s is due to volatile and very mobile fraction of the fresh bitumen. Conversely the ILT of the

bitumen extracted from RAP present only two peaks as the volatile fraction disappeared due to the oxidation process in the aged bitumen. In addition the peaks related to the two main components of the sample are shifted toward shorter times so indicating that the material is more rigid. In particular the asphaltene peak is now close to 10^{-5} s. The ILT of the extracted with the WML additive it can be noted that the relaxation times go back to values similar to the fresh but obviously without the presence of the volatile-mobile fraction. If we perform the integration of the peaks area we can obtain the percentage of the different fractions that compose the given material. Results are collected in table 2.

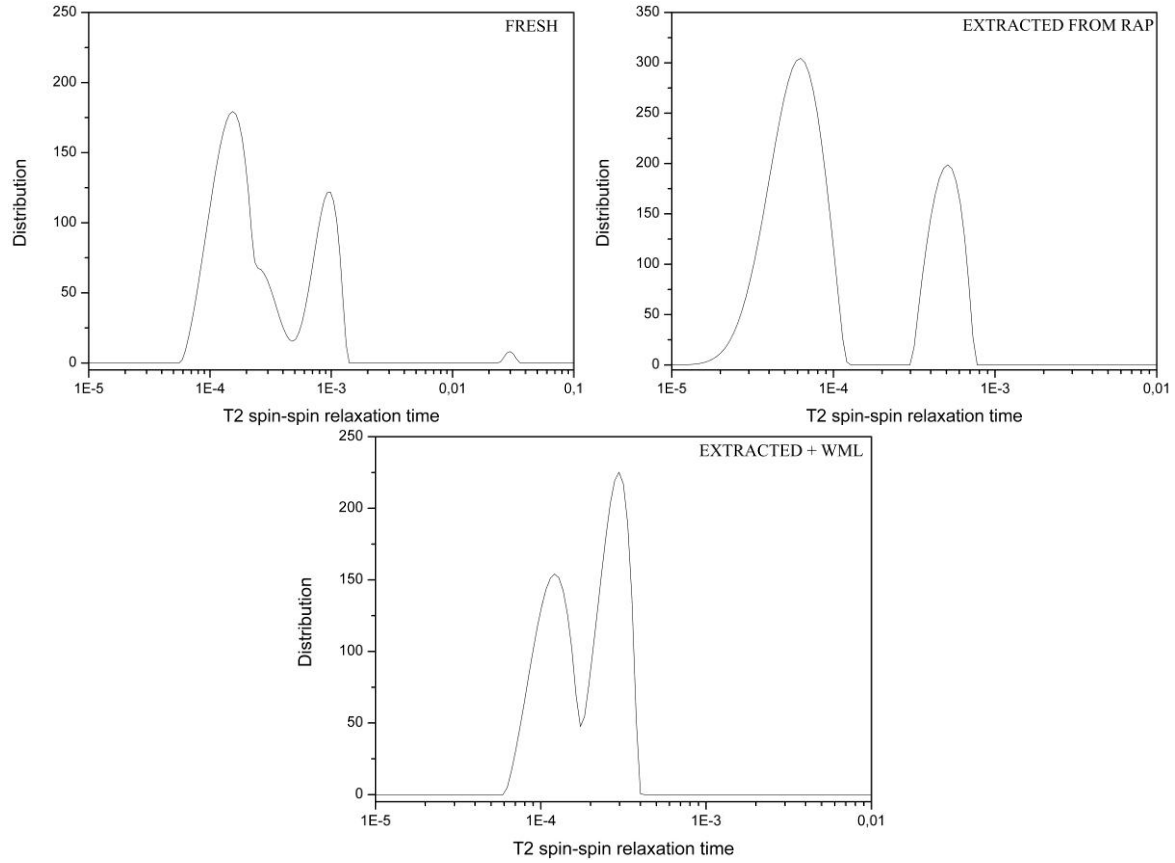

Figure 4. Inverse Laplace Transform of the echo decay in NMR relaxation experiments for the investigated samples.

SAMPLE	Asphaltenes: T_2 (s), ILT Peak Area (%)	Maltenes: T_2 (s), ILT Peak Area (%)	Fluid Volatile Fraction : T_2 (s), ILT Peak Area (%)
Fresh bitumen	$1.50x10^{-4}$; 20%	$1.00x10^{-3}$; 45%	$3x10^{2}$; 35%
Extracted bitumen	$6.30x10^{-5}$; 23%	$5.09x10^{-4}$; 77%	
Extract. +0.4%WML	$7.50x10^{-5}$; 23%	$5.00x10^{-4}$; 77%	

Table 2. Integral of the peaks area for the calculated ILT.

From these data we can say that although the asphaltene content is the same in the bitumen extracted from RAP and in the additivated, the last is more soft as we can appreciate a shift of the relaxation T_2 towards longer times.

Conclusions.

Warm mix asphalt is a promising technique to be also used to recycle aged road pavements. In this work we investigated a commercial additive, WML, to enhance the benefits of this industrial process. By means of AFM we found that the additive is able to restructure the lost colloidal network of an aged bitumen. This very likely is due to the mediator character of the additive which may act as a pseudo-organosurfactant interposing itself between the more polar asphaltenes and the less polar maltenes. The quantitative Inverse Laplace Transform of the echo decay in the NMR spin-spin relaxation time was quite in agreement with the asphaltene content as measured with the conventional procedure [14] and also revealed that the use of the additive does not alter the asphaltene content but make the entire system more fluid namely less viscous, hence more workable at a lower temperature than the usual hot recycling process.

References

[1] Karlsson, R., Isacsson, U. Material-Related Aspects of Asphalt Recycling・State-of-the-Art. J. Mater. Civ. Eng., 18, 81, 2006.

[2] Roberts, F L, Kandhal, P S, Brown, E R, Lee, D-Y, Kennedy, T W Hot Mix Asphalt Materials, Mixture Design And Construction. Second Edition ,National Asphalt Pavement Association Research and Education Foundation 5100 Forbes Boulevard Lanham, MD 20706-4413 USA, 1996.

[3] McKay,J.F. and Latham.D.R. Polyaromatic hydrocarbons in highboiling petroleum distillates: isolation by gel permeation chromatography and identification by fluorescence spectrometry. Anal. Chem., 45, 1050- 1055, 1973.

[4] Hurley, G. C., Prowell, B. D., Evaluation of potential processes for use in warm mix asphalt, Journal of the Association of Asphalt Paving Technologists 75: 41–90, 2006.

[5] Sanchez-Alonso, E.,Vega-Zamanillo, A., Castro-Fresno, D., DelRio-Prat, M. Evaluation of Compactability and Mechanical Properties of Bituminous Mixes with Warm Additives, Construction and Building Materials 25(5): 2304-2311, 2010.

[6] Silva H. M. R. D., Oliveira, J. R. M., Ferreira, C. I. G., Pereira, P. A. A. Assessment of the Performance of Warm Mix Asphalts in Road Pavements, International Journal of Pavement Research and Technology 3(3): 119-127, 2010.

[7] Baldino, N., Gabriele, D., Oliviero Rossi, C.; Seta, L., Lupi, F. R., Caputo, P. Low temperature rheology of polyphosphoric acid (PPA) added bitumen. Constr. Build. Mater., 36, 592, 2012.

[8] Gentile, L., Filippelli, L., Oliviero Rossi, C., Baldino, N., Ranieri, G. A. Rheological and H-NMR spin-spin relaxation time for the evaluation of the effects of PPA addition on bitumen. Mol. Cryst. Liq. Cryst., 558, 1, 2012.

[9] Hakseo Kima, Soon-Jae Leeb, Rheology of warm mix asphalt binders with aged binders, Construction and Building Materials, Volume 25, Issue 1, Pages 183–189, January 2011.

[10] Ali Jamshidia, Meor Othman Hamzaha, Performance of Warm Mix Asphalt containing Sasobit®: State-of-the-art, Construction and Building Materials, Volume 38, , Pages 530–553, January 2013.

[11] StarDope ACF20; Star Asphalt S.p.A, Saracena (CS), Italy. http://starasphalt.com/STARDOPEACF20_engl.PDF (accessed Oct 31, 2013).

[12] WML; Star Asphalt S.p.A, Saracena (CS), Italy. http://www.starasphalt.com/additivi1F_engl.asp (accessed Oct 31, 2013).

[13] Luigi Filippelli, Luigi Gentile, Cesare Oliviero Rossi, Giuseppe A. Ranieri, and Filipe E. Antunes Structural Change of Bitumen in the Recycling Process by Using Rheology and NMR, Ind. Eng. Chem. Res., 51, 16346−16353, 2012.

[14] Altgelt, K. H.; Boduszynski, M. M. Composition and Analysis of Heavy Petroleum Fractions; Marcel Dekker Inc.: New York, 1994.

[15] Carr, H. Y.; Purcell, E. M. Effects of Diffusion on Free Precession in Nuclear Magnetic Resonance Experiments. Phys. Rev., 94, 630, 1954.

[17] S.W. Provencher: A constrained regularization method for inverting data represented by linear algebraic or integral equations. Comput. Phys. Commun. 27, 213, 1982.

[18] S.W. Provencher: CONTIN: A general purpose constrained regularization program for inverting noisy linear algebraic and integral equations. Comput. Phys. Commun. 27, 229, 1982.

[19] Tikhonov, A. N.; Arsenin, V. Y. Solutions of Ill-Posed Problems; John Wiley & Sons: New York, 1977.

[20] S.N. Magonov , V. Elings, M-H Whangbo, Phase imaging and stiffness in tapping-mode atomic force microscopy, Surf. Sci. 375 L385-L391, 1997.

[21] Loeber L, Sutton O, Morel J, Valleton JM, Muller G., New direct observations of asphalts and asphalt binders by scanning electron microscopy and atomic force microscopy., Journal of Microscopy, 182, pages: 32-39, 1996.

[23] Buonomenna MG, Golemme G, Tone CM, De Santo MP, Ciuchi F, Perrotta E, Zappone B, Galiano F, Figoli A, Ordering phenomena in nanostructured poly(styrene-b-butadiene-b-styrene) (SBS) membranes for selective ethanol transport, Journal of Membrane Science, 385 (1-2), pages 162-170, 2011.

[24] Lesueur, D. The colloidal structure of bitumen: Consequences on the rheology and on the mechanisms of bitumen modification. Advances in Colloid and Interface Science, 145, 42, 2009.

[25] Long, J.; Zhang, L.; Xu, Z.; Masliyah, H. J. Colloidal Interactions between Langmuir−Blodgett Bitumen Films and Fine Solid Particles. Langmuir, 22 ,8831, 2006.

[26] Benjamin McCarron "The Investigation of 'Bee-Structures' in Asphalt Binders" Major Qualifying Project 2011-2012, Dept. of Physics, Worcester Polytechnic Institute, (2012).

Rheological performance of ultrasound crumb rubber modified bitumen.

Cesare Oliviero Rossi[*1], Filipe E. Antunes[2], Luigi Filippelli[1], Luigi Gentile[1], Giuseppe A. Ranieri[1]

[1]Department of Chemistry and Chemical Technologies, University of Calabria, Via P. Bucci, Cubo 14/D - 87036 Arcavacata di Rende (Cs), Italy.

[2]Department of Chemistry, University of Coimbra, 3004-535 Coimbra, Portugal.

*e-mail address: cesare.oliviero@unical.it

Abstract.

Several road pavement inconvenience are related to rheological properties of bitumen. Rutting and fatigue cracking are the major distresses that lead to permanent failures in pavement performances [1]. Adding crumb rubber to bitumen is a way to improve bitumen mechanical behaviour. By means of NMR and Rheological dynamic experiments we investigated the influence of ultrasound treated crumb rubber modifier (UCRM) on the structure and rheological properties of bitumen binder at both high and low temperatures. The ultrasounds cause the devulcanization of the crumb rubber and this seems to result into enhanced mechanical properties in a wide range of temperatures. Morphology changes were also analyzed.

1. Introduction

Approximately 9 to 10 kg of rubber from tyres per inhabitant and year are currently discarded in the industrialized societies [2]. It is a waste material with a highly valuable constituent: vulcanized natural and synthetic rubber. Thus, the introduction of crumb rubber in the production of asphalt rubber (AR) mixes for road pavements should be considered as a sustainable technology which transforms an unwanted residue into a new bituminous mixture highly resistant to fatigue and fracture [3].

Additionally the rheological weakness of the conventional bitumen has generated an increasing interest in the use of polymer modified binders to enhance the conventional bitumen properties. A limited number of polymers has been used as modifying agents due to their high cost [4]. Because of the high cost of these polymers compared to bitumen, the amount needed to improve pavement performance should be as small as possible. The use of discarded vehicle tires in pavement construction was one of the steps that were taken in this direction. Research on crumb rubber has been going on for the last three decades [5-9]. The characteristics of crumb rubber depend on the

rubber type, asphalt composition, and size of rubber crumbs, as well as time and temperature of reaction. These factors have considerable affect on pavement performance [10-12].

However, the increasing demands in relation to the quality and durability of pavements lead to the need of a profound knowledge in the physicochemical changes of the materials which constitute the AR binders.

When crumb rubber is blended with bitumen at high temperatures to produce a modified binder, i.e. wet process, the two materials interact as bitumen components migrate into the rubber causing it to swell. Initially, the interaction between CR and bitumen is a non-chemical reaction where the rubber particles are swollen by absorption of the bitumen's aromatic oils [13]. Absorption of bitumen components by the rubber inevitably depletes the bitumen of the absorbed components and, consequently, modifies its properties making it stiffer and more brittle [14].

After substantial swelling occurs the polymer macromolecules may start to separate and transfer to the solvent where they may dissolve completely. This is called the dissolution stage. Dissolution can generally occur only if the vulcanization cross links are thoroughly destroyed and the devulcanization is complete. Rubber polymers with a dense vulcanization grid can only allow minimal swelling so no significant quantity of oil can enter the polymer.

The challenge is to subject the rubber to a devulcanization regime that will produce a substance capable of maximum swelling yet maintaining sufficient cross links to prevent the rubber from dissolving in bitumen.

In this work base bitumens interacted with neat crumb and ultrasound devulcanized crumb rubber in order to produce AR binders.

Devulcanization is the process of cleaving the C-S and S-S bonds in the cross-linked rubber.

There are numerous ways to complete this process but most are expensive, cumbersome, and time-consuming. In this investigation the devulcanization method, utilizes ultrasonic energy to break the C-S and S-S bonds.

In fact the high-energy ultrasound can focus energy into localized sites for selective bond rupture. The research work reported to date suggests that the ultrasonic technology is more suited to convert rubber waste to a usable material efficiently, effectively and environmental friendly, therefore this method can be considered the most efficient method. Thus, the main objective of this paper is to characterize the influence of ultrasound devulcanized crumb rubber on the mechanical properties of the bitumen.

In the present study, we focus on understanding the physical-chemistry interactions between neat and ultrasound devulcanized crumb rubber and bitumen. To reach this goal we performed empirical mechanical test and dynamic rheological tests in a wide temperature range.

2. Experimental section

2.1 Material and Samples

Plain bitumen from Saudi Arabia and Russia), already tested for low temperature behavior [15], were used in this study. The Saudi Arabia bitumen was 70/100 penetration grade bitumens.

The crumb rubber used in this work was obtained by the mechanical means. According to the supplier, the crumb rubber was constituted by truck tyres and car tyres. In addition samples of crumb rubber were supplied ultrasound devulcanized. The sample called 266 is made by ultrasound devulcanized wasted truck tyres and the sample called 277 is also ultrasound devulcanized but the crumb rubber comes from car tyres. The supplied crumb rubber was sieved through a sequence of sieves in the laboratory, in order to use only the fraction passed through the sieve, the size was 0.1-0.5 mm.

The sieved crumb rubber obtained in the laboratory was washed with toluene and dried in an oven at 135 ºC. The clean and dry rubber particles where observed and measured, using an optical microscope . Crumb rubber was also analyzed to determine its soluble percentage (ASTM D 6814-02) [16] and density (apparent and bulk density – AG:PT/T144) [17].

The procedures for the production and collection of samples followed the next steps:

– Heating approximately 1 kg and collection of a sample of base bitumen (B) at 180 ºC;

- Measurement of the bitumen density;

– Introducing 10.0% w/w of crumb rubber (CR) and re-heating of the mix at 180 ºC;

– Measurement of the “asphalt rubber” density;

– Maintain the temperature at 180 ºC, while stirring the “asphalt rubber” at a velocity at 400 rot/min for 120 minutes;

– Measurement of the density and collection of a sample of the asphalt rubber (AR) produced;

– Suspension of the basket in a oven at 180 ºC for 15 min;

– Collection of a sample of the recovered rubber (RR) retained in the basket;

– Measurement of the density and collection of a sample of residual bitumen.

2.2 Rheological Measurements

Rheological tests on bitumen samples were carried out using a shear stress controlled rheometer SR5 (Rheometric Scientific, USA) equipped with a parallel plate geometry (gap 2 mm, Φ 25 mm in the temperature range 20-130°C, gap 2 mm, Φ 8 mm in the temperature range 20-130°C) and a Peltier system (±0.1°C) for temperature control.

Dynamic tests, carried out in conditions of linear material behaviour where measured material functions are independent on the amplitude of applied load and are only function of microstructure [18], were adopted for material characterization. During these tests samples are subjected to oscillatory motions by applying small deformations (or stresses) to maintain linear viscoelastic conditions [19] and the resulting dynamic modulus can be split in two components: the storage modulus, G', being the in-phase part, is a measure of the reversible, elastic energy, whilst the loss modulus, G", being the out-of-phase component represents the irreversible viscous dissipation of the mechanical energy. The dependence of these quantities on the oscillating frequency gives rise to the so-called mechanical spectrum, allowing the quantitative rheological characterization of studied materials [18]. The loss tangent, tan(δ), is a measure of the ratio of energy lost to energy stored in a deformation cycle.

$$\tan(\delta) = \frac{G''(\omega)}{G'(\omega)}$$

Aiming at investigating the material phase transition, temperature sweep tests were performed at 1 Hz increasing temperature from 25 to 120°C at 1 °C/min and applying the proper stress values to guarantee linear viscoelastic conditions (previously determined by stress sweep test) at all tested temperatures. The adopted heating rate represents a suitable compromise between the experimental times and an acceptable accuracy of data.

Aiming at investigating the material at low temperature, temperature sweep tests were performed at 1 Hz decreasing temperature from 20 to -30°C at 1 °C/min and applying the proper stress values to guarantee linear viscoelastic conditions (previously determined by stress sweep test) at all tested temperatures. The adopted cooling/heating rate represents a suitable compromise between the experimental times and an acceptable accuracy of data.

2.3 Empirical characterization

The ring and ball test (ASTM D36-37) [(ASTM Standard D36)-D36M, 2009] is used to determine the bitumen softening temperature (TR&B, ring and ball temperature). The test was performed by ball and ring apparatus B530 (Tecnotest®, Italy). A bitumen sample is poured into two standard brass rings and the obtained specimens are kept at room temperature for 30 minutes and then levelled. Afterwards the samples are placed in a support provided of two guides for centring two steel balls, one for each ring, and finally they are immersed in a thermostatic bath at 5°C (at 30° C if expected TR&B is higher than 80°C). After a conditioning period, to guarantee a uniform sample temperature, spheres are placed on the rings and temperature is increased at 5°C/min. The softening point is reported as the mean of the temperatures at which the two specimens soften enough to allow each ball, enveloped in bitumen, to reach a plate positioned on the first level under the rings.
According to the standard procedure (ASTM D946 / D946M), CNR B.U. 24/71 the bitumen consistency was evaluated by measuring the penetration depth of a stainless steel needle of standard dimensions under determinate charge conditions (100 g), time (5 s) and temperature (25 °C,) using penetrometer 531/2-T101 (Tecnotest®, Italy)..

3. Discussion

In Table 1 the transition temperatures for the investigated samples are reported.

Sample	T °C ± 0.5
Plain	62.9
266	87.4
267	85.9
Piumatti-NOT devulcanized	93.8

Table 1. Transition temperature of samples

As it is possible to observe the sample Piumatti shows higher transition temperature, the sample Plain, that is pure bitumen, presents the lowest transition temperature (62.9 ° C), while the samples 266 and 267 (ultrasound partially de-vulcanized) have similar transition temperatures with a value of about 25 ° C higher than the pure bitumen. Important information can be determined from the analysis of the trends of tan δ throughout the temperature range. The pure sample shows a viscous behavior markedly compared to the other samples. The samples 266, 267 and Piumatti show similar

rheological behaviors, even if the samples 266 and 267 are characterized by values of dynamic viscosity slightly greater than the sample Piumatti (pure bitumen).

The samples 266 and 267 have values of G' lower than the not devulcanized (Piumatti) in the temperature range from 10 to -30 ° C. At low temperatures the samples 266 and 267 show intermediate behavior, considering the values of tan δ , between the pure sample and the sample Piumatti.

The observed data indicate that, at high temperatures, the 266 and 267 have a higher transition temperature than the sample Puro and, having a higher elastic modulus, are able to "recover" a possible further applied deformation.

At low temperatures the samples 266 and 267 have greater tan δ and lower elastic modulus therefore, they better dissipate the applied stress.

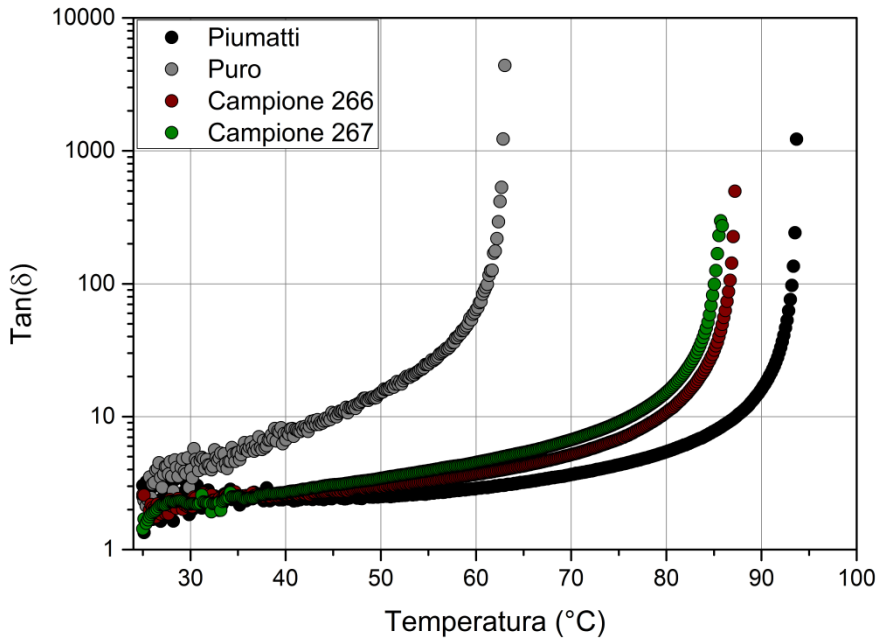

Figure 1. Plot of tan(δ) as a function of temperature.

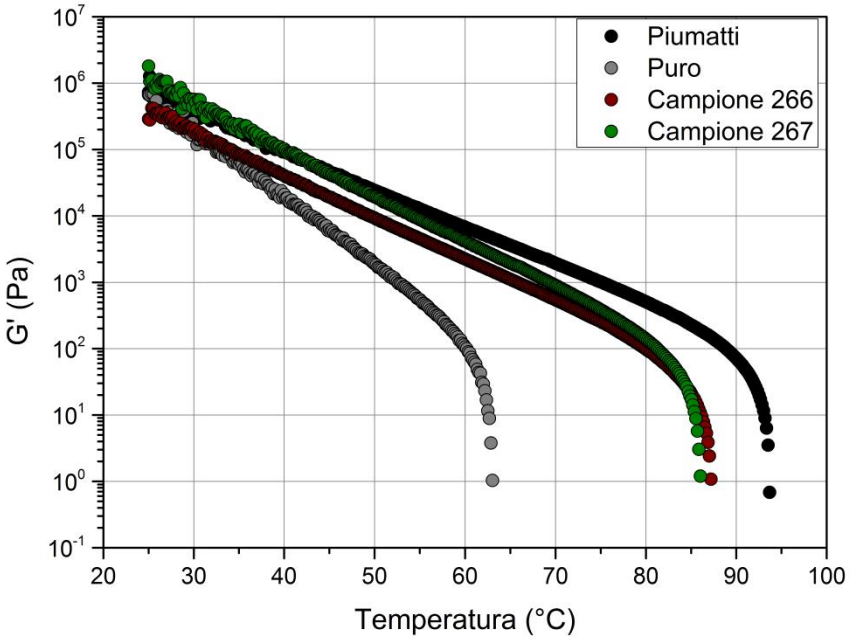

Figure 2. Plot of, G' as function of temperature. Frequency 1Hz, stress 100Pa.

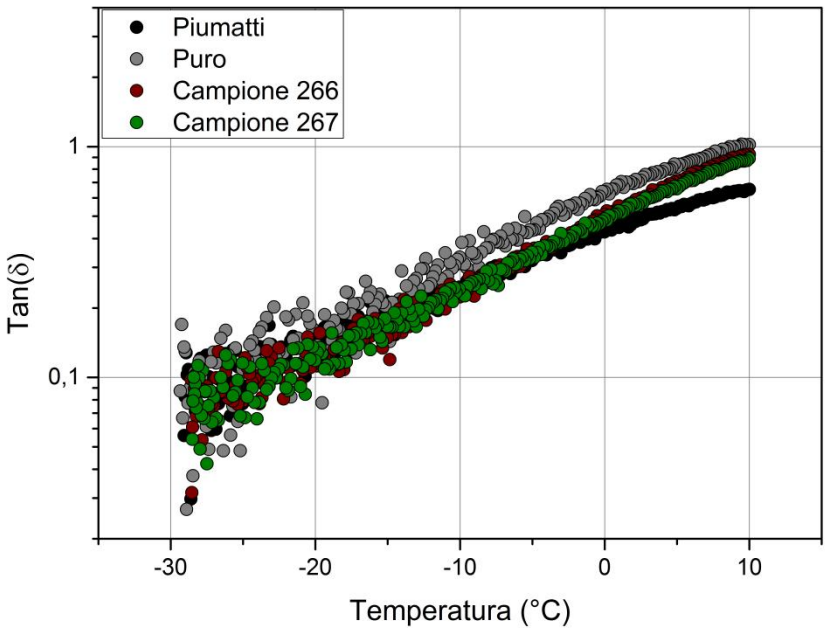

Figure 3. Plot of tan(δ) as a function of temperature. Low temperatures.

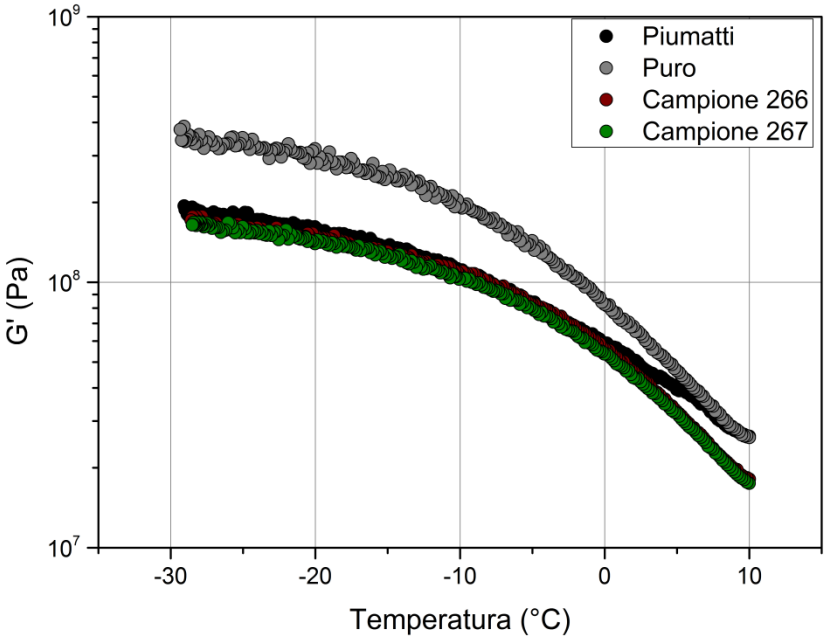

Figure 4. Plot of, G' as function of temperature. Low temperature.

4. Conclusions

The ultrasound devucanized crumb rubber is a technology that enables homogeneity, stability and consistent properties of bitumen binder. To achieve this, a special manufacturing process is adopted and the result is a high performance bituminous binder with unique properties that are consistent. Ultrasound devucanized crumb rubber is ideally suited for hot climates. It enhances the key properties of asphalt mixes, i.e. deformation resistance and fatigue life. These improvements are the result of three crucial physical changes which the polymer makes in the conventional binder structure: reduces temperature susceptibility, increases stiffness modulus and enhances elasticity.

References

[1] The Asphalt Handbook ISBN 193415427X , Ed. Asphalt Institute (first published January 1st 1989). (2007).

[2] Qiou Qinghua, Jia Diming, Wang Feidi. Development on Using of Crumb Rubber. Rubber Industry, ,44,11, 691 – 695. (1997).

[3] Heitnaaan M. Design and Construction of Asphalt Paving Malerials with Crumb Rubber Modifier. Transportation Research Record, 1, 8, 1339 – 1345. (1992).

[4] Wang Shifeng, Wang Dizhen. Rubber Modified Bitumen for Highways. Rubber Industry,47,8, 503 – 506. (2000).

[5] Takallou, H. B.; Hicks, R. G.; Esch, D. C.Transp. Res. Rec. 1096, 68-80 (1986).

[6] Coplantz, J. S.; Yapp, M. T.; Finn, F. N. Review of Relationships between Modified Asphalt Properties and Pavement Performance; SHRP-A-631; Strategic Highways Research Program, National Research Council: Washington, DC, (1993).

[7] Roberts, F. L.; Kandhal, P. S.; Brown, E. R.; Lee, D. Y.; Kennedy, T. W. Hot Mix Asphalt Materials, Mixture Design and Construction, 1st ed.; NAPA Education Foundation: Lanham, MD, pp 68- 382. (1991)

[8] Airey, G. D.; Rahman, M. M.; Collop, A. C. Int. J. Pavement Eng., 4, 105-119.(2003).

[9] European Tire Recycling Association (ETRA). Summary of the Post-Consumer Tire Market; France, (1999).

[10] M.A. Abdelrahman and S.H. Carpenter, Mechanism of Interaction of Asphalt Cement with Crumb Rubber Modifier, Transportation Research Record 1661. Washington, D.C.: Transportation Research Board, pp. 106–113. (1999)

[11] L. Raad, S. Saboundjian, and G. Minassian, “Field Aging Effects on Fatigue asphalt Concrete and Asphalt Rubber Concrete”, Transportation Research Record 1767. Washington D.C.: National Academy Press, 2001.

[12] S. Kim, S.W. Loh, H. Zhai, and H.U. Bahia, “Advanced Characterization of Crumb Rubber-Modified Asphalts, using Protocols Developed for Complex Binders”, Transportation Research Record 1767. Washington, D.C.: Transportation Research Board, pp. 15–24. (2001).

[13] Heitzman, M., “Design and Construction of Asphalt Paving Materials with Crumb Rubber Modifier”. Transportation Research Record 1339, TRB, National Research Council, Washington,DC., pp. 1-8. (1992).

[14] Artamendi, I., Khalid, H.A., “Diffusion Kinetics of Bitumen into Waste Tyre Rubber”. Journal ofthe Association of Asphalt Paving Technologists. Proceedings of the Technical Sessions, Vol. 75, Savannah, Georgia, pp. 133-164. (2006).

[15] Baldino N. , Gabriele D. , Oliviero Rossi C. , Seta L. , Lupi F. R. , Caputo P. , " Low temperature rheology of polyphosphoric acid (PPA) added bitume". Construction and Building Materials, Vol. 36, pp. 592-598. (2012).

[16] online - http://www.doceng.com/product.php?productid=3193410&cat=0&page=7103

[17] AG:PT/T144 Morphology of crumb rubber – Bulk density test - http://www.austroads.com.au/images/stories/T144_Rubber_morphology.pdf.

[18] Barnes, H.A., Hutton, J.F., Walters, K.,. An Introduction to Rheology, first ed. Elsevier Science Publisher, Amsterdam. 212p. (1989).

[19] Steffe, J.F., Rheological Methods in Food Process Engineering, second ed. Freeman Press, Michigan. 418p. (1996).

6. Results part III – Published Papers not related to the doctoral project.

Molecular Crystals and Liquid Crystals
Publication details, including instructions for authors and subscription information:
http://www.tandfonline.com/loi/gmcl20

Analysis of the Solubilisation Power of Detergents by Photochromic Probe

Cesare O. Rossi [a] , Marialuigia Macchione [a] & Luigi Filippelli [a]
[a] Department of Chemistry, University of Calabria, via P. Bucci, 87036 Arcavacata di Rende (CS) , Italy
Published online: 07 Oct 2011.

To cite this article: Cesare O. Rossi , Marialuigia Macchione & Luigi Filippelli (2011) Analysis of the Solubilisation Power of Detergents by Photochromic Probe, Molecular Crystals and Liquid Crystals, 549:1, 160-165, DOI: 10.1080/15421406.2011.581527

To link to this article: http://dx.doi.org/10.1080/15421406.2011.581527

Mol. Cryst. Liq. Cryst., Vol. 549: pp. 160–165, 2011

ISSN: 1542-1406 print/1563-5287 online
DOI: 10.1080/15421406.2011.581527

Taylor & Francis
Taylor & Francis Group

Analysis of the Solubilisation Power of Detergents by Photochromic Probe

CESARE O. ROSSI,* MARIALUIGIA MACCHIONE, AND LUIGI FILIPPELLI

Department of Chemistry, University of Calabria, via P. Bucci, 87036 Arcavacata di Rende (CS), Italy

The ability of micelles to solubilize organic substances is a property of fundamental importance in many practical applications, such as in detergents. In this work, a new method to determine the solubilisation power of SDS, in terms of the amount of captured organic substance, was used for the first time.

A photochromic probe has been dispersed into an organic phase and its incorporation in the micellar system was monitored. The volume of the organic phase entrapped within the micellar hydrophobic core has been measured by the absorbance peak of the dye sensitizer.

In our work, three organic compounds were used to determine the amount of organic solvent solubilised by SDS/water system.

Keywords: photochromic probe; solubilization power; detergents; SDS.

Introduction

Surfactants play an important role in chemistry with considerable implications for the environment [1]. Above a certain concentration, that is the critical micelle concentration (cmc), surfactants undergo a reversible self-aggregation to form micelles [2]. With increasing surfactant concentration, the micelles exhibit a special set of macro-structural transitions, changing from a spherical shape into cylindrical and other shapes. Depending on the chemical nature of surfactant, temperature and water content, different types of ordered liquid-crystalline phases can also exist (cubic, lamellar and hexagonal phases) [3]. Such a fascinating variety of self-assembled structures lead to occurrence of a wide range of physical chemistry behaviour [4].

Soaps (sodium oleate etc.) are fatty acid salts [5] (later on, we will recognise them to be a type of anionic surfactant). They are characterised by a long hydrocarbon chain which represents the hydrophobic portion of the molecule, also called "tail". This hydrocarbon chain may be mono-unsaturated (it contains one C-C double bond), poly-unsaturated (more than one double bond) or saturated (no double bonds). A carboxylate group, attached at the end of the hydrocarbon chain, represents the hydrophilic portion of the molecule, also called "polar head". A surfactant that does not possess the above described molecular chemical characteristic, is considered a detergent. Detergents could be produced easily from

*Corresponding author: cesare.oliviero@unical.it, tel.: +39 0984 492045, fax: +39 0984 492044

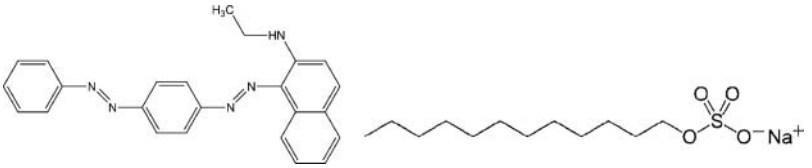

Figure 1. Oliviero R. Cesare et al. "Molecular structure of Sudan Red 7B (on the left) and schematic draw of the structure of SDS (on the right)".

petrochemicals. The procedure was developed during World War I and World War II as an answer to the scarcity of the animal and vegetable fats. Aqueous solutions of detergents or soaps are used for cleaning dirt, which is essentially made by organic non polar substances. Because of its polar nature, pure water can't remove those grimy compounds. Soap allows oil and water to mix acting as an emulsifier so that oily stains can be removed during rinsing.

The ability of a micelle to solubilize water-insoluble organic molecules is usually described through the solubilization power of the detergent, *Ps*, defined as the molar amount of solute dissolved in the micellar pseudophase per mole of micellized detergent at

Table 1. Oliviero R. Cesare et al. "Spectrometric properties of the dye solutions"

Dye solution conc., (mol/L $*10^{-7}$)	Absorbance at 534 nm, (-)	Molar absorption coefficient, ε (L/mol*cm)
	Toluene	
2.2	0.0224	$4.56*10^{-4}$
7.3	0.0371	
8	0.0746	
22.8	0.1024	
34	0.1366	
56	0.2536	
	P-xylene	
9,46	0,04	$4.11*10^{-4}$
12	0,058	
24	0,095	
56	0,23	
83	0,33	
98,6	0,4	
	Benzene	
5,9	0,0399	$3.40*10^{-4}$
18	0,0733	
34	0,1241	
45	0,1654	
96,3	0,3229	
144	0,484	

Table 2. Oliviero R. Cesare et al. "Spectrometric properties of the SDS/water/dye solutions at saturation. The solubilization power of SDS/water solutions is expressed as the volume of organic solvent inside micelles"

SDS/water solution conc.,(%)	Absorbance at 534 nm, (-)	Dye conc. in the organic solvent dispersed inside micelles, (mol/L*10^{-7})	Volume of organic solvent inside micelles, (ml*10^{-4})
		Toluene	
0.1 (below CMC)	0	0	0
0.3 (c.a. CMC)	0.0066	2.00	2.11
0.75 (above CMC)	0.0076	2.20	2.32
1.5	0.0144	4.10	4.32
8	0.1548	34.5	36.3
16	0.5644	111	117
		P-xylene	
0.1	0	0	0
0.3	0.0035	0.83	0.874
0.75	0.0058	1.30	1.37
1.5	0.0105	1.76	1.85
8	0.0242	5.70	6.00
16	0.0704	16.6	17.5
		Benzene	
0.1	0	0	0
0.3	0	0	0
0.75	0.0074	1.10	1.16
1.5	0.0105	2.00	2.11
8	0.0334	9.70	10.2
16	0.0568	21.0	22.1

saturation [6,7]. In the present work we tested a new method for the direct measurement of the volume of three different organic compounds dissolved into micelles made by Sodium Dodecyl Sulphate (SDS, figure 1) dispersed in water [8]. A oil-soluble dye sensitizer, Sudan Red 7B which is a well known marker to visualize lipid bodies in plant cells [9], has been dissolved into the organic phases. When the SDS/water micellar system incorporates the dye-organic solvent composite, one can get informations of the amount on solute entrapped into micelles by the absorbance peak of the dye in the UV-Vis spectrum.

Materials and Methods

As reported in Table 1, Sudan Red 7B was dissolved in each of the three organic compounds Benzene, Toluene and p- Xylene at different concentration ratios. The measured absorbance at the different concentrations allowed us to calculate the linear calibration line and to determine the molar absorption coefficient ε by the Lambert-Beer law :

$$A = C \varepsilon d \tag{2}$$

Where A is the absorbance at 534nm, C is the concentration of the dye and d is the optical path corresponding to the length (1cm) of the quartz cuvette probe For our measurements a Varian Cary 50 Scan spectrophotometer, virtual double beam equipped, has been used. All the measurements were performed in a thermostated room at 25.0°C. Little amounts of the dye stock-solution at the fixed concentration of 9.5×10^{-4} mol/L, were added to SDS/water micellar solutions under stirring (Table 2) and left to reach the phase separation for at least 3 days. Spectrophotometer measurements were then performed on SDS/water micellar solutions in the saturation state. By measuring the intensity of the absorbance peak of the dye micellar solutions, it was possible to calculate the concentration of the dye inside micelles. These data were used to calculate the volume of the organic solvent inside micelles (Table 2).

Results and Discussion

It is well known [10] that at concentrations well above the cmc of SDS/water solutions (Figure 2) the system is able to solubilize great amounts of organic solvents. The solubilisation power strongly depends not only on the surfactant type but also on the type of organic solvent.

In this study UV/Visible spectroscopy technique was used for the first time to calculate the volume of three different benzene-derivates organic solvents inside SDS/water micelles.

The presence of a dye dispersed in the organic solvent, allowed to perform this characterization and to obtain the quantity of solvent inside micelles by the simple Lambert-Beer law. Results are collected and shown in Tables 1, 2 and Figure 3 for all of the investigated systems.

Although further investigations are needed for the standardization of the procedure, it clearly appears that toluene is the organic solvent that better is absorbed into SDS/water

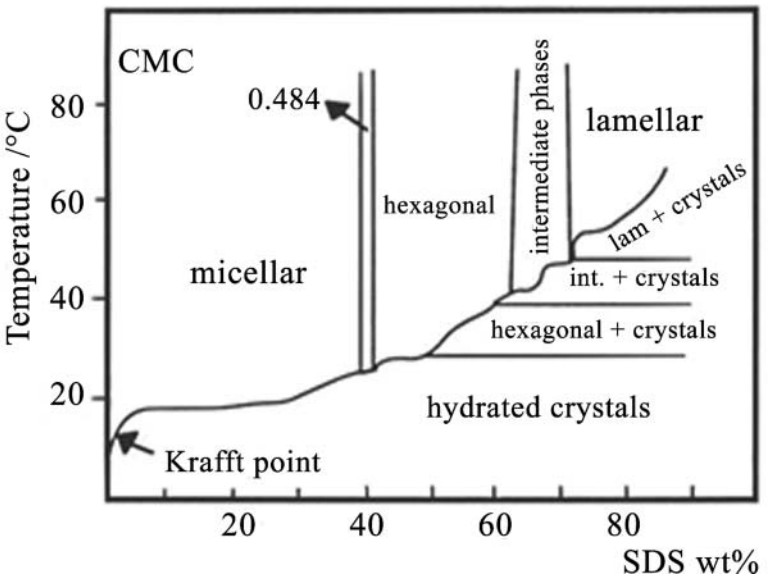

Figure 2. Oliviero R. Cesare et al. "Phase diagram of the SDS/water system, (R.G. Laughlin, The aqueous phase behavior of surfactants, Academic Press, London, 1994)".

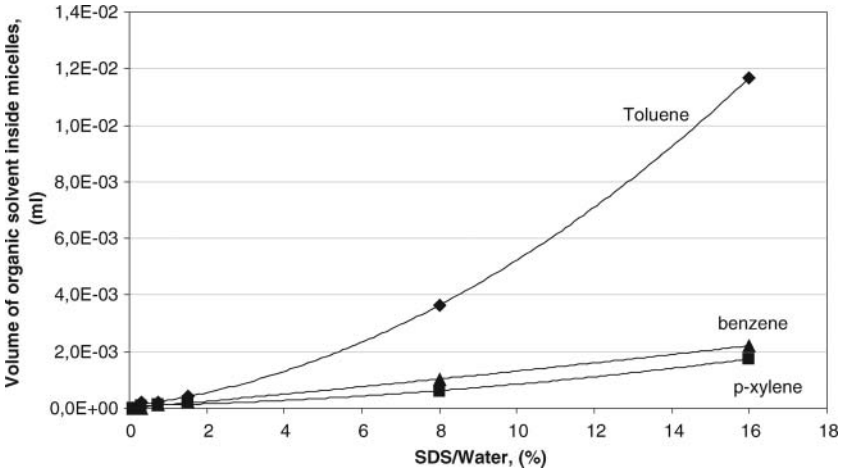

Figure 3. Oliviero R. Cesare et al. "The volume of the organic solvents inside SDS/water micelles at the saturation".

micelles. On the other hand benzene and p-xylene have a similar affinity for the micellar system that was tested. This behaviour might be interpreted by considering the methyl group and its position on the benzene ring as the only chemical difference in the three organic solvents. How this little chemical difference can lead to a different absorption by the SDS/water micelles? A possible explanation involves the dipole moment of the organic solvents. Indeed, benzene has no dipole moment and p-xylene possesses a very low dipole moment, 0.07 D, whereas toluene dipole moment is 0.36 D. From these data we can say that toluene molecule is relatively more polar than the other two benzene derivatives. A micelle created as we did for the present study is a complex macro-structure, but we can essentially think about it as a two shells onion. The external shell, in contact with water, is the polar layer while the inner shell is the non polar layer where the organic solvents are confined. The greater is the hydrophobic character of a compound, the better it will be confined in the core of the micelle. Hence toluene molecule distribute better than benzene and p-xylene throughout the hydrophobic layer because it can go closer to the polar head shell leading to a greater volume of substance that can be absorbed by the SDS/water micelles.

Conclusions

In the present study we tested a new method for the measurement of the solubilisation power of detergents. For the first time, a photochromic probe allowed us to easily calculate the volume of organic solvents confined inside a micellar phase made up by the well-known SDS/water binary system. In a more general frame, results revealed also that the affinity of the benzene-derivative organic solvents with surfactant/water system strongly depends on the groups bounded to the aromatic ring. Even small chemical differences can produce great discrepancy in the volume of organic solvent absorbed by the micellar system. A more general conclusion is that benzene-derivates organic solvents with relatively high dipole moment, better solubilize in the micellar phase of a SDS/water system. Further investigations are in progress also by testing other surfactants as micellar system. This will clarify the role of the chemical nature of surfactant in solubilising organic solvents.

References

[1] Schoberl, P., Ecological assessment of surfactants (1996). *Tenside Surfactants Detergents*, vol. *33 Issue 2*.
[2] Lindmann B., Wennerstrom H in *Topics in current chemistry*, *Sprinter-Verlag – Berlin*.
[3] Tanford C. in "*The Hydrophobic effect: Formation of Micelles and Biological Membranes"*, (1980)- *Wiley-Intersciences* – New York.
[4] Filippelli L., Medronho B., Oliviero Rossi C., Miguel M. G., Olsson U., (2009) *Mol. Cryst. & Liq. Cryst*. **500**, 166–181.
[5] *"IUPAC Gold Book - soap" Compendium of Chemical Terminology, 2nd ed. (the "Gold Book"). Compiled by* A. D. McNaught and A. Wilkinson (1997), *Blackwell Scientific Publications*, Oxford.
[6] Liu, G.G.H., Roy, D., Rosen, M.J. (2000). *Langmuir*, **16**, 3595.
[7] Kim, J.H., Domach, M.M., Tilton, R.D. (2000). *Langmuir*, **16**, 10037.
[8] Youssry M., Asaro F., Coppola L., Gentile L., Nicotera I.,(2010), *Journal of Colloid and Interface Science*, **342**, 2, 348–353.
[9] Brundett M.C., Kendrick B., Peterson C.A. (1991), *Biotech Histochem*, **66**, 111–116.
[10] Daniel E. Kile, Cary T. Chiou,(1989), *Environ. Sci. Technol.*, **23** (7), 832–838.

Colloids and Surfaces B: Biointerfaces 82 (2011) 13–17

Contents lists available at ScienceDirect

Colloids and Surfaces B: Biointerfaces

journal homepage: www.elsevier.com/locate/colsurfb

E, *Z* and positional-monoenoic phyto-fatty acids influencing membrane fluidity: DSC and NMR experiments

Luigi Filippelli[a], Cesare Oliviero Rossi[a], Nicola A. Uccella[a,b,*]

[a] *Chemistry Department, Calabria University, via P. Bucci, Arcavacata, 87036 Rende, CS, Italy*
[b] *IRESMO Foundation, via Cavour, 5, 87040 Montalto Uffugo, CS, Italy*

ARTICLE INFO

Article history:
Received 2 February 2010
Received in revised form 21 July 2010
Accepted 23 July 2010
Available online 3 August 2010

Keywords:
Biomembrane fluidity
Monoenoic lipids
DSC
NMR

ABSTRACT

The membrane fluidity of biological tissues is highly influenced by the π-bond position and isomeric configuration in the long chain of phyto-fatty acids (FAs). *Z*, *E* and positional isomeric monoenoic lipids, i.e. the phytomolecules oleic (OA), elaidic (EA), vaccenic acid (TV) and its *Z*-isomer (CV), have been evaluated for their effects on the fluidity of cellular membranes. To this purpose the Differential Scanning Calorimetry (DSC) and Deuterium Nuclear Magnetic Resonance (^{2}H-NMR), are suitable techniques to understand the supramolecular lamellar structure during the order (gel)–disorder (fluid) transition. It was found that the presence of CV concentration, induces the biomimetic system to reach the first step to fluid phase earlier than the membrane containing OA. DSC showed that the endothermic peak onset of the membrane containing CV occurs at a lower temperature than that of a membrane containing an equal amount of OA. ^{2}H-NMR investigation confirmed the last statement. In fact the study of the main phase transition of the two different systems, revealed that model membrane containing a 3% (w/w) of CV goes in ripple phase, i.e. the first step to the fluid state, at a lower temperature as compared to the membrane of an identical system with OA.

1. Introduction

The strong relation between the protective effects of Mediterranean Aliment Culture (MAC), associated with complex component intake, having functional food activity, has been largely documented [1]. Long-chain fatty acids, essentially represent a benign dietary material that can, for instance, markedly increase the dopamine content of dopaminergic phenotype neurons, providing an interesting approach to Parkinson's disease treatment [2]. In this view, the phytomolecules oleic (OA), elaidic (EA), *Z* and *E* vaccenic acids isomers (CV and TV respectively), have been studied for their effects on the fluidity of cellular membranes exploiting lyotropic liquid crystals as model membranes. DSC [3] and NMR [4,5] techniques, allowed us to look into model bilayer structure and dynamics when a 3% (w/w) of fatty acid is present in the membrane. This concentration represents the typical CV concentration in olive oil from olives harvested from hill orchards. Further investigations will have to be performed to clarify the CV concentration effects on the membrane fluidity.

The "tail-packing" rationalization in model bilayer membrane, has been derived by DSC method, while ^{2}H-NMR reinforced the DSC results studying the lineshape of the heavy water deuterium signal in the biomimetic systems. Experimentally membrane-lipid bilayers manifest, under temperature control, a reversible change of state from a *disordered* fluid to an *ordered* nonfluid (gel) array of fatty acyl chains. The *order–disorder* transition temperature (main phase transition) [6–8] depends on lipid composition and, under cholesterol deficiency, it mainly relies on fatty acid ratios in membrane-lipids. In fact membrane fluidity of model biological tissues, is highly influenced by the π-bond position and configuration in the long chain isomers of phyto-fatty acids.

Our biomimetic experiments, give a clear rationalization of the different fatty acid ratios found in some bio-active food, like olive oil obtained from olives harvested in orchards grown under severely different pedoclimatic environments, i.e. hill or plan fields [9]. When the growth temperature is lowered, isomeric phyto-fatty acids are competitively biosynthesized by olive cells. This mechanism, for example, allows olive tissues to regulate membrane fluidity, thus optimizing its function at the variable growth temperature. Biomimetic systems are relatively easy to prepare and they provide the possibility to isolate some chemical-physics parameter which would be hindered in a natural biological membrane by its complexity.

These model membranes are basically a mix of amphiphile molecules and water. Depending on the temperature and hydration grade of the samples, a variety of mesophases, with macroscopic

* Corresponding author. Fax: +39 0984 492044.
E-mail address: n.uccella@unical.it (N.A. Uccella).

0927-7765/$ – see front matter © 2010 Elsevier B.V. All rights reserved.
doi:10.1016/j.colsurfb.2010.07.052

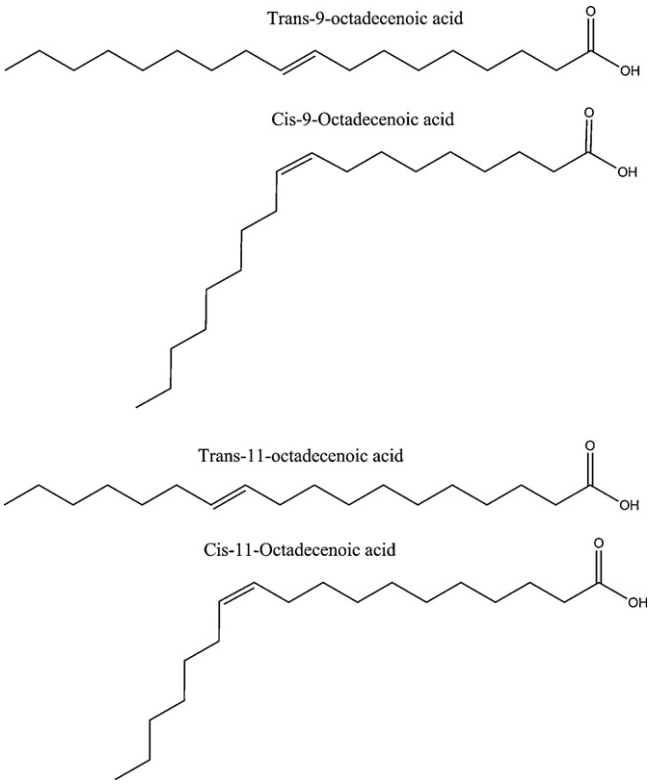

Fig. 1. Molecular structures of monoenoic acids investigated in this work.

arrangement of lipids/water systems, can be produced. Among them, the double layered L_α phase reproduces biomembranes with good approximation [10,11]. Dimyristoylphosphatidylcholine (DMPC) is a phospholipid commonly used in model membrane studies dealing with the understanding of biophysical properties of membranes in absence or presence of other lipids, sterols, and so forth [12,13].

In the present work, the ^{2}H-NMR analysis of a bilayer made by DMPC, and a 3% (w/w) of monoenoic fatty acid, has been performed.

2. Materials and methods

2.1. Materials

Z-9-Octadecenoic acid, i.e. the oleic one, 18:1Δ9z, OA, *E*-9-octadecenoic acid, the elaidic isomer (18:1Δ9e, EA), *Z*-11-octadecenoic acid, the *cis*-vaccenic or asclepic, positional isomer (18:1Δ11z, CV) and *E*-11-octadecenoic acid, the proper vaccenic acid (18:1Δ11e, TV), whose molecular structures are shown in Fig. 1, DMPC and ^2H_2O, heavy water, have been purchased from Sigma Chemicals, Steinheim, Germany. All materials have purity higher than 97% and have been used without further purification.

2.2. Samples preparation

Model membranes were prepared by dissolving the suitable amount of DMPC and a 3% (w/w) of FA in chloroform. The obtained solution has been evaporated under a nitrogen stream and then samples have been dried under vacuum overnight. Membranes were then reconstituted by ^2H_2O to observe both quadrupolar splitting and lineshape of the resulting NMR spectra. The same samples were analyzed with the DSC technique.

2.3. Methods

2.3.1. Differential Scanning Calorimetry (DSC)

DSC has been used in this research for the measurement of the *order–disorder* transition temperature. The experiments were performed on the samples by using a Setaram micro DSC III instrument. The indium was used to calibrate temperature and energy scales. Samples (20–30 mg) were sealed in aluminium-cells and brought to the initial temperature. As a reference, a sealed pan with the corresponding amount of heavy water was used. To check water evaporation, the pans have been weighed before and after the DSC measurements. The DSC thermograms were recorded in the temperature range from 5 to 80 °C. The heating rate was 1 °C min^{-1}. Thermograms were digitized by an IBM computer, which allowed the determination of the phase transition temperatures with the associated heat changes by the use of the commercial software Origin 7.5 (OriginLab, MA, USA).

2.3.2. NMR measurements

A Bruker Avance 300 has been used to record deuterium NMR spectra at 46.043 MHz. Temperature control was achieved with a Bruker Variable Temperature Unit B-VT 1000 with a sensitivity of ±0.1 °C. ^{2}H-NMR spectra were acquired using a quadrupole echo sequence [14]. In the echo sequence, the 90° pulse length was 9 μs, and time delays of 100 μs. Typically the number of averaged transients were from 32 to 64. Considering the abundance of the deuterium nuclei in the samples, the number was sufficient to obtain an adequate signal to noise ratio.

The polar heads of the used lamellar systems have been hydrated with heavy water. As for the resulting ^{2}H-NMR spectra, both quadrupolar splitting and lineshape bring information on the macroscopic arrangement and the hydration grade of the biomimetic system. As matter of fact the observed splitting is related to the order and mobility of the deuterium nuclei within the sample and its value, $\Delta\upsilon$, is given by the following equation [15]:

$$\Delta\upsilon = \frac{3}{2}\upsilon_Q\left(\frac{3\cos^2\theta - 1}{2}\right)S$$

where υ_Q is the quadrupolar coupling constant, θ is the angle formed by the director of the mesophase and the static magnetic field. *S* is an order parameter describing the ordering of the O–^{2}H bonds in ^2H_2O, with respect to the director of each microdomain. Furthermore, the value of the order parameter *S* is time averaged. Another contribution to the splitting value is given by the fraction of deuterium nuclei of water molecules bound to the polar head group of the amphiphile (p_b). Taking into account that an exchange process between interlayer and bound water occurs, we may express an average $\overline{\Delta\upsilon}$ value by the following equation:

$$\overline{\Delta\upsilon} = \frac{3}{4}\nu_Q p_b \bar{S}$$

where p_b is the fraction of water bound to the membrane. Hence from a typical ^{2}H-NMR spectrum of heavy water within a model membrane system, one can have a precise idea on the macroscopic arrangement that the amphiphile molecules adopt at a certain temperature. This is of great advantage for the aim of the present study. In fact pure DMPC/^2H_2O system experiences the gel-fluid, *order–disorder*, transition at 25 °C and the resulting spectra of the two mesophases are completely different in both splitting and line shape as shown in Fig. 2. This is mainly due to the fact that between gel and fluid phase, an undulated macro-arrangement called ripple phase, occurs. This undulation make the deuterium signal of heavy water furthermore averaged and the spectrum became a characteristic wide singlet. It is worthy to point out that the hydra-

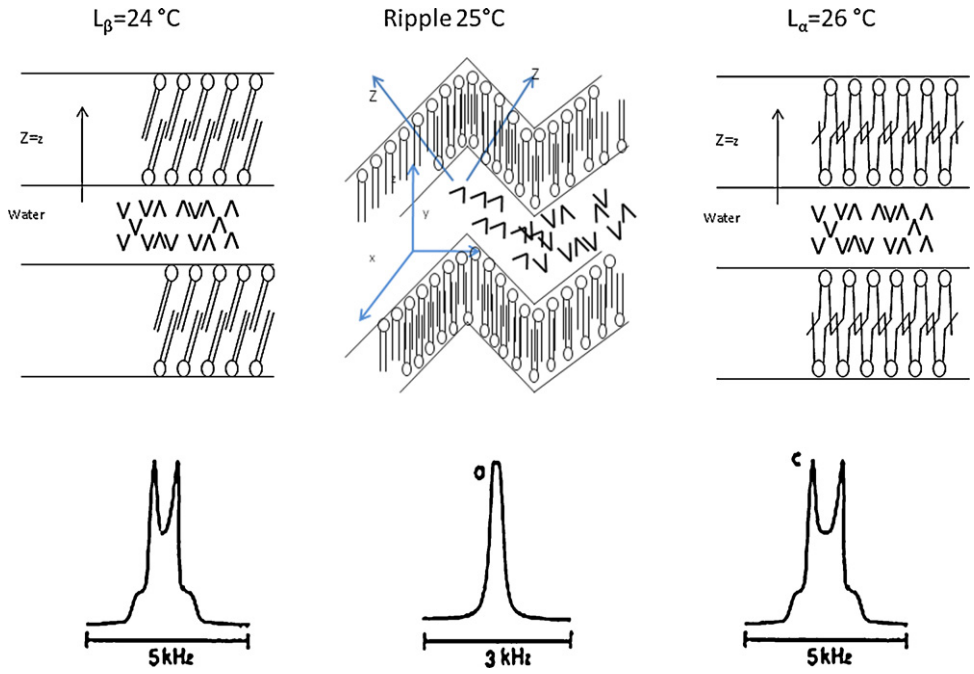

Fig. 2. ^{2}H-NMR profiles of the *order–disorder* transition in DMPC/^2H_2O model system.

tion grade of the membrane increase going from gel to fluid phase that is, the disordered phase bound more water than the ordered phase.

3. Results and discussion

The two hydrogen atoms which lie on a *E* π bond of a monoenoic fatty acid (MEFA), are located on opposite sides of the carbon chain. In contrast to the more typical *Z* isomeric configuration, the π bond angle of the *E* Fatty Acids (TFAs) is smaller and the acyl chain is more linear, resulting in a more rigid molecular structure with a higher melting point. In the *Z* configuration, the hydrogen atoms reside on the same side of the carbon chain, resulting in a "kink" in the acyl chain and a more flexible molecule. The spatial structure of TFAs is between that of saturated fatty acids and *Z* unsaturated fatty acids. As a result, oleic acid or *Z* C18:1*n*-9 melts at 13 °C, while its *E* isomer elaidic acid (*E* C18:1*n*-9) melts at 44 °C. Therefore the number, geometry, and position of π bonds in fatty acids affect the melting behavior of the fats of which they form part. For instance, triglycerides high in saturated fatty acids easily stack in a crystal lattice and appear solid at room temperature. "Bends" in the triglyceride molecule, introduced by *Z* unsaturated π bonds, hinder crystals formation and that explains why oils are liquid at room or even lower temperature.

The DC *vs.* temperature measured on DMPC membranes with 3% (w/w) of monoenoic fatty acids gives a broad endothermic peak attributable to the well known *order–disorder* transition (Fig. 3).

A TA processor has been employed to obtain Δ*H* values for each peak using an integration method.

DSC data are summarized and reported in Table 1. From DSC scans it has been found that both the *order–disorder* transition temperature and the area of endothermic peak Δ*H* are lower when *Z* monoenoic phyto-fatty acids are present in the DMPC membrane. In addition it is worthy to note the effect of the π bond position on the transition. The peak related to the CV-based membrane is broader and it starts at 18.5 °C while the OA-based membrane peak starts at 19 °C. The peaks have a minimum point at 22.3 and 20.9 °C, end at 26.8 and 25.6, respectively, with a calculated Δ*H* values of 25.7 and 24.1 J/g.

Table 1
DSC results relative to the endothermic peak of the monoenoic based DMPC membrane.

DMPC membranes	T_m (°C)	Minimum (°C)	End (°C)	Δ*H* (J/g)
EA	20.5	22.5	26.5	28.2
TV	21.0	23.5	27.5	25.7
CV	18.5	22.3	26.8	26.0
OA	19.0	20.9	25.6	24.1

Fig. 4 shows the ^{2}H-NMR profile of two biomimetic systems containing respectively Oleic Acid (OA-dashed spectra) and CV, black spectra. The signals were recorded at 24 °C (Fig. 4a) and successively at 25 °C (Fig. 4b). The sample containing CV has a profile at 24 °C narrower than the one containing OA. Conversely at 25 °C the two spectra show no appreciable differences.

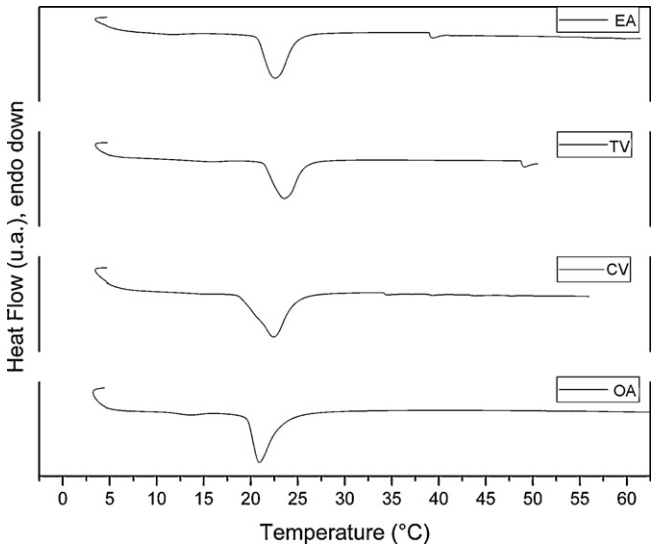

Fig. 3. DSC thermograms of OA, CV, TV and EA based DMPC membranes. Heating rate 1 °C/min.

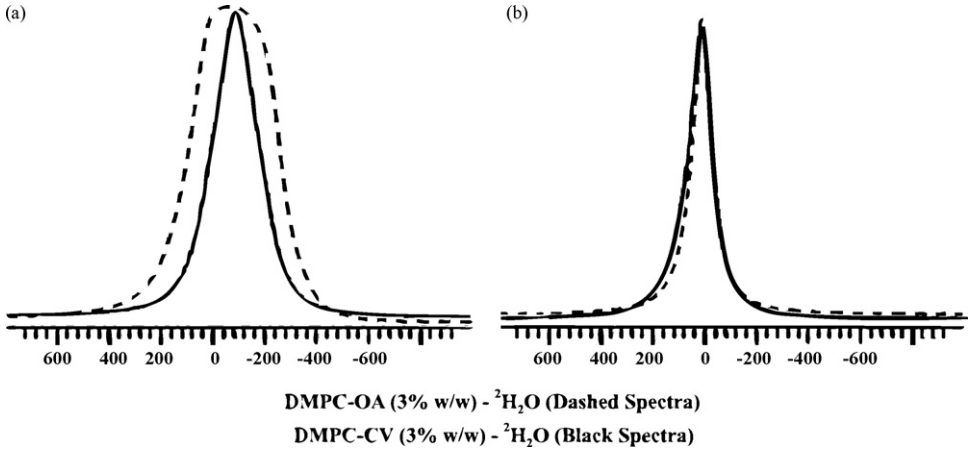

Fig. 4. ^{2}H-NMR profiles of DMPC/OA/^2H_2O (dashed line) and DMPC/CV/^2H_2O (solid line) model systems at 24 (a) and 25 °C (b).

Regarding the samples containing elaidic acid and vaccenic acid, an identical experiment has been performed. In this case the difference was not so large like the previous test on the *Z* conformers. However at 24 °C it was found that the sample containing TV resulted into a lower $\Delta\nu$ while at 25 °C there is no substantial difference.

When the bilayer prepared from phospholipid species undergoes the thermally induced gel to fluid phase transition, an equilibrium state is reached between the gel phase and liquid crystalline phase at the phase transition temperature T_m. Assuming the transition to be a first order equilibrium transition, the T_m is then equal to the ratio of the transition enthalpy and the transition entropy, as follows: $T_m = \Delta H/\Delta S$.

The contribution of the energy term ΔH to the magnitude of T_m is greater than ΔS, consequently as a first approximation, the term T_m may be expressed as a function of some structural parameters that are directly related to the energy term ΔH without invoking the ΔS term.

The main endothermic peak, observed with all the mixtures we examined, undoubtedly reflects the transition from gel to liquid crystalline phases. Values of T_m and ΔH for all the membranes that contained the *Z*-unsatured fatty acids, are lower than those containing *E* fatty acids in agreement with data reported in literature [16]. These effects have been considered to reflect principally the destructive influence of a $Z\,\pi$ bond on the packing of the hydrocarbon chains in the gel state, a less compact arrangement resulting in a lower T_m and ΔH values.

The *E* configuration has a completely different effect on the fluidity of the phospholipid bilayer [8]. TFAs can take up a long extended structure, which is similar to that of saturated fatty acids so that phospholipids result more rigidly packed in the membrane.

The measurement of phase transition temperatures of membranes containing *E* rather than *Z* isomers results in higher transition temperatures according to Wever et al. [17]. Therefore, the conversion of *Z* unsaturated fatty acids (CFAs) into their *E* configuration results in a significant reduction of the membrane fluidity which is, however, smaller than the replacement of CFAs by saturated fatty acids.

A slight increase in the minimum point of the endothermic peak was observed as the π bond moves to the methyl end. This seems to be in agreement with data reported in literature when similar systems have been analyzed [18].

The effect of the shift of the minimum point could be interpreted as a progressive increase in van der Waals interactions. In general when π bonds occupy the middle part of the chain, the maximum point is lowest because the greatest effective length of interaction for chain with all *E* chain is minimized. As π bonds move towards the carboxyl or methyl terminus of the chain, there is a longer region of the chain not interrupted with π bonds interacting with all *E* and this leads to a higher transition temperature.

In the present investigation the endothermic peak of the CV-based membrane shows a particular heat flow profile. In fact it is important to point out that even though a slight increasing of the minimum point is observed moving the position of π bond from 9 to 11, the onset temperature is lower.

This result is really interesting and it led us to interpret this observation in terms of membrane higher fluidity induced by the presence of CV acid. The onset temperature in fact reflects the starting of the *order–disorder* transition.

The results and conclusions presented in this paper appear partially in disagreement with those of Barton et al. [18] and with data from the melting points of fatty solids. Barton and Gunstone found that the T_m was lowest when the $Z\,\pi$ bond was in $\Delta 9$ position.

This can be ascribed mainly to a different biomimetic system they utilized, which was formed by phospholipid bilayers of pure unsaturated lecithin/water mixture. In fact the thermodynamic values for *Z*-unsatured lecithins are different than those for saturated systems having the same chain length [19]. Additionally, the disruptive influence of the $Z\,\pi$ bond is more pronounced when the monoenoic fatty acid is embedded in model membranes prepared with saturated acyl chain phospholipids [20].

It seems also inappropriate to consider the melting points of crystalline solid fats as a reference for the study of the fluidity of the biomimetic membranes.

In fact the molecular organization of the solid fats is different from the one they adopt in the liquid- crystalline phase. Furthermore the long chain fatty acids may exist in different crystalline forms, a phenomenon known as polymorphisms. Fat polymorphism therefore describes phase changes and structural modifications of a solid fat. The different polymorphic fat forms turn into different melting points, solubility, crystal morphology and network. The adopted crystal structure depends on the type of lipid molecule, fatty acid distribution, lipid purity, and crystallization conditions (temperature, rate of cooling, shear, solvent).

When the molecule crystallizes, the chains will align side by side to maximize van der Waals interactions. In general long spacing reflects the distance between methyl end groups for triacylglycerols and are usually comprised of two or three chains lengths of the fatty acid. The DSC data that we measured led us to investigate this system at a deeper level in order to clarify the effect of CV on the membrane fluidity. The onset temperature in fact reflects

the starting of the *order–disorder* transition. To this purpose the ^{2}H-NMR results allowed to better understand the structural organization during the *order–disorder* transition when a monoenic acid is present in the membrane bilayer.

The ^{2}H-NMR investigation has clearly revealed that model membrane containing a 3% (w/w) of VA makes the membrane more fluid compared to an identical system with OA. Fig. 4 evidenced indeed that at 24 °C the profile of the sample with CV is that of a system which is turning into ripple phase, while the sample containing OA is still in the ordered phase L_β. This means that the presence of CV induces the system to reach the first step to fluid phase earlier than OA. The spectra of the same systems were then recorded at 25 °C and no appreciable difference was found. According to the brief theoretical background mentioned above, the quadrupolar splitting, considering $\theta = 90°$, is the distance between the two highest peaks. When the system is around the *order–disorder* transition the splitting of D_2O in a hydrated DMPC system, became smaller because of the averaging effect of water diffusion on the undulated surface, which is faster than NMR time scale measurement. The observed effect of CV is consistent with the expected assumption that its π bond is situated deeper within the double layer than OA. This surely enhances the entropy content in the vicinity of the hydrophobic core, consequently the mobility of the inner of the bilayer results increased pushing the system towards a more hydrated membrane. The effect on the temperature transition caused by the *E* conformers is less evident. This is because of VA and EA have a straight molecular shape and the hindrance of the two molecules related to the π bond position has minor consequences on the mobility of the bilayer core.

These conclusions are in agreements with studies using spin label techniques [21] and subsequently nuclear magnetic resonance [22] which indicated that from the carboxyl group end to C10 the hydrocarbon chains are relatively ordered. From C10 to C18 there is an increase in the molecular motion. This is often referred to as (nonlinear) "gradient of fluidity". The molecular motion experienced by hydrocarbons chain can be associated with the existence of several gauche isomers [23].

4. Conclusion

The study of the molecular structure in the liquid crystalline phase has attracted the attention of many researchers in order to clarify some of the main active processes involving biological cell membranes, such as the in/out transport mechanism rather than mitosis process by which cells divide themselves and create a new daughter cells. When phospholipids are dispersed in water, they form globules of bilayer structures often referred as model membranes or biomimetic systems. Disordering, fluidizing and dilating effects of MEFAs on biomimetic membranes have been precisely measured by DSC and NMR. DMPC model membrane undergoes transition from gel phase (ordered and less fluid) to liquid crystalline (less ordered and fluid) phase according to the temperature, the hydration grade, the degree of packing, and the chemical environment. The phase transition occurs in a cooperative way. This investigation demonstrated the fluidizing effect of CV acid when it is intercalated in the phospholipid bilayer structure. The CV acid in the DMPC model membrane causes a shift of the main phase transition of about 0.5 °C lower than OA acid evidencing its more fluidifying effect. Future investigations by using complementary techniques and varying the amount of embedded fatty acids within the model membranes are necessary to understand better the supramolecular organization during the *order–disorder* transition when MEFAs are present in the membrane bilayer.

References

[1] A. Saija, N.A. Uccella, Trends Food Sci. Technol. 11 (2001) 357–363.
[2] A. Hellera, L. Wona, N. Bubulaa, S. Hesseforta, J.W. Kurutzb, G.A. Reddyc, M. Grossd, Neurosci. Lett. 367 (2005) 35–39.
[3] N. Iannotta, C. Oliviero Rossi, G.A. Ranieri, N.A. Uccella, Eur. Food Res. Technol. 212 (2001) 240–243.
[4] L. Filippelli, A. Beneduci, G. Chidichimo, Proceedings of 4th International Workshop on Biological Effects of Electromagnetic Fields, October, Crete, Greece, 2006, pp. 574–581.
[5] L. Coppola, R. Gianferri, I. Nicotera, C. Oliviero Rossi, Cryst. Liquid Cryst. 398 (2003) 157–167.
[6] D. de Mendoza, J.E. Cronan, Trends Biochem. Sci. 8 (1983) 49–52.
[7] L. Vigh, B. Maresca, J.L. Harwood, Trends Biochem. Sci. 23 (1998) 369–374.
[8] G. Cevc, Biochemistry 30 (1991) 7186–7719.
[9] M. D'Imperio, G. Dugo, M. Alfa, L. Mannina, A.L. Segre, Food Chem. 102 (2007) 956–965.
[10] F. Aussenac, M. Laguerre, J.M. Schmitter, E.J. Dufourc, Langmuir 19 (2003) 10468–10479.
[11] M. Pasenkiewicz-Gierula, Y. Takaoka, H. Miyagawa, K. Kitamura, A. Kusumi, Biophys. J. 76 (1999) 1228–1240.
[12] H.L. Kantor, J.H. Prestegard, Biochemistry 17 (1978) 3592–3597.
[13] A.C. Rowat, J.H. Davis, Biochim. Biophys. Acta 1661 (2004) 178–187.
[14] A.D. Ronemus, R.L. Vold, R.R. Vold, J. Magn. Reson. 70 (1986) 416–426.
[15] L. Coppola, R. Gianferri, I. Nicotera, C. Oliviero, Mol. Cryst. Liquid Cryst. 398 (2003) 157–167.
[16] V. Pedrotta, B. Witholt, J. Bacteriol. 181 (1999) 3256–3261.
[17] F. Wever, S. Isken, J. De Bont, Microbiology 140 (1994) 2013–2017.
[18] P.G. Barton, F.D. Gunstone, J. Biol. Chem. 250 (1975) 4470–4476.
[19] B.D. Ladbrooke, R.M. Williams, D. Chapman, Biochim. Biophys. Acta 160 (1968) 333–340.
[20] F. Nielloud, G. Marti-Mestres, Pharmaceutical Emulsions and Suspensions, Marcel Dekker, New York, 2000, p. 229.
[21] W.L. Hubbell, H.M. McConnell, J. Am. Chem. Soc. 93 (1971) 314–326.
[22] Y.K. Levine, N.J.M. Birdsall, A.G. Lee, J.C. Metcalfe, Biochemistry 11 (1972) 1416–1421.
[23] J.G. Batchelor, J.H. Prestegard, R.J. Cushley, S.R. Lipsky, Biochem. Biophys. Res. Commun. 48 (1972) 70–75.

Bioelectrochemistry 84 (2012) 18–24

Contents lists available at SciVerse ScienceDirect

Bioelectrochemistry

journal homepage: www.elsevier.com/locate/bioelechem

Microwave induced shift of the main phase transition in phosphatidylcholine membranes

Amerigo Beneduci [a,b,*], Luigi Filippelli [a], Katia Cosentino [a], Maria L. Calabrese [c], Rita Massa [c,d], Giuseppe Chidichimo [a,b]

[a] Department of Chemistry, University of Calabria, Via P. Bucci-Cubo 17/D, 87036 Arcavacata di Rende (CS), Italy
[b] Consorzio TEBAID c/o Department of Chemistry, University of Calabria, Via P. Bucci-Cubo 15/D, 87036 Arcavacata di Rende (CS), Italy
[c] Interuniversity Center on Interaction Between Electromagnetic Fields and Biosystems (ICEmB), Italy
[d] Department of Physical Science, University Federico II, Naples, Italy

ARTICLE INFO

Article history:
Received 17 June 2011
Received in revised form 11 September 2011
Accepted 6 October 2011
Available online 13 October 2011

Keywords:
Biological membrane
Membrane phase transition
Deuterium NMR spectroscopy
Microwave nonthermal effects
Dosimetry

ABSTRACT

Numerous experimental evidence show that exposure of biological systems to extremely high frequency microwaves may induce significant effects even at low powers. These effects are thought to occur via non-thermal mechanisms involving primarily the interaction of microwaves with phospholipid membrane structures. However, no conclusive experimental evidence that biomembranes exhibit remarkable sensitivity to this radiation has been provided up to now. Here, deuterium nuclear magnetic resonance spectroscopy is used to study the effects of microwaves on 1,2-Dimyristoyl-sn-glycero-3-phosphatidylcholine/^2H_2O multilamellar vesicles that serve as biomimetic membranes. Here we show that, if the membrane is brought into close proximity to the transition point, microwaves induce a reduction of water ordering at the membrane interface, an upward shift of the main phase transition temperature and a broadening of the transition region. A deep dosimetric analysis shows that the above effects are nonthermal, indicating the need for a nonthermal hypothesis to explain them. This study suggests that exposure to high-frequency microwaves can have far reaching consequences on active biological systems.

1. Introduction

Within the extremely high frequency microwave (MW) region of the electromagnetic spectrum (30–300 GHz), the 50–80 GHz sub-band is of particular interest due to its current applications in biomedicine [1–5] and its next use in wireless communication technologies [6]. For these reasons, there is an increasing interest on the potential biological effects that such waves may induce even at power exposure conditions within the recommended safety standard limits [7], above which thermal effects arise [8]. In fact, numerous experimental studies have shown that MW may induce a variety of biological effects at low power densities that cannot arise from heating [1,8,9]. Depending on the exposure conditions, an increased or decreased growth of several cell types in vitro has been reported [10,11]. A resonant-like or frequency-dependent interaction mechanism has been theoretically suggested [13] and, in a few notable cases, observed experimentally [1,12–14]. However, this idea has been discredited by independent studies [8]. Therefore, no conclusive experimental proofs demonstrate the nonthermal nature of the MW-induced effects. Two main intriguing, challenging and related questions are still unsolved: i. what biological structures are the site of interaction? ii. on which mechanisms the above nonthermal biological effects are based.

Strong evidence shows that biological membranes are likely to be highly sensitive to frequencies in the 1–80 GHz range [1,15–21]. As far as ionic transmembrane current is concerned, a significant activation of the Ca^{2+} pump in the sarcoplasmic reticulum of skeletal muscle cells and in those of the rat heart exposed to 61 GHz at 4 mW/cm^2 has been observed [1] as well as significant alterations in the transport of calcium ions across the single Ca^{2+}-activated K^+ channel of kidney cells exposed to nonthermal 42.25 GHz radiation [16]. Frequency specific and reversible effects have been reported on the Cl^- transmembrane current in cells of the *Nitellopsis obtusa* giant algae exposed to 41–76 GHz at a power density of 5 mW/cm^2 where thermal increase was <1 °C [1,15]. Further results have shown that in vitro exposure of human cells in the 42–78 GHz MW range induced nonthermal changes on cell membranes, such as reversible externalization of phosphatidylserine [17] and morphological alterations in tumor cells [8]. An intrinsic effect of MW has been claimed even in the presence of thermal effects, to fully explain the K^+ and Na^+ permeability increase observed in erythrocytes exposed to 8.42 GHz [17] and the MW-stimulated drug release from liposomes [18]. Even if controversy finding has been found from nonreproducible experimental results on multilamellar vesicles exposed to 1.0 GHz radiation [20], the above

* Corresponding author at: Department of Chemistry, University of Calabria, Via P. Bucci-Cubo 17/D, 87036 Arcavacata di Rende (CS), Italy. Tel.: +39 0984492117; fax: +39 0984492041.
E-mail address: beneduci@unical.it (A. Beneduci).

1567-5394/$ – see front matter © 2011 Elsevier B.V. All rights reserved.
doi:10.1016/j.bioelechem.2011.10.003

studies [18,19] suggest that membrane phase transition may play a significant role in microwave induced biological effects.

Further evidence on model membrane systems have shown that exposure at 60 GHz significantly increased the lateral pressure of phospholipid monolayer films at power densities as low as 9 μW/cm^2, though without a statistical significant phospholipid microdomain reorganization [21]. Moreover, 130 GHz pulsed wave exposure affects the permeability of cationic vesicles by a nonthermal mechanism [22]. Recently, we have shown that 53.57 GHz exposure of giant unilamellar vesicles (GUVs) at average SAR up to 0.55 W/kg, induced shape changes of GUVs, diffusion of the fluorescent dye D-8-ANNEPS into the membrane bilayer and increased attraction between vesicles [23], suggesting that MW mainly affects the membrane-water vesicle interface.

To better understand the two main issues outlined above, here we have studied the impact of MW on pure phospholipid membranes made of 1,2-Dimyristoyl-sn-glycero-3-phosphatidylcholine-^2H_2O (DMPC/^2H_2O) multilamellar vesicles (MLVs) that serve as biomimetic membranes. Samples were exposed in the 53–78 GHz frequency range, at Specific Absorption Rate (SAR) <12 mW/kg. We have used deuterium nuclear magnetic resonance spectroscopy (^{2}H-NMR) of heavy water to determine the properties of the membrane polar interface and their changes as a response to MW in strictly controlled temperature conditions. Heavy water can be appropriately used as a probe of membrane surface geometry and is particularly suitable for studying membrane phase transitions because a change in water quadrupole splitting ($\Delta\nu_Q$) can be related to changes in bilayer structures [24–28]. In fact, for unoriented MLVs (powder sample), $\Delta\nu_Q$ is measured by the distance in Hz between the principal peaks of the powder spectrum (see below) and is given by [24,28]:

$$\Delta\nu_Q = \frac{3}{4}\nu_Q|S| \quad (1)$$

where, ν_Q is the quadrupole coupling constant equal to 220 KHz; S is the water molecular order parameter averaged over the fast anisotropic molecular reorientations and is a direct measure of the ordering of water molecules at the polar interface [29,30]. It brings information on the dynamic processes involved at the membrane/water interface and is therefore sensitive to the membrane phase.

2. Experimental

2.1. Sample preparation

1,2-Dimyristoyl-sn-glycero-3-phosphatidylcholine (DMPC) was purchased from Sigma Aldrich with a 98.8% purity and used without further purification. ^2H_2O was obtained from Cambridge Isotope Inc. having a purity of 99.98%. When hydrated, this phospholipid can assume different liquid crystalline mesophase, depending on the water/lipid mole ratio and temperature. The phase diagram for the binary system DMPC/water shows that the fluid lamellar phase is obtained within a range of composition at temperatures above about 25 °C [24–28]. In this phase, lipids are arranged in bilayers (lamellae) like those characteristic of any biological membranes. DMPC powder was dried to constant weight in vacuum at room temperature and then hydrated with heavy water to yield multilamellar vesicles (MLVs) containing 11 ± 1 water moles per mole of lipids (n_w). Glass tubes containing the samples were subsequently flame-sealed. Due to the high viscosity of the samples, they were homogenized by heating to 45 °C, well above the main phase transition temperature (25.5 °C), for approximately 8 h and centrifuging back and forth in the tubes. In order to prevent potential lipid oxidation the small volume of air left above the sample was removed inserting a piston plug of Teflon (WG-805, Wilmad LabGlass, USA) in the tube provided with an air vent in the center assuring easy insertion by means of a stainless steel positioning road (WG-504, Wilmad LabGlass, USA).

As will be seen later, sample thickness in the tube is crucial in determining SAR uniformity. Each sample was prepared with a total weight of about 50 mg in order to have an optimal thickness of about 3 mm. Samples were weighted and stored at 37 °C for at least three days. Before performing the exposure treatment, ^{2}H NMR spectra were recorded over 48 h to ensure the time stability of the observed splitting. After any exposure, samples were weighted to check out for water evaporation.

2.2. ^{2}H-NMR acquisitions

Deuterium spectra were acquired with a Bruker Avance 300 spectrometer at 46.52 MHz using a phase cycled quadrupole echo sequence with $\pi/2 = 7$ μs, $\tau_2 = 50$ μs and a recycle delay of 1 s followed by Fourier transformation. 32 to 128 transients were averaged with a spectral width of 30 KHz. A 20 Hz exponential multiplication was performed on the free-induction decay (FID).

Phase transition was monitored with a precision on T of ± 0.2 °C, controlled by the Bruker VT 2000 unit. Samples were brought in the L_α phase, above T_m, and their temperature was gradually decreased in steps of 0.2 °C in order to enter into the $P_{\beta'}$ phase. For each new T value, the systems were equilibrated for at least 30 min prior to acquisition. The reverse process ($P_{\beta'}$ to L_α) was studied increasing the temperature in the same way.

2.3. Real-time NMR acquisition under exposure

MW exposure was performed by means of a microwave wide-band generator (Amphit-32, MicroMedTech, Nizhny Novgorod, Russia) in the 53.57–78.33 GHz frequency (f) range (Supplementary Fig. 1A). The frequency-dependent emission spectrum of this generator (Supplementary Fig. 1B), measured by a radiometer (IMG Panorama, MicroMedTech, Nizhny Novgorod, Russia), exhibited several relative maxima and minima with output power in the range 5–20 μW (being the signal not leveled but stable in time). This radiation source was chosen due to its wide-band characteristic and its use in biomedicine [1–5]. To allow real time detection of NMR spectra during exposure, the MW generator was connected to a diamagnetic cylindrical waveguide of variable length terminating with a dielectric Teflon antenna inserted into the NMR probe provided with a vertical radiofrequency coil (Supplementary Fig. 1A and C). A schematization of the exposure set-up showing the antenna and the sample inside the probe is reported in Fig. 1. The dielectric antenna was inserted into a 10 mm glass tube, containing a sample tube of 5 mm. The waveguide was kept outside the NMR acquisition volume to avoid interference with the radiofrequency signal of the coil (Fig. 1 and Supplementary Fig. 1A and C). Spectra recorded with this set-up show that the antenna did not affect the measurement. Sham exposure conditions correspond to the same set-up but with the generator turned off (incident power density = 0). NMR spectra were acquired in real-time in strictly controlled temperature conditions.

2.4. Dosimetry

The exposure set-up was made up of different modules of circular waveguides (internal radius of 2 mm), feeding at one end by the MW source and terminated on the other end with a dielectric antenna (Supplementary Fig. 2). The dielectric antenna was made up of Teflon, with a radius of 3 mm and height of 40 mm (Supplementary Fig. 2A). At the end of the dielectric antenna the NMR tube (internal radius 3 mm, height 15 mm) filled with the sample (thickness between 3 and 5 mm, depending on the sample preparation) is positioned (Supplementary Fig. 2).

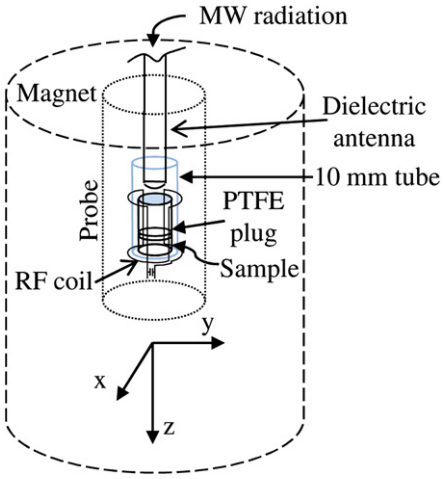

Fig. 1. Schematic diagram of the exposure set-up showing the interior of the NMR probe with the saddle radiofrequency coil where the sample is inserted. Microwaves are propagated into the probe by a diamagnetic metallic waveguide terminating with a dielectric antenna positioned above the tube containing sample (see Suppl. Fig. 1), outside the NMR acquisition volume. Relative dimensions are not in scale.

The power deposition pattern inside the sample was evaluated numerically by using Ansoft HFSS, a commercial code based on the Finite Element Methods (FEM) [31], running on a typical laptop (2 GB RAM).

Due to the wide range investigated, several simulations were carried out considering different medium complex relative permittivities, $\varepsilon = \varepsilon_r' - j\,\varepsilon_r''$, while the density was $\rho = 1110$ kg/m^3. In Table 1 the assumed parameters are reported, being $\omega = 2\pi f$; $\varepsilon_0 = 1/(36\pi \times 10^9)$ F/m and $\varepsilon_r'' = \sigma_{eq}/\omega\varepsilon_0$. Permittivity values of DMPC membranes at these frequencies are unknown. We have therefore assumed that they can be described by those of the analogous membrane system 1,2-Dioleoyl-sn-Glycero-3-Phosphocholine (DOPC), for which they have been measured in the 0.2–1.2 THz frequency range [32]. We have calculated the dielectric properties at frequencies <0.2 THz simulating a double-Debye dispersion equation $\hat{\varepsilon}(f) = \varepsilon_\infty + \frac{\Delta\varepsilon_1}{1+i2\pi f\tau_D} + \frac{\Delta\varepsilon_2}{1+i2\pi f\tau_2}$ with $\Delta\varepsilon_1 = 8.8, \Delta\varepsilon_2 = 0.89, \varepsilon_\infty = 2.3, t_D = 8$ ps and $\tau_2 = 121$ fs that holds for DOPC membrane at $n_w = 9$ in the range 0–1.2 THz [32].

According to the FEM method, the region of interest was divided in tetrahedral elements (134,891); the mesh generation (Supplementary Fig. 2B) was based both on the material wavelength λ_m (at 53.57 GHz $\lambda_m = 2.5$ mm, at 74 GHz $\lambda_m = 1.3$ mm) refinement and on the length based mesh refinement; thus the length of the tetrahedral elements were refined until they were below a specified value. In this case we adopted as the maximum length of a tetrahedron (i.e. the length of its longest edge) $l = 0.5$ mm.

In particular the following dosimetric parameters were calculated [33]:

- E^u (x,y,z) : the local electric field amplitude per unit incident power [(V/m)/W]. This was evaluated at each node of the computing domain (Supplementary Fig. 2C).

Table 1
Electromagnetic parameters adopted in numerical simulations.

Medium	f [GHz]	ε_r'[a]	ε_r''[a]	σ_{eq}[b] [S/m]
DMPC-^2H_2O	53.57	4.3	3.0	8.9
(MLVs) $n_w = 11$	65.00	4.0	2.6	9.4
	74.00	3.8	2.3	9.5
Quartz glass (NMR tube)		3.78		
Teflon		2.10		

[a] Calculated by a double-Debye equation $\hat{\varepsilon}(f) = \varepsilon_\infty + \frac{\Delta\varepsilon_1}{1+i2\pi f\tau_D} + \frac{\Delta\varepsilon_2}{1+i2\pi f\tau_2}$ with $\Delta\varepsilon_1 = 8.8$, $\Delta\varepsilon_2 = 0.89$, $\varepsilon_\infty = 2.3$, $\tau_D = 8$ ps and $\tau_2 = 121$ fs.
[b] Calculated by $\sigma_{eq} = 2\pi f\varepsilon_0\varepsilon_r''$.

E^u (x,y,z) : the local electric field amplitude per unit incident power [(V/m)/W]. This was evaluated at each node of the computing domain (Supplementary Fig. 2C).

- SAR^u (x,y,z) $= \sigma_{eq}\ E^{u\,2}/2\,\rho$: the local absorbed power per unit mass and per unit incident power [(W/kg)/W]. This is also the local specific efficiency, and it is zero outside the sample ($\sigma_{eq} = 0$).
- AV^u: the average SAR^u (x,y,z) over the sample per unit incident power [(W/kg)/W].

It is understood that, should the incident power be $P_0 \neq 1$ W, the local absorbed power per unit mass would be:

- P_0 x SAR^u (x,y,z) = SAR (x,y,z) = specific absorption rate [W/kg] and, consequently,
- P_0 x $AV^u = SAR_{av}$ the average SAR (x,y,z) over the sample [W/kg].

3. Results and discussion

3.1. Dosimetry

Dosimetric simulations were run at three different frequencies considering samples with 5 or 3 mm thickness. Fig. 2 displays the electric field amplitude found in a 3 mm thick sample at 74 GHz for 1 W incident power. It shows that the SAR is not uniform either along the axis of radiation propagation (z axis) or in the xy plane. It can be also noted that the sample layers closer to the glass (Fig. 2B) as well as the layers at the top, absorb most of the microwave

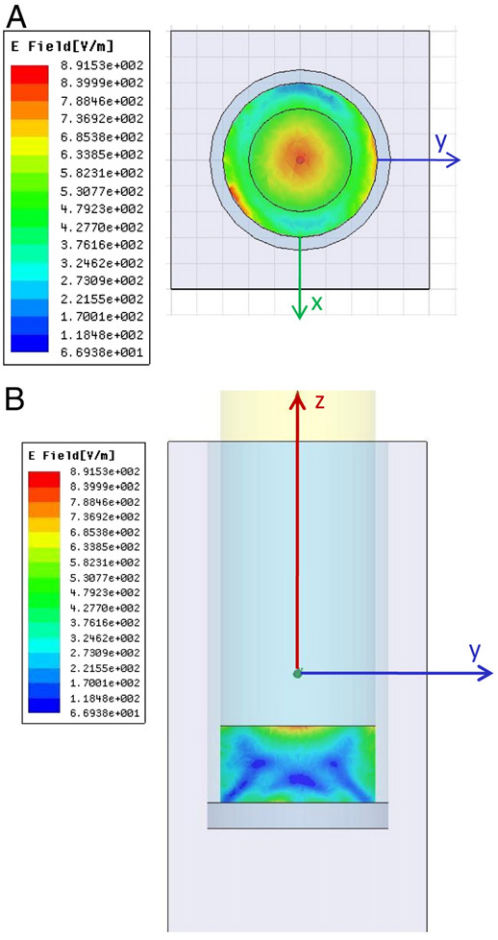

Fig. 2. Local electric field amplitude [V/m] at 1 W incident power. Electric field amplitude on the top layer (A) and on the yz plane of the exposed sample (B) for $f = 74$ GHz and 3 mm sample thickness.

power, as expected due to the small skin depth. In the top layer, "hot spot areas" with peak electric field amplitude, can be clearly distinguished (Fig. 2A). Table 2 reports the following results for the whole sample: the Average SAR per 1 W incident power (AV^u); the SAR values scaled down to the incident power (P_0) emitted by the generator at the frequency *f* (see Supplementary Fig. 1B); the time rate of initial temperature rises $\frac{dT}{dt}$, proportional to the SAR (Eq. (2)) in the first few seconds of exposure over which heat diffusion and convection do not occur [34,35] :

$$SAR = c\frac{dT}{dt}|_{t=0} \quad (2)$$

where *dT* is the temperature increment, *dt* is the duration (sec) over which T is measured and c is the specific heat, assumed to be that of water $c = 4186$ J/kg K.

It can be seen that the average SAR depends on the frequency of the radiation as well as on the sample thickness and it is larger for samples with 3 mm thickness.

Average SAR was also calculated for layers of sample 1 mm thick, starting from the sample surface (layer 1) down to the bottom (layer 3 or 5) along the z direction (Fig. 3A). The results show that, as expected due to the high conductivity (σ_{eq}) of the membrane system (Table 1), SAR values are higher on the top of the sample and decrease approaching the bottom layer (Fig. 3A); the latter is mostly higher than the next internal layer because of the coupling with the walls of the NMR tube. This trend is less pronounced in the sample with 3 mm thickness, indicating that average SAR uniformity along the z axis increases with decreasing sample thickness. However, thicknesses smaller than 3 mm deteriorate the quality of the measurements due to the low concentration of deuterium nuclei in the preparation. Therefore, optimal sample thickness conditions for the best trade off between SAR uniformity and measurement quality were 3 mm.

In all cases, SAR levels are of the order of mW/kg, much lower than 1.6 W/kg, the currently accepted safety limit for nonthermal effects [7]. These SAR levels correspond to negligible initial linear temperature rise in the first few seconds (<30 s) of exposure, being the average slope of the transient temperature response curve of the order of 10^{-6} K/s (Table 2). It can be also seen that the temperature is homogeneous inside the sample (especially for the 3 mm thick sample) and only negligible thermal gradients are induced between the top sample layer and the internal layers (Fig. 3B).

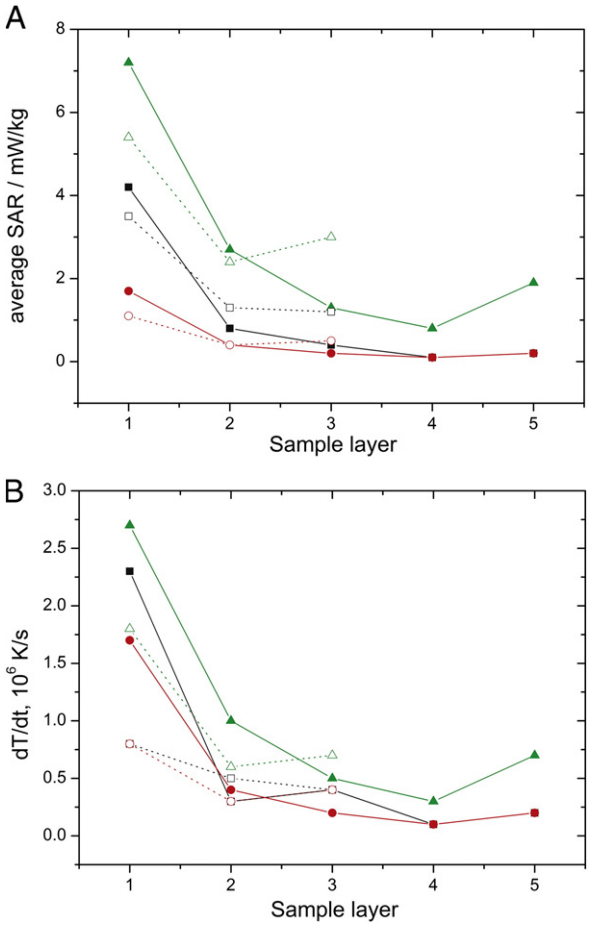

Fig. 3. Dosimetric analysis for DMPC samples with thickness of 5 (solid lines) and 3 mm (dotted lines). Average SAR calculated for each sample layer 1 mm thick along the z direction. Layer 1 identifies the sample top while layer 3 or 5 the bottom one (A). Average time rate of initial temperature rises in the first few seconds (<30 s) of exposure (B) for each sample layer.

3.2. Membrane main phase transition

Fig. 4A shows a sequence of ^{2}H-NMR spectra acquired at different temperatures across the main phase transition temperature T_m (25.5 °C) of the DMPC-^2H_2O membrane having a water/lipid mole ratio (n_w) of 11. The spectra a and b are typical powder patterns of the fluid phase (L_α). When the system reaches T_m, a clear discontinuity in the lineshape occurs and the spectrum becomes a singlet, typical of the ripple $P_{\beta'}$ phase (spectrum d) [27]. The $L_\alpha \rightarrow P_{\beta'}$ phase transition can be advantageously monitored by the decrease of the water splitting upon cooling, as shown in Fig. 4B. The discontinuity near T_m, at which the splitting drops to ≈110 Hz, reflects the discontinuity in the NMR lineshape. A reduced splitting effectively indicates a loss of water order (Eq. (1)) that becomes maximum at the main phase transition point. It must be noted that $\Delta\nu_Q$ decreases in the fluid phase and increases in the ripple phase as the temperature decreases (Fig. 4A a–c and d–g, respectively).

Table 2
Whole SAR values (average) for two different sample thickness and the expected initial temperature rise.

Sample thickness (mm)	*f* [GHz]	AV^{ua} [(W/kg)/W]	SAR_{av}[b] (mW/kg)	$\Delta T/\Delta t \times 10^{6c}$ (K/s)
5	53.57	86.0	1.1	0.3
	65.00	68.9	0.5	0.1
	74.00	133.9	2.5	0.6
3	53.57	209.1	2.7	0.6
	65.00	135.7	1.0	0.2
	74.00	133.9	2.5	0.6

[a] Average SAR per 1 W incident power.
[b] average SAR ($P_0 \times AV^u$) scaled down to the incident power (P_0) emitted by the generator at the frequency *f*.
[c] average time rate of initial temperature rise.

3.3. MW induced effects on the ripple-to-fluid transition

In order to evaluate the potential effects of MW on the membrane at different temperatures, a real-time exposure set-up was conceived (see "Experimental"). ^{2}H-NMR spectra were acquired during the wideband exposure in the frequency range 53–78 GHz, while strictly controlling and accurately adjusting the temperature of the membrane samples inside the probe. The response of the DMPC-^2H_2O membrane to MW, was first evaluated near the transition point, at 25.0 °C. In these conditions, the membrane was in the ripple phase close to T_m and its spectrum was a singlet analogous to those of the spectra d and e reported in Fig. 4A. The results of the exposure experiment are summarized in Fig. 5 where, the dependence of $\Delta\nu_Q$ on the exposure time and temperature, is reported for the sham and MW exposed samples. No significant changes were observed

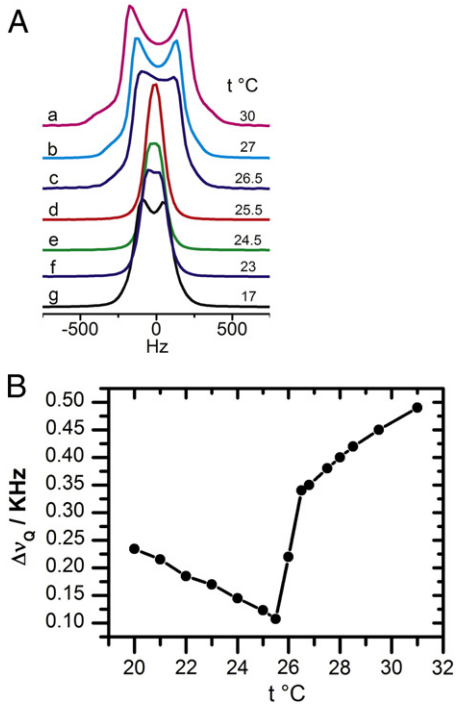

Fig. 4. DMPC-^2H_2O membrane phase transition. Sequence of ^{2}H-NMR spectra for the DMPC-^2H_2O membrane with $n_w = 11$ acquired at different temperatures across the fluid/ripple first order transition (a–c, fluid phase; d–g ripple phase) (A). Heavy water quadrupole splitting temperature dependence across the transition point. At $T_m = 25.5$ °C, a discontinuity occurs due to the transition from the fluid (L_α) to the ripple ($P_{\beta'}$) phase (B).

after 3 h of exposure on both samples neither in the lineshape (still a singlet), nor in the width of the signal. It should be further noted that, at constant temperature, both samples showed a long term thermal stability. After 3 h of exposure, the temperature was gradually raised above T_m, still under exposure, in order to induce the transition to the fluid phase. The splitting increased in both samples as expected, but significantly less in the MW exposed one (Fig. 5).

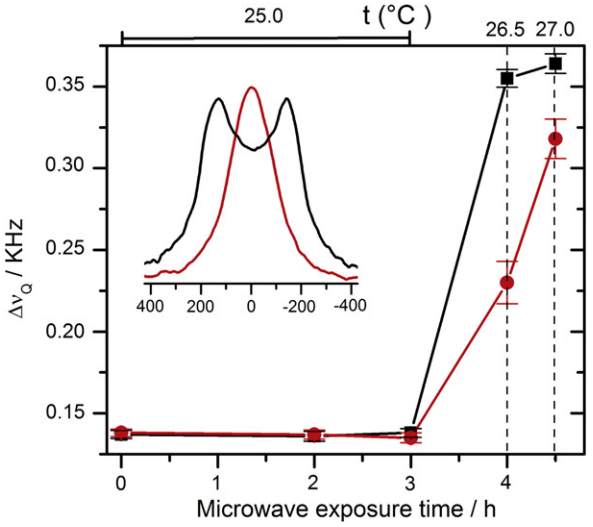

Fig. 5. Effects of the 53–78 GHz wideband exposure on the $P_{\beta'} \rightarrow L_\alpha$ transition in the 53–78 GHz wideband mode. Heavy water quadrupole splitting as a function of the microwave exposure time and temperature for the DMPC-^2H_2O membrane ($n_w = 11$). Error bars are the standard deviation calculated on three independent experiments. No effects were observed in the first 3 h ($T = 25.0$ °C) on the sham (black line) and microwave exposed (red line) samples. The inset shows representative spectra acquired for the sham (black spectrum) and the microwave exposed (red spectrum) samples at 26.5 °C ($T > T_m$). The transition to the fluid phase occurred only in the sham exposed sample (doublet).

In this case, the analysis of the NMR lineshapes is even much more informative, as displayed in the inset of Fig. 5, that compares representative deuterium spectra acquired at 26.5 °C after 4 h of sham (black line) and MW exposure (red line): the doublet appearance under sham exposure indicates that the membrane was already in the L_α phase, as should be at this temperature (see Fig. 4A), whereas the singlet observed under MW exposure indicates that the transition to the fluid phase was not yet completed and that the sample was still in a $P_{\beta'}$ phase, despite the fact that it was brought to a temperature T (26.5 °C) > T_m. Under microwave exposure conditions, a resolved doublet, indicative of a transition into the fluid phase, was observed only after a further temperature increase, at about 27 °C. This phase transition temperature delay (~1.5 °C) is to be clearly attributed to the radiation that acts against the opposite thermal trend.

3.4. MW induced effects on the fluid-to-ripple transition

In order to gain insight into this very interesting effect, the response of the membrane was studied from the fluid phase side of the transition region as a function of the exposure time and temperature. In this experiment, the sample was initially brought into the fluid phase and constantly maintained at 27 °C, close to the transition temperature (25.5 °C). Under these conditions, microwave exposure was started. The sequence of one hour interval spectra reported in Fig. 6A shows a representative time course of the experiment over the first 4 h of exposure, after which no relevant effect were anymore detected. It can be seen that a relevant narrowing of the spectra occurs during the exposure treatment that, however, did not alter the canonical powder pattern lineshape of the deuterium spectra, indicating that the effect induced by the radiation involved the entire mesophase. This MW-induced-spectral narrowing reveals a loss of water ordering at the membrane interface, qualitatively similar to that observed in the sham exposed system during the cooling-induced $L_\alpha \rightarrow P_{\beta'}$ transition (Fig. 4A). The difference is that the spectral doublet did not completely disappear under microwave exposure.

The loss of water ordering can be quantified by means of the decrease of the heavy water quadrupole splitting as a function of the microwave exposure time (Fig. 6B, red line). After about 4 h of microwave exposure, a relevant splitting decrease of almost 30% was detected. In contrast, a parallel analysis made under sham exposure conditions showed that, as long as the temperature was kept constant (27 °C in the first 4 h of sham exposure), the splitting of the sham exposed sample did not change (black line). This long term thermal stability, clearly implies that the splitting decrease observed under microwave exposure, has to be necessarily attributed to the action of microwaves.

Once the smallest splitting value was induced under microwave exposure (after about 4 h), the sample was gradually cooled towards T_m, always under exposure. Fig. 6B shows that, after an initial slight reduction at 26.5 °C, a significant splitting increase occurred for $T \geq 25.5$ °C. This trend reversion is as surprising as important because: a) in the fluid phase ($T > T_m$), a temperature decrease would have to cause, instead, a splitting decrease and b) it marks a turning point that should be related to some relevant structural change in the membrane.

The overall trend is qualitatively analogous to that observed in the sham exposed sample during the cooling-induced $L_\alpha \rightarrow P_{\beta'}$ phase transition, as displayed in Fig. 6B. The main differences are that, under microwave exposure the transition point is shifted to a higher temperature and the discontinuity in the splitting is less pronounced compared to that characteristic of the unperturbed (sham exposed) system.

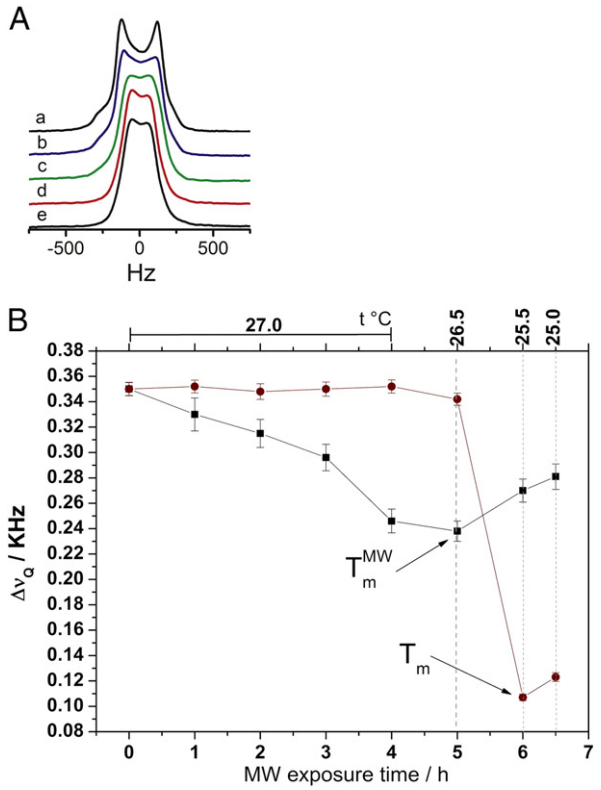

Fig. 6. Effects of the 53–78 GHz wideband exposure on the $L_\alpha \rightarrow P_{\beta'}$ transition. Representative deuterium NMR lineshape changes for the DMPC-^2H_2O membrane ($n_w = 11$) induced by microwaves at constant T = 27 °C as a function of the exposure time (see Fig. 3A for comparison) (A). Quadrupole splitting of water (^2H), as a function of the exposure time and temperature for the sham (■) and microwave exposed (●) samples (B). Microwaves induce an upwards shift of the transition point. Black and red lines are drawn to show the different trends. Error bars are the standard deviation calculated on three independent experiments.

All of these results do effectively indicate that the microwave exposed DMPC membrane is pointing towards a transition point at $T_m^{MW} \approx 27^{\circ}C > T_m$.

Summarizing the above results, we can say that under microwave exposure there is an upward shift of the transition point, a broadening of the transition region and a smaller change of the water order parameter at the membrane phase transition.

3.5. Thermal vs. nonthermal mechanism

We have seen that if the membranes are exposed close to the transition point from the fluid phase side (i.e., for $T > T_m$), the transition to the gel-ripple phase is induced at a constant temperature close to T_m (Fig. 6 A, B). The fluid to gel transition can be alternatively induced by cooling the sample (Fig. 4 A, B) or, again at a constant temperature, by imposing osmotic pressures with energies < kT [36]. On the contrary, if the membrane is exposed in the ripple phase close to the transition point and the temperature is gradually raised up to T_m, the effect of the radiation is to delay the transition to the fluid phase in the temperature scale (Fig. 5). Thus, all these effects appear to be nonthermal since the radiation always acts in opposition to the thermal trend.

On the other hand, no induction of significant heating is expected, as already shown in the dosimetric analysis. Moreover, even if the 50–80 GHz radiation has a small penetration depth in the membrane sample (~1 mm, see Table 1) which leads to the nonuniform SAR pattern before described, thermal gradients in the sample are of negligible entity (Fig. 3B), even when "hot spot areas" are considered. Indeed, in the worst case scenario, the simplest thermal model that neglects all heat transfer mechanisms except microwave radiation energy deposition, we can estimate (Eq. (2)) that the largest thermal gradient between the local maximum and minimum peak SAR is ~0.08 °C, after 4 h of exposure and for 20 μW incident power, 74 GHz and 5 mm sample thickness. This value, neglects many potentially significant heat transfer mechanisms as thermal conduction, surface cooling (convection, radiation), that should occur in a so long exposure time [34,35] and, in any case, is too small to activate significant thermal processes like convective effects, as previously observed in the range 40–70 GHz on other systems [37]. Besides, convection phenomena are restricted to "convection-enabled" media, like aqueous solutions, where water is the most abundant component. In contrast, in "convection-disabled media" like gels, they are inhibited even under exposure at high SAR up to 80 kW/kg [37]. This is the case applicable to our samples that are rather viscous gel systems (see Materials and methods).

These argumentations suggest that the thermal mechanisms can hardly be invoked for interpreting our results.

3.6. Nonthermal effect

The hypothesis that the effects here described would be caused by some nonthermal mechanism must be therefore taken into consideration. A nonthermal hypothesis should answer to the following crucial questions: i. How can these small amounts of MW energy (<kT) affect the membrane behavior in such a relevant way? ii. Which are the biophysical phenomena involved in the MW-membrane interaction? Is there a mechanism that accounts for the unique sensitivity of the DMPC membranes at temperature close to the melting transition and that provides a quantitative explanation for the systematic changes observed in the deuterium NMR spectra?

Since the photon energy involved in the above experiments is of the order of the thermal energy, it is at least plausible that collective oscillations of the membrane might be excited. Such a hypothesis has been formerly suggested by Fröhlich who showed that MW can trigger the condensation of a set of oscillators (biological structures), sustained by metabolic energy, to a coherent single mode of oscillation with the lowest energy, if the total energy supply exceeds a threshold [13], suggesting the possibility of nonthermal biological effects. Recently, Reimers et al. reanalyzed (revised) Fröhlich's model showing that "weak condensates", that do not require coherence, may be produced by microwave energy and may significantly affect biological systems [38]. However, this model has not yet been unambiguously proven and remains a conjecture.

A mode of excitation of the membrane in the 50–80 GHz range, should be found in order to involve a nonthermal effect. By excluding the direct effect of the radiation on ion motion because of inertia effects [39], another potential mode of excitation could be the local fluctuation of water molecules bound to the membrane among different hydration sites of the polar headgroups, occurring in the neighboring of T_m [40]. This exchange mechanism, occurring in the ps-time scale, falls in the range of high frequency MW and may provide the dipole interaction triggering with the microwave radiation. If microwaves interact with the water exchange between phosphocholine binding sites, mechanism relevant near the transition point, such an hypothesis could explain the strong influence of the radiation on the main phase transition. This hypothesis is now under study and will be the subject of another paper.

4. Conclusions

In conclusion, this work provides strong evidence of the extreme sensitivity of biological membranes to low power long term MW exposure near the phase transition point. Since all membrane systems

exhibit a change of hydration across the membrane main phase transition, like that observed in DMPC model membranes, we believe that the phenomena here reported may play a common and crucial role in all the effects observed both in vitro and in vivo as a consequence of microwave exposure.

Supplementary materials related to this article can be found online at doi:10.1016/j.bioelechem.2011.10.003.

Acknowledgments

A.B., G.C. and L.F. are grateful to P. W. Westermann for critical discussions. A.B. thanks Yuri Koshurinov for the cooperation in the design of the experimental set-up and the technical support with waveguide circuits. The authors thank N. Gagliardi for carefully reading the manuscript.

A.B., G.C. and L.F. were funded by Regione Calabria (POR 2000/2006, misure 3.16, progetto PROSICA).

References

[1] A.G. Pakhomov, Y. Akyel, O.N. Pakhomova, B.E. Stuck, M.R. Murphy, Current state and implication of research on biological effects of millimeter wave, Bioelectromagnetics 19 (1998) 393–413.
[2] A.G. Pakhomov, M.R. Murphy, Low intensity millimeter waves as a novel therapeutic modality, IEEE Trans. Plasma Sci. 28 (2000) 34–40.
[3] M.A. Rojavin, A.A. Radzievsky, A. Cowan, M.C. Ziskin, Pain relief caused by millimeter waves in mice: results of cold water tail flick tests, Int. J. Radiat. Biol. 76 (2000) 575–580.
[4] A.A. Radzievsky, O.V. Gordiienko, I. Szabo, S.I. Alekseev, M.C. Ziskin, Millimeter wave-induced suppression of B16 F10 melanoma growth in mice: involvement of endogenous opioids, Bioelectromagnetics 25 (2004) 466–473.
[5] M.A. Rojavin, M.C. Ziskin, Medical applications of millimeter waves, QJM 91 (1998) 57–66.
[6] M. Marcus, B. Pattan, Millimeter wave propagation: spectrum management and implications, IEEE Microwave Mag. 6 (2005) 54–62.
[7] CNIRP, Guidelines for limiting exposure to time varying electric, magnetic, and electromagnetic fields (up to 300 GHz), Health Phys. 74 (1998) 494–522.
[8] A. Beneduci, Review on the mechanisms of interaction between millimeter waves and biological systems, in: E.M. Bernstein (Ed.), Bioelectrochemistry Research Developments, Nova Science Publishers Inc, New York, 2008, pp. 35–80.
[9] E. Postow, L. Swicord, Modulated fields and "window" effects, in: C. Polk, E. Postow (Eds.), Handbook of Biological Effects of Electromagnetic Fields, Second Edition, CRC Press LLC, Boca Raton, Florida, 1996, pp. 537–541.
[10] I.Y. Belyaev, Nonthermal biological effects of microwaves: current knowledge, further perspective, and urgent needs, Electromagn. Biol. Med. 24 (2005) 375–403.
[11] A. Beneduci, G. Chidichimo, S. Tripepi, E. Perrotta, F. Cufone, Antiproliferative effect of millimeter radiation on human erythromyeloid leukemia cell line K562 in culture: Ultrastructural- and metabolic-induced changes, Bioelectrochemistry 70 (2007) 214–220.
[12] S.J. Webbs, A.D. Booth, Absorption of microwaves by microorganisms, Nature 222 (1969) 1199–1203.
[13] H. Fröhlich, Theoretical physics and biology, in: H. Fröhlich (Ed.), Biological Coherence and Response to External Stimuli, Springer-Verlag, Berlin (DH), 1988, pp. 1–24.
[14] S. Hadjiloucas, M.S. Chahal, J.W. Bowen, Preliminary results on the non-thermal effects of 200–350 GHz radiation on the growth rate of *S. cerevisiae* cells in microcolonies, Phys. Med. Biol. 47 (2002) 3831–3841.
[15] A. Ramundo-Orlando, Effects of millimeter waves radiation on cell membrane-A brief review, J. Infrared Milli. Terahz. Waves 31 (2010) 1400–1411.
[16] V.I. Geletyuk, V.N. Kazachenko, N.K. Chemeris, E.E. Fesenko, Dual effect of microwaves on single Ca^{++} activated K^{+} channels in cultured kidney cells Vero, FEBS Lett. 359 (1995) 85–88.
[17] I. Szabo, J. Kappelmayer, S.I. Alekseev, M. Ziskin, Millimeter waves induced reversible externalization of phosphatidylserine molecules in cells exposed in vitro, Bioelectromagnetics 27 (2006) 233–244.
[18] R.P. Liburdy, A. Penn, Microwaves bioeffects in the erythrocyte are temperature and pO_2 dependent: cation permeability and protein shedding occur at the membrane phase transition, Bioelectromagnetics 5 (1984) 283–291.
[19] R.P. Liburdy, R.L. Magin, Microwave-stimulated drug release from liposomes, Rad. Res. 103 (1985) 266–275.
[20] J.W. Allis, B.L. Sinha, Fluorescence depolarization studies of the phase transition in multilamellar phospholipid vesicles exposed to 1.0-GHz microwave radiation, Bioelectromagnetics 3 (1982) 323–332.
[21] M. Zadhobov, et al., Interactions between 60-GHz millimeter waves and artificial biological membranes: dependence on radiation parameters, IEEE Trans. Microwave Theory Tech. 54 (2006) 2534–2542.
[22] A. Ramundo-Orlando, G.P. Gallerano, P. Stano, A. Doria, E. Giovenale, G. Messina, M. Cappelli, M. D'Arienzo, I. Spassovsky, Permeability changes induced by 130 GHz pulsed radiation on cationic liposomes loaded with carbonic anhydrase, Bioelectromagnetics 28 (2007) 587–598.
[23] A. Ramundo-Orlando, G. Longo, M. Cappelli, M. Girasole, L. Tarricone, A. Beneduci, R. Massa, The response of giant phospholipid vesicles to millimeter waves radiation, Biochim. Biophys. Acta, Biomembr. 1788 (2009) 1497–1507.
[24] J.F. Nagle, S. Tristram-Nagle, Structure of lipid bilayers, Biochim. Biophys. Acta 1469 (2000) 159–195.
[25] G. Chidichimo, A. Golemme, J.W. Doane, P.W. Westermann, Investigation of ribbon lyotropic structures by deuterium magnetic resonance, Phys. Rev. Lett. 48 (1985) 1950–1954.
[26] J.H. Davis, The description of membrane lipid conformation, order and dynamics by ^{2}H-NMR, Biochim. Biophys. Acta 737 (1983) 117–171.
[27] R.L. Smith, E. Oldfiel, Dynamic structures of membranes by deuterium NMR, Science 225 (1984) 280–288.
[28] J.M. Pope, L. Walker, B.A. Cornell, G.W. Francis, NMR study of synthetic lecithin bilayers in the vicinity of the gel–liquid–crystal transition, Biophys. J. 35 (1981) 509–520.
[29] S.-J. Marrink, D.P. Tieleman, A.R. Van Buuren, H.J.C. Beredsen, Membranes and water: an interesting relashionship, Faraday Discuss. 103 (1996) 191–201.
[30] J.X. Cheng, S. Pautot, D.A. Weitz, X.S. Xie, Ordering of water molecules between phospholipid bilayers visualized by coherent anti-Stokes Raman scattering microscopy, Proc. Natl. Acad. Sci. U. S. A. 100 (2003) 9826–9830.
[31] J. Jin, Electromagnetic Analysis and Design in Magnetic Resonance Imaging, CRC Press LLC, Florida, USA, 1999.
[32] K.J. Tielrooij, D. Paparo, L. Piatkowski, H.J. Bakker, M. Bonn, Dielectric relaxation dynamics of water in model membranes probed by Terahertz spectroscopy, Biophys. J. 97 (2009) 2484–2492.
[33] M.L. Calabrese, G. D'Ambrosio, R. Massa, G.A. Petraglia, High-efficiency waveguide applicator for in vitro exposure of mammalian cells at 1.95 GHz, IEEE Trans. Microwave Theory Tech. 54 (2006) 2256–2264.
[34] S. Kühn, N. Kuster, Experimental EMF exposure assessment, in: F.S. Barnes, B. Greenebaum (Eds.), Handbook of Biological Effects of Electromagnetic Fields. Bioengineering and Biophysical Aspects of Electromagnetic Fields, Third Edition, Taylor and Francis, CRC Press, Boca Raton, Florida, 2007, pp. 381–409.
[35] E.G. Moros, W.F. Pickard, On the assumption of negligible heat diffusion during the thermal measurement of a nonuniform specific absorption rate, Radiat. Res. 152 (1999) 312–320.
[36] V.A. Parsegian, R.P. Rand, N. Fueller, D.C. Rau, Osmotic stress for the direct measurement of intermolecular forces, Methods Enzymol. 127 (1986) 400–416.
[37] E.P. Khizhnyak, M.C. Ziskin, Temperature oscillations in liquid media caused by continuous (nonmodulated) millimeter wavelength electromagnetic irradiation, Bioelectromagnetics 17 (1996) 223–229.
[38] J.R. Reimers, L.K. McKemmish, R.H. McKenzie, A.E. Mark, N.S. Hush, Weak, strong, and coherent regimes of Frohlich condensation and their applications to terahertz medicine and quantum consciousness, Proc. Natl. Acad. Sci. U. S. A. 106 (2009) 4219–4224.
[39] J.E. Moulder, L.S. Erdreich, R.S. Malyapa, J. Merritt, W.F. Pickard, Vijayalaxmi, cell phones and cancer: what is the evidence for a connection? Rad. Res. 151 (1999) 513–531.
[40] K. Åman, E. Lindahl, O. Edholm, P. Håkansson, P.-O. Westlund, Structure and dynamics of interfacial water in a L_{α} phase lipid bilayer from molecular dynamics simulations, Biophys. J. 84 (2003) 102–115.

ACKNOWLEDGEMENTS

I would like to thank all the people who contributed directly or indirectly to this work. First of all my supervisor Dr. Cesare Oliviero Rossi, who gave me the right stimuli and suggestions to carry out the research. He supported me not only in the research project but we also shared some difficult moment of my life, contributing to raise my condition again. I also would like to express my gratitude to Prof. Giuseppe Ranieri for the useful scientific discussions and for his support. I appreciate his vast knowledge and skill in many areas. I would like to thank the other member of my research group, Dr. Luigi Gentile for the assistance he provided of the research project and for taking time out from his busy schedule. I'm also grateful to dott. Paolino Caputo whose expertise in the bitumen and asphalt conglomerate resulted in a precious help. A special thank to Dr. Filipe Antunes from University of Coimbra, Portugal. He provided me with direction, technical support and in the end became a friend. He gave me the opportunity to learn about the great value of people of Portugal. I must acknowledge my wife Francesca and my daughter Giorgia for making my days more interesting and worthy to be lived. In the end I really would like to thank my parents that have been going through the most hard time of their entire lives and for not to be a burden on me. I love you mom and dad.